NOTICE

The quality of this microform is heavily dependent upon the quality of the original thesis submitted for microfilming. Every effort has been made to ensure the highest quality of reproduction possible.

If pages are missing, contact the university which granted the degree.

Some pages may have indistinct print especially if the original pages were typed with a poor typewriter ribbon or if the university sent us an inferior photocopy.

Reproduction in full or in part of this microform is governed by the Canadian Copyright Act, R.S.C. 1970, c. C-30, and subsequent amendments.

AVIS

La qualité de cette microforme dépend grandement de la qualité de la thèse soumise au microfilmage. Nous avons tout fait pour assurer une qualité supérieure de reproduction.

S'il manque des pages, veuillez communiquer avec l'université qui a conféré le grade.

La qualité d'impression de certaines pages peut laisser à désirer, surtout si les pages originales ont été dactylographiées à l'aide d'un ruban usé ou si l'université nous a fait parvenir une photocopie de qualité inférieure.

La reproduction, même partielle, de cette microforme est soumise à la Loi canadienne sur le droit d'auteur, SRC 1970, c. C-30, et ses amendements subséquents.

Investigation on a Multi-Point Direct Injection and Control System for Gaseous Fuels in Diesel Engines

Domenico Patrizio Miele

A Thesis

in

The Department

of

Mechanical Engineering

Presented in Partial Fulfillment of the Requirements
for the Degree of Master of Engineering at
Concordia University
Montreal, Quebec, Canada

November 1990

ISBN 0-315-64735-3

ABSTRACT

Investigation on a Multi-Point Direct Injection and Control System for Gaseous Fuels in Diesel Engines

Domenico P. Miele

The gaseous fuels are the recognized alternatives for hydrocarbon liquid fuels in automotive engine use. While methanol and other alcohols are more suitable for use in automobiles, mainly due to the existing infrastructure for liquid fuel distribution, Natural Gas is considered as the prime replacement candidate for the commercial vehicles. This is because most commercial vehicles operate from a centrally located distribution center.

To obtain the highest efficiency, the gaseous fuel has to be directly injected into the cylinder of an engine and a suitable technology has still to be developed to allow the proper use of the alternative gaseous fuels.

The direct injection system proposed consists of solenoid operated injectors interfaced with a metering valve that is controlled by a linear digital actuator. The injected gas dose can be controlled by both the metering valve opening and the time of injection, or injection duration. The mathematical model for the injection system has been formulated and validated experimentally. It was

then used to calculate the injected gas dose for various metering valve flow area and time of injection. The obtained gas discharge characteristics could be used to select the required design parameters of the injectors and the metering valve and also to optimize the gas injection system for a particular diesel engine.

ACKNOWLEDGEMENTS

The author would like to express his greatest gratitudes to his supervisors Dr. T. Krepec and Dr. G.H. Vatistas, for their constant encouragement, support and understanding throughout the course of this investigation and its final preparation. Extended thanks go to Dr. R.M.H. Cheng for his assistance and advice.

Many thanks are directed to several of the author's friends and colleagues, who also egged him on during this investigation and during its final submission. The thankful group consists of Carmine Lisio, Dr. Antonios I. Georgantas, and Gino Carrese in the Fuel Control Lab, Daniel Quinz and Stewart Cassof, for their programming support and evolution from assembler to C, Tom Montor, Henry Hong, and Simon Poon, for their assistance with the use of facilities and equipment.

Most of all, the author expresses the deepest of gratitudes to his wife, Anna Maria Mancini, for her support, encouragement and understanding for all those long hours and weekends that were not spent together.

Finally, the author would like to thank all the societies with whose funds made this investigation possible, "Fonds pour la Formation et l'Aide a la Recherche" (FCAR), Bendix Avelex Inc., Imperial Oil, and Energy Mines and Resources Canada.

TABLE OF CONTENTS

LIST OF FIGURES

LIST OF TABLES

NOMENCLATURE

a	- speed of sound, m/s
A_{12}	- metering valve flow area, m^2
A_{23}	- injector flow area, m^2
A_o	- injector orifice area, m^2
A_{needle}	- injector needle cross sectional area, m^2
A_{nozzle}	- injector nozzle area, m^2
A_{pipe}	- fuel pipeline cross-sectional area, m^2
cf	- conversion factor, 448.93 GPM-s/ft^3
C_d	- discharge coefficient
C_m	- mass flow coefficient, s $\sqrt{K}$/ m
C_v	- flow coefficient, GPM/ $\sqrt{psi}$
C+	- positive wave flow characteristic
C-	- negative wave flow characteristic
d, D_{pipe}	- diameter of fuel pipeline, m
d_{needle}	- diameter of the injector needle, m
d_{si}	- diameter of the injector inner seat, m
d_{se}	- diameter of the injector exterior seat, m
d_o	- nozzle orifice diameter, m
d_{met}	- metering valve hole diameter, m
D_f	- damping force, N
D_T	- diameter of injector needle + clearance, m
dt	- time increment, s
dx	- length increment, m

f - Darcy-Weisbach friction factor

FA_{stoich} - stoichiometric fuel/air ratio, kg/kg

FA_{actual} - actual fuel/air ratio, kg/kg

F_{eff} - effective force on injector needle, N

F_{elec} - electrical or solenoid force, N

F_{fric} - friction force acting on injector needle, N

F_{gas} - gas forces on injector needle, N

F_{pre} - spring preload force on injector needle, N

g - gravitational constant, 32.2 lb/s

h - injector needle displacement, m

dh - injector velocity, m/s

d^2h - injector acceleration, m/s^2

K_s - injector spring constant, N/m

l_{pipe} - fuel pipeline length, m

L - length, m

m - mass, kg

m_{acc} - mass of gas in accumulator, kg

m_{air} - mass of air, kg

$m_{armature}$ - mass of solenoid armature, kg

m_{needle} - mass of needle, kg

m_{spring} - mass of spring, kg

m_2 - mass in injection chamber, kg

m_{2i} - initial mass in injector chamber, kg

m_{2f} - final mass in injector chamber, kg

m_f - mass of fuel, kg

$\dot{m}_f$ - mass flow of fuel, kg/s

$\dot{m}_{12}$ - mass flow, supply to injector, kg/s

$\dot{m}_{23}$ - mass flow into combustion chamber, kg/s

$\dot{m}_{24}$ - mass flow, leakage from injector, kg/s

$\dot{m}_{n-1}$ - mass flow at increment n-1, kg/s

$\dot{m}_n$ - mass flow at increment n, kg/s

$\dot{m}_x$ - mass flow at position x at t = t, kg/s

$\dot{m}_y$ - mass flow at position y at t = t, kg/s

$\dot{m}_z$ - mass flow at position z at t = t +Δt, kg/s

n - number of increments for the fuel pipeline

N - engine speed, rpm

P_{acc} - pressure in accumulator, bar

P_1 - fuel supply pressure, bar

P_2 - injector chamber pressure, bar

P_3 - combustion chamber pressure, bar

P_4 - ambient pressure, bar

P_x - pressure at position x at t = t, bar

P_y - pressure at position y at t = t, bar

P_z - pressure at position z at t = t + Δt, bar

Q - water flow rate, GPM

R - gas constant, kJ/kg-K

$\bar{R}$ - Universal Gas Constant, kJ/kmol-K

t - time, s

T - temperature, K

u,U - gas velocity, m/s

V	- volume, m^3
V_{acc}	- volume of accumulator, m^3
V_2	- injector chamber volume, m^3
V_{2i}	- initial injector chamber volume, m^3
V_{2f}	- final injector chamber volume, m^3
x	- distance, m
Y,y	- metering valve handle revolutions
Z,z	- compressibility factor

GREEK SYMBOLS

γ	- isentropic gas constant
δ	- clearance, m
λ	- multiplying factor
μ	- viscosity, $N-s/m^2$
ρ	- density, kg/m^3
τ_o	- shear stress along pipe wall, kPa
τ_{yx}	- shear stress on yx plane, kPa
υ	- specific volume, m^3/kg
ϕ	- equivalence ratio
ψ	- crank angle, degrees

1. THESIS CONCEPT DEFINITION

A large quantity of fuel available as an alternative energy source for combustion engines is in the gaseous state. Most of these fuels are Hydrogen, Natural Gas, and Propane. Some of these gaseous fuels have been already used as a secondary source of energy, together with gasoline for spark ignition engines, in so called dual fuel engines. In the case of gas fueled diesel engines, called dual fuel diesel engines, liquid diesel fuel is still injected in small doses to obtain ignition due to the low cetane number of the gaseous fuels, which are introduced into a diesel engine by aspiration, through the intake manifold, as in spark ignition engines. The main objective of this investigation is to develop an improved design of electronically controlled multi-point diesel fuel supply system which would provide direct injection of gaseous fuels into the cylinder of the diesel engine, rather than by the method of aspiration. See Figure 1.1.

There are several known advantages of the direct injection system for gaseous fuels; the most important being: higher specific power output and thermal efficiency. The proposed addition of an electronic control system allows for a large degree of flexibility in shaping of the gas discharge characteristic and of the fuel delivery dose

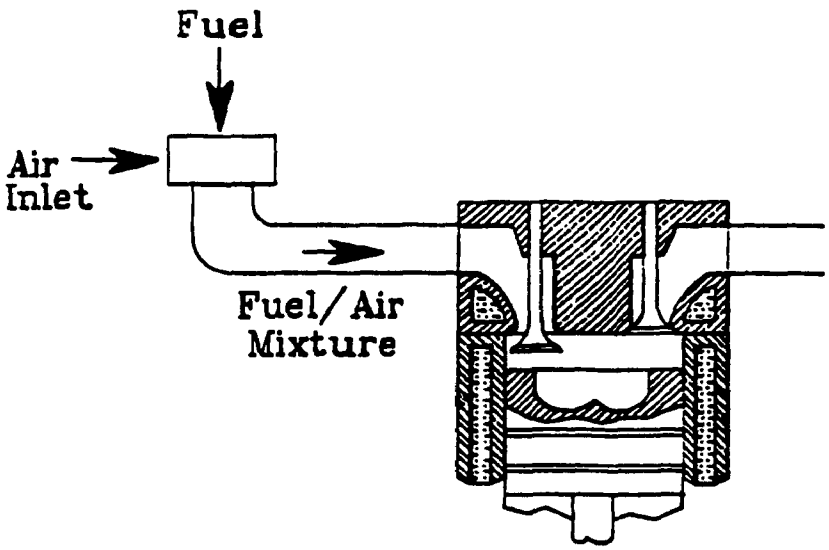

a) Fuel/Air Mixture by Aspiration

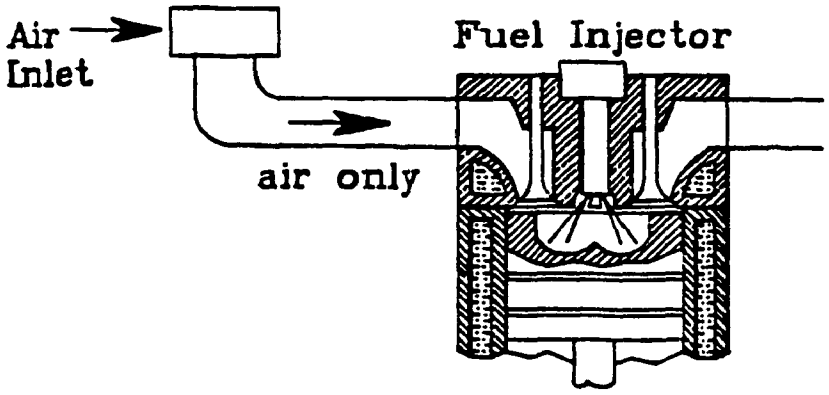

b) Fuel/Air Mixture by Direct Injection

Figure 1.1. Methods of Achieving Fuel/Air Mixtures.

versus the engine speed, i.e. in producing the required engine's operational characteristic.

The design of the proposed gaseous injection system consists of several injectors actuated by solenoids which are interfaced with one metering valve actuated by a stepper motor, which is placed at some distance from the injectors. In the design of this injection system, the pressure waves propagating in the pipe between the metering valve and the injectors are taken into account due to their impact on the instant rate of gas injection and on the gas mass dose injected. These two factors affect the performance of the diesel engine and must be well optimized in order to produce the required characteristic of a gas fueled diesel engine. The control of the direct gas injection process will be accomplished by adjusting both: the metering valve flow area and the time of injection duration (pulse width regulation).

The existing version of the gas injection system will be reviewed first and then the modifications will be shown. Next, a mathematical model of a multi-point injection system for gaseous fuels will be formulated including the effects of pressure waves propagating between the injectors and the metering valve, on the injected fuel mass dose and the rate of fuel discharge. Then, experiments will be performed to validate the mathematical model and to match the operational characteristic of a diesel engine. The

validation will be followed by an attempt to optimize the gaseous injection system via the simulation process. Finally, a summary will be made and recommendations for improvements of the injection system for gaseous fuels will be presented.

2. GASEOUS FUEL INJECTION AND CONTROL SYSTEMS. LITERATURE REVIEW

The potential for the use of alternative gaseous fuels in automotive engines can be judged presently as being high. In current research, four critical areas of challenge can be observed leading towards the implementation of these fuels which are: 1) their inexpensive availability, 2) the effective on-board storage systems for gaseous fuels, 3) the efficient energy conversion in the combustion engine, and 4) the effective control system for the gaseous fuel supply, as required for the automotive engine characteristics.

The ability to retrieve commercially competitive gaseous fuels is dependent on the relative cost of the production or extraction method. A fuel such as Hydrogen can be obtained from water by electrolysis; however, quite a substantial amount of electrical energy is required to obtain Hydrogen by this method because the ionization energy of water is quite high. As a solution, the inexpensive off-peak hours energy abundance could be used to produce Hydrogen. Natural Gas is a more readily available fuel which is found in large quantities in North America. Natural Gas is extracted from the underground reservoirs by drilling and piping methods combined with those of obtaining crude oil.

On-board storage systems for Hydrogen and Natural Gas are vital for the implementation of gaseous fuels which are occupying a considerable amount of space in the vehicle. This represents a significant problem because the gas storage system should provide sufficient amount of fuel for the required operational range of the vehicle, while leaving enough space for passengers and their cargo.

The next major concern is the energy conversion of gaseous fuels in automotive engines. The existing types of gas supply systems, through the intake manifold, may be considered as adequate but they are usually not quite able to extract the maximum efficiency from the engine. The main problems remained to be solved are related to the fuel supply mode and to some undesirable combustion characteristics of the gaseous fuels. Some progress has been made recently, thanks to the advancing microprocessor technology in the area of electronic controls, which can now be applied to improve the effectiveness of gaseous fuel use in automotive engines.

There are two ways in which an air-fuel mixture can be obtained: by external mixing in the intake manifold or by internal mixing in the engine cylinder chamber. External mixing can be achieved by aspiration, single point (throttle body) injection, and by multi-point port injection, which is usually found in spark ignition

engines. Internal mixtures are achieved by direct injection of fuel into the combustion chamber of an engine. Under the term of direct injection, the fuel injection into the divided chambers of a diesel engine is also considered, which in diesel engine technology is designated as indirect injection (IDI) chambers. Direct injection (DI) chambers are now being favored in diesel engines because they offer several advantages such as higher thermal efficiency and improved starting. Presently, in some research, direct injection has been also used in spark ignition engines, as well as in diesel engines with ignition support from the spark plugs.

H. R. Ricardo was one of the first researchers to investigate the possibilities of a Hydrogen fueled spark ignition engine back in 1923. He determined that Hydrogen was impractical for most uses due to the flashback and the pre-ignition phenomena [1].*

Rudolf Erren, before World War II, designed several direct Hydrogen fueled engines in which no detonation occurred. This was due to the direct injection of the Hydrogen fuel, which Erren introduced early in the compression stroke in order to maximize mixing [1]. Other researchers such as Oehmichen and Schoeppel, followed Erren's path, in realizing that direct injection of Hydrogen fuel was the best solution to avoid undesirable

---

* Number in brackets refers to References.

combustion phenomena.

Homan et al [1] addressed the undesirable combustion and emissions in Hydrogen fueled engines and they proposed some remedies to rectify these problems. Homan found that mixtures achieved by aspiration or manifold point injection are prone to pre-ignition, knock and flashback. Some remedies to these undesirable phenomena are water injection, exhaust gas recirculation, and low equivalence ratios. Homan developed a scheme called LIRIAM, for Late Injection Rapid Ignition And Mixing, in a spark ignition engine. The advantages of this scheme were: no flashback and no pre-ignition due to the late direct injection of the fuel dose into the cylinder of a combustion engine. The pressure rise in the cylinder was controlled by the pressure changes in the injector, which affected the rate of injection. Homan found that the most difficult problems to overcome in direct gas injection were: creation of the high injection pressure necessary for rapid mixing of the Hydrogen with air and the lack of fast operating injectors with sufficiently high flow rates to supply the required fuel dose during the required short injection time period. Homan confirmed that with Hydrogen fueled diesel engines, the best results are achieved with direct injection as compared to manifold supply and diesel fuel injection to provide ignition. He acknowledged that the majority of

research is directed towards the use of direct injection diesel engines converted to run on Hydrogen, using some type of ignition support such as spark plugs, glow plugs, and other hot surfaces.

Varde [2], using a spark ignition engine, managed to avoid pre-ignition and knock by developing a scheme where the port injector released Hydrogen late in the suction stroke so that the residual exhaust gases were first cooled by the incoming air, before coming into contact with the Hydrogen gas.

Peschka [3,4], using a spark ignition engine, applied water injection, as denoted by Homan et al [1], to solve the flashback problem and to obtain higher power output from the engine, when using multi-point port injection. Peschka [4] also experimented with direct injection of both: liquid Hydrogen as well as gaseous Hydrogen in a spark ignition engine and he received favorable results. He found that direct gas injection eliminated the need for water injection to prevent pre-ignition and flashback, as well as reduced nitrous oxide (NO_x) emissions.

Furuhama [5,6,7,8] has accomplished the most successful research results using direct injection of Hydrogen, in both spark ignition and diesel engines. Furuhama succeeded in developing a complete supply system for Hydrogen fueled two stroke and four stroke engines. He

built a special pump, to bring the cold liquid Hydrogen to the required high operating pressure. He also used a hot surface igniter (glow plug), with a platinum wiring producing a catalytic effect to ensure fast Hydrogen ignition. Furuhama's success has been demonstrated by several "Musashi" vehicles which operated on Hydrogen fuel.

Martorano [9] adopted a two-stroke spark ignition engine for direct Hydrogen injection. With the aid of spark plugs, he received favorable results in power output which was much higher than that of the gasoline engine.

Ikegima et al [10] used indirect injection diesel engines for his experiments with Hydrogen because of their lower sensitivity to the "diesel knock". One engine had a swirl chamber while the other was equipped with a prechamber. By experiments, he found that the swirl chamber diesel engine did not run smoothly and misfired intermittently [10]. Even though ignition did occur, the ignition delay varied from cycle to cycle and sometimes produced the "diesel knock" phenomena. The outcome was similar with the prechamber diesel engine, in which explosions occurred in the prechamber and additionally severe explosions followed in the exhaust pipe due to the accumulated unburnt fuel. When normal ignition did occur by chance in the prechamber, the engine ran in a knock-free manner, probably due to hot residual gases in the

prechamber, but there was no ability to reproduce the results when the engine was stopped and restarted. Finally, the swirl chamber engine was chosen for further development, because it showed less undesirable phenomena as compared to the prechamber engine. Ikegima noted that minute gas leakage from the injector, between injections, allowed for a smooth combustion to take place in the swirl chamber engine, so consequently he tried with the pilot injection. He found that the earlier the pilot fuel jet was released, the smaller was the pilot fuel dose necessary to achieve a smooth engine operation over a certain speed range. However, at lower speed range, the pilot injection caused a pre-ignition and the engine was prone to rough operation. Thus, it was confirmed that the gas dose of pilot injection played an important role in the ignition of the main dose, similar to the amount of the residual gases remaining in the swirl chamber [ ] Overall, a conclusion was drawn that the swirl chamber diesel engine may successfully operate on Hydrogen if the correct pilot gas dose is introduced prior to the injection of the main dose.

Most of the direct injection systems for gaseous fuel in diesel engines being investigated presently by the researchers, have injectors which are actuated mechanically by rocker arms and camshafts, or hydraulically by modified in-line diesel engine pumps. However, the port injectors

used in spark ignition engines with gaseous fuel supply, are actuated electronically by means of a solenoid. Following this lead, MacCarley [11] developed a high speed electronically controlled injector for injection of Hydrogen in spark ignition engines. This injector operated at high frequency during short time periods for engine speeds of 4000 revolutions per minute (rpm) and it was capable of reaching maximum lift in 0.6 milliseconds. Presently available solenoid actuated injectors [12,13,14] for spark ignition engines, deliver quite similar results for opening time and injection duration as those developed by MacCarley. A new concept on fuel control systems for gas fueled diesel engines was suggested by Krepec et al. [15,16,17] which consists of a complete fuel supply system under microprocessor control. The fuel supply system contains a semi-cryogenic tank for gaseous fuels, a gas pressure regulating system, a preheating system using engine exhaust gases to increase the temperature and pressure of the fuel, a gas injection and metering system and an electronic control unit, with sensors and actuators.

Krepec et al's concept led Tebelis [18] to develop an electronically controlled gas injector for high speed diesel engines. This injector was a modified diesel injector which was actuated by a solenoid, whose power was supplied by a standard 12 Volt car battery. Tebelis'

injectors were able to operate with engine speeds exceeding 2000 revolutions per minute (rpm).

Giannacopoulos (nee Tebelis) [19,20] also proposed further development possibilities of more advanced electronically controlled Hydrogen gas injection systems in diesel engines, which will be discussed more specifically in the ensuing chapter. He investigated three different injection system configurations, which are: a) a simple common rail supplied solenoid operated injector, b) a metering valve and a solenoid actuated injector, and c) a control valve and a solenoid actuated injector in series [20]. He found the metering valve-injector configuration as the most promising. However, he developed a mathematical model for the simplest configuration only. This model did not account for the case of pressure waves and considered all the processes occurring instantaneously in the injection system. In the case of multi-point injection, the mathematical model for an injection system with a metering valve placed at some distance from the injector, would differ greatly from the aforementioned model and would include the pressure waves traversing between the injectors and the metering valve, and the volumetric changes in the injector's volume due to the movement of the needle.

3. PROPOSED MULTI-POINT DIRECT INJECTION SYSTEM FOR GASEOUS FUELS

As mentioned in the literature review, several researchers have used various types of injector opening mechanisms to inject Hydrogen Gas into the combustion chamber of an internal combustion engine, mainly spark ignition engines. The aim of this research is to investigate the feasibility of an electronically controlled multi-point direct injection system for gaseous fuels for application in the diesel engines.

This electronically controlled injection system offers several advantages over mechanically operated injectors. One of the major advantages is the high degree of flexibility which the electronic system offers in matching the engine's operational characteristics to the requirements of the vehicle.

The proposed multi-point injection system will be affected by the pressure waves in the injection system tubing, between the injectors and the metering valve. These pressure fluctuations can alter the injected fuel dose and the rate of injection of the proposed system, as compared to a single injector connected to a common rail gas supply system, as analyzed by Giannacopoulos [19,20].

3.1 BACKGROUND

Present conventional injection systems for liquid fuels are not suited to appropriately inject gaseous fuels such as Hydrogen and Natural Gas. Some sort of injection pump cannot be used and it is clear that an external force must participate in the lifting of the injector's needle together with the gaseous fuel supply pressure, or even without the assistance of the gas pressure.

The proposed multi-point gaseous injection system is a modified and extended version of the one developed by Giannacopoulos [20]. Some similarities are in the switching circuit, in the control circuit, and in the solenoid actuated injector, see Figures 3.1, 3.2 and 3.3; however, significant controlling parameters had to be altered so that the solenoid actuated injectors could achieve the required gas flow rates at much lower supply pressure of 100 bar only. The new gaseous injection system also differs by: a) the addition of a digitally actuated metering valve, b) the incorporation of the second injector, in order to obtain a multi-point injection system, and c) the location of the components, which are at some distance of each other and are connected by steel tubing.

In this chapter, the injector's adaptation to lower

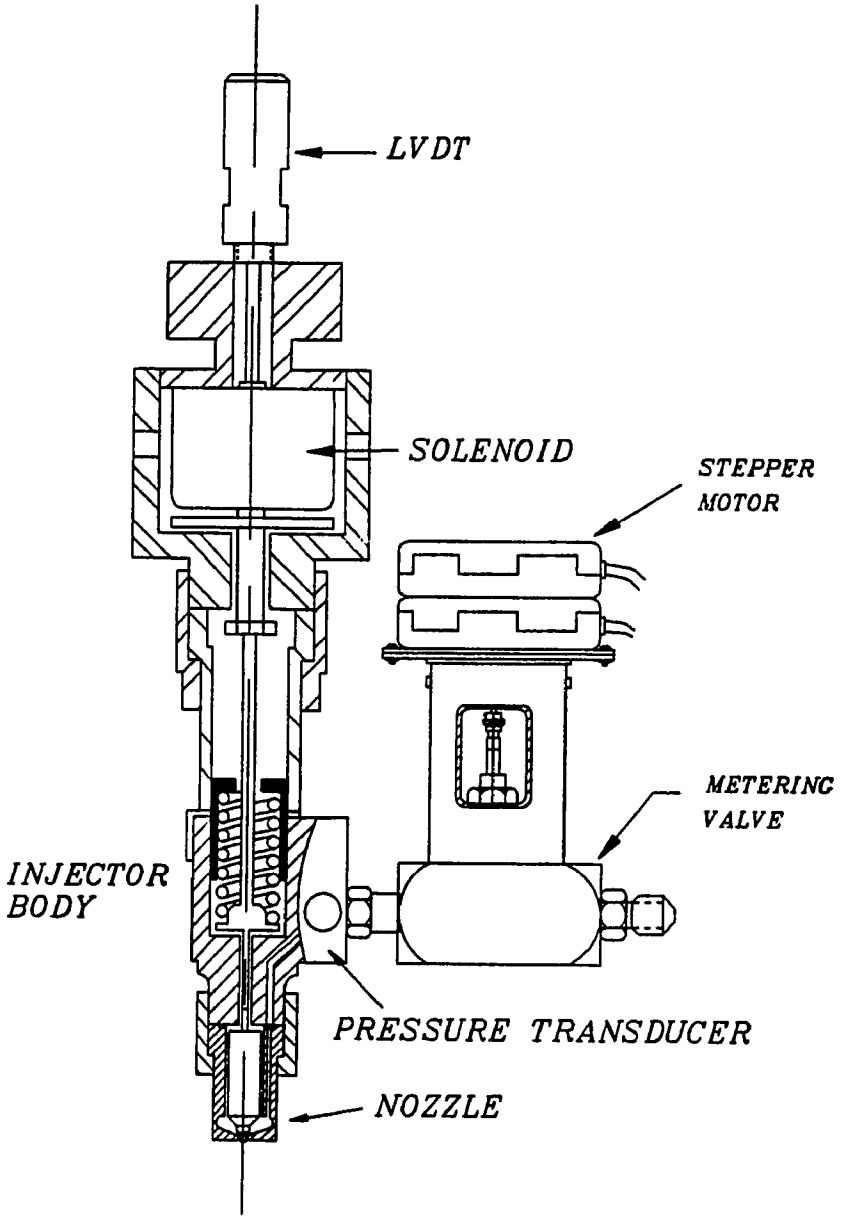

Figure 3.1 Solenoid Actuated Injector and Motorized Metering Valve.

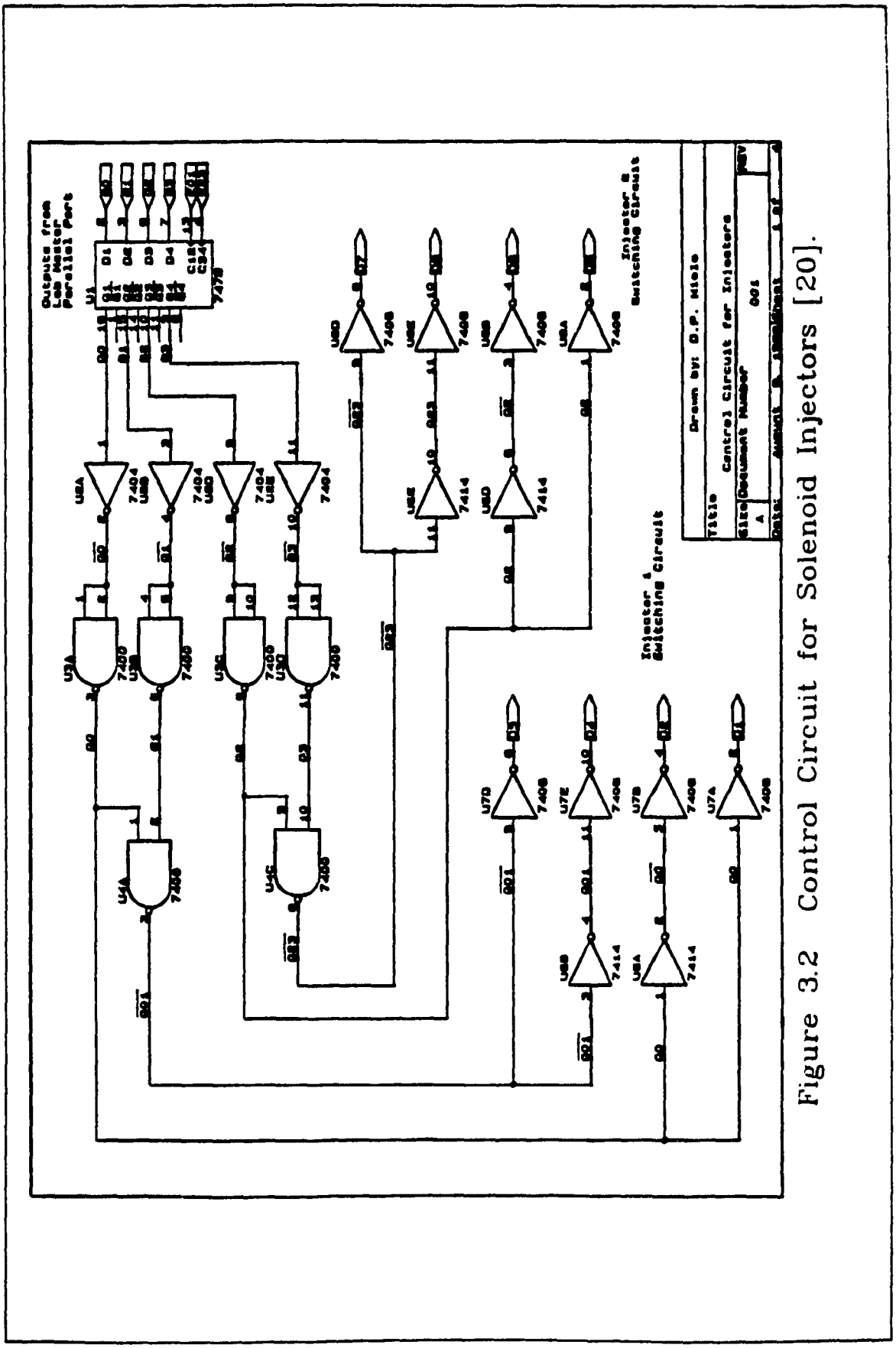

Figure 3.2 Control Circuit for Solenoid Injectors [20].

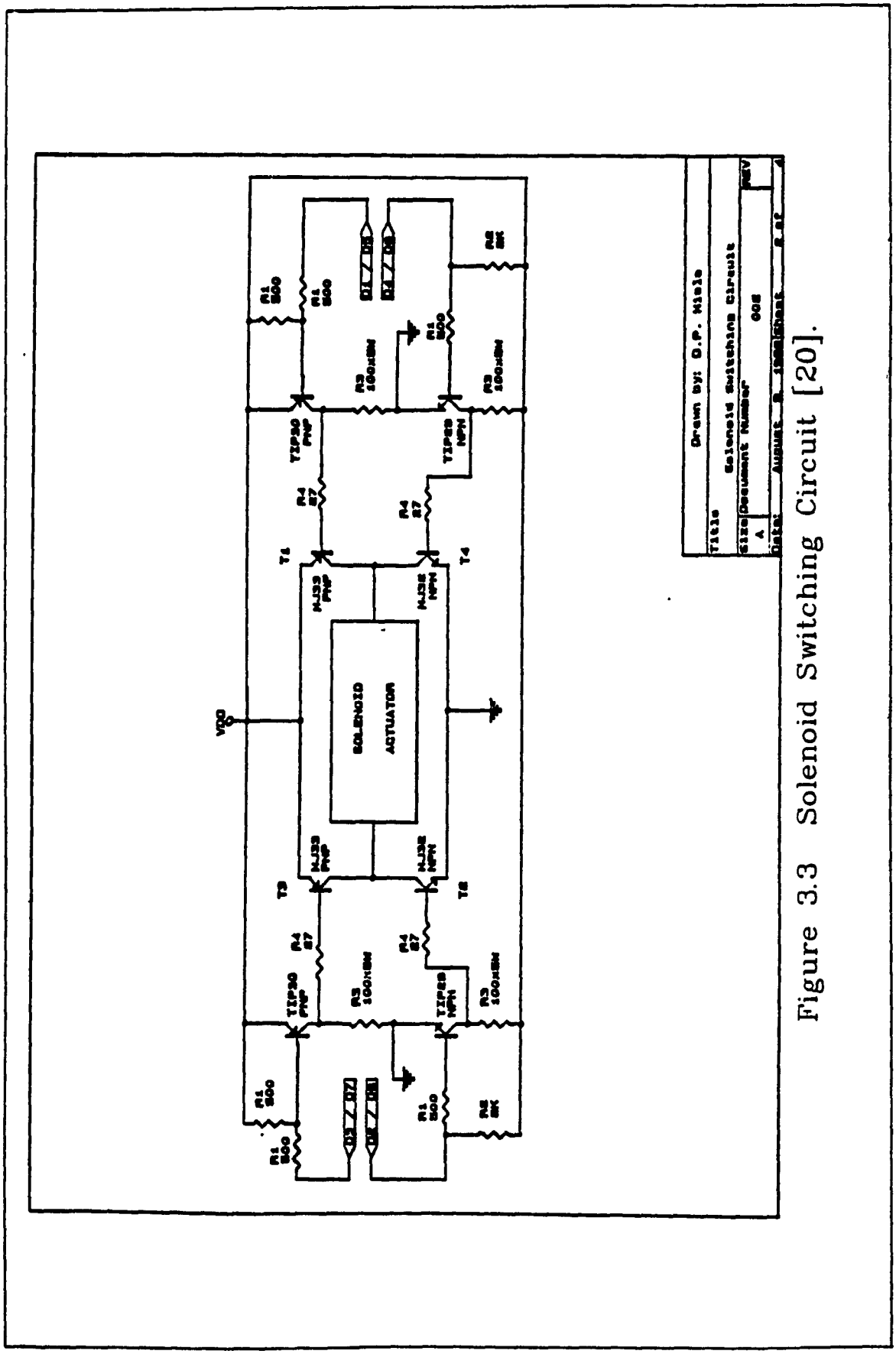

Figure 3.3 Solenoid Switching Circuit [20].

supply pressure will be discussed along with the metering valve and the electronic fuel control unit, being used to operate the solenoid actuated injectors and the digitally actuated metering valve. First, the concept of a multi-point gaseous fuel injection system will be reviewed.

3.2 PROPOSED GASEOUS INJECTION SYSTEM MODIFICATIONS

The proposed multi-point gaseous fuel injection system is a part of a concept for Gaseous Fuel Supply System [21], as seen in Figure 3.4. It consists of the following major components: a semi-cryogenic storage tank, a pressure regulator, a gas conditioner, a digitally actuated metering valve, the solenoid actuated injectors, different sensors and a central processing unit. The electronic control unit's function is to acquire the input signals regarding the fuel supply parameters and the engine demand to compute and to command the injection of the required fuel dose for maximum engine performance. The use of an electronic control allows for greater flexibility in engine operation due to its ability to adequately adapt to the constantly changing engine parameters.

This system differs significantly from previous proposals made by Furuhama [5,6,7] and Krepec [15,17] for a Hydrogen fuel supply system. High pressure pump for liquid Hydrogen is no longer required as well as the cryogenic tank operating at liquid Hydrogen temperatures. The semi-cryogenic tank concept allows the storage of gaseous fuels at much higher temperature than in the cryogenic tank; however, at higher energy density than in standard cylinders for compressed gas. The concept can be explained

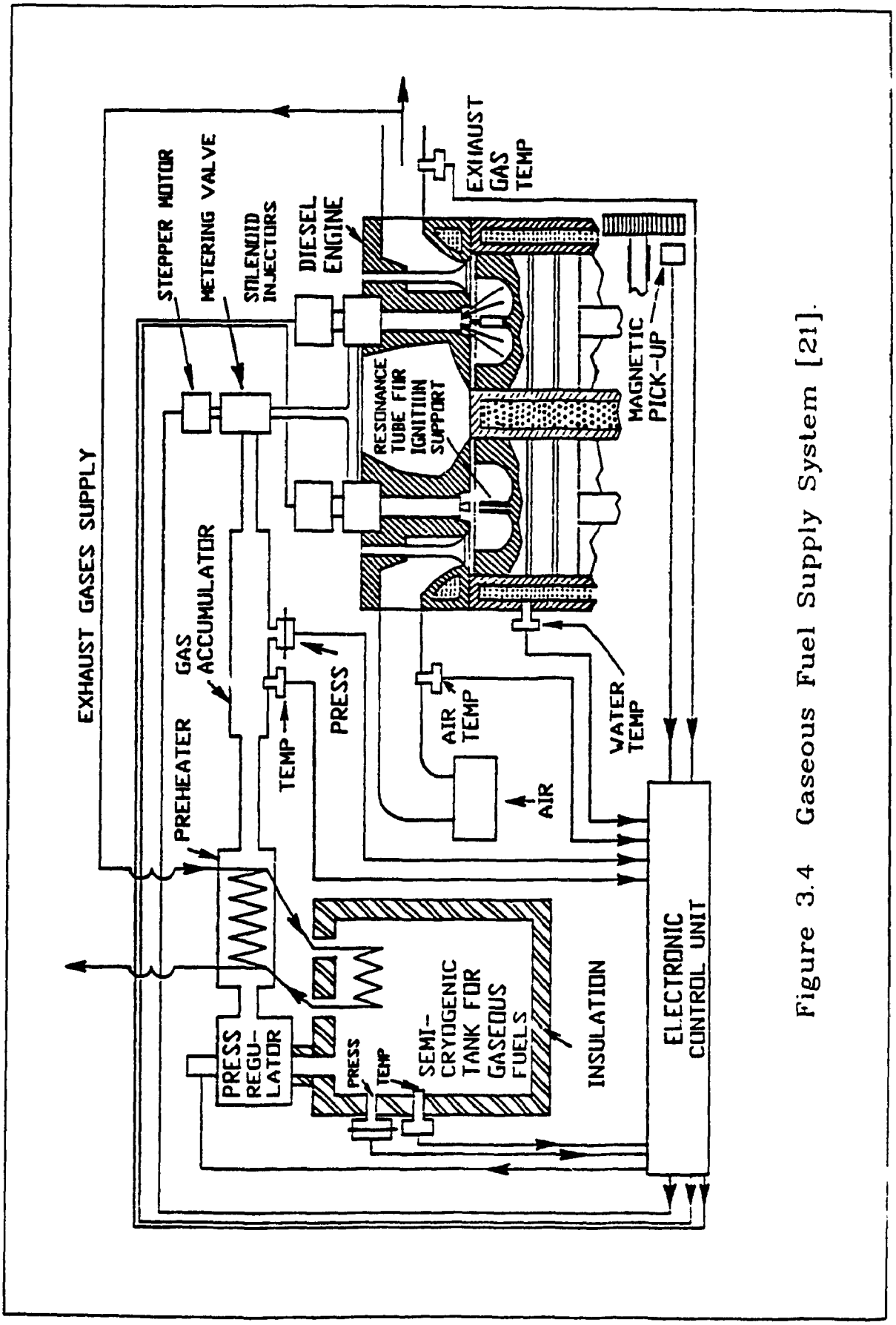

Figure 3.4 Gaseous Fuel Supply System [21].

by viewing the T-ν diagrams for Natural Gas and Hydrogen presented in Figures 3.5 (a) and (b) respectively.

Point 1 on the diagram for Natural Gas, based on Methane Gas tables [22], is at atmospheric pressure and at the temperature of 110 K; it corresponds to the cryogenic tank storage point. Point 2 corresponds to the storage of compressed Methane Gas in standardized cylinders at 200 bar pressure and atmospheric temperature. It can be seen that three times more Methane can be stored in a cryogenic tank than in a standard cylinder of equal volume [13]. Point 3 is the proposed storage point for Methane in a semi-cryogenic tank at a pressure of 200 bars and at a temperature of 200 K. The amount of Methane stored in the semi-cryogenic tank is approximately twice higher than that in the present standardized cylinders for compressed Natural Gas (CNG); however, it is one and a half times lower than in a cryogenic tank of equal volume. The most important issue is that the gas is already under high pressure and does not require to be pumped to the required injection pressure level; it rather has to be regulated down to the injection pressure of 100 bar.

When the pressure in the semi-cryogenic tank drops to the 100 bar level, due to the gaseous fuel consumption, an exhaust gas preheating system would be used to increase the temperature of the gas in the tank as required, up to 400 K

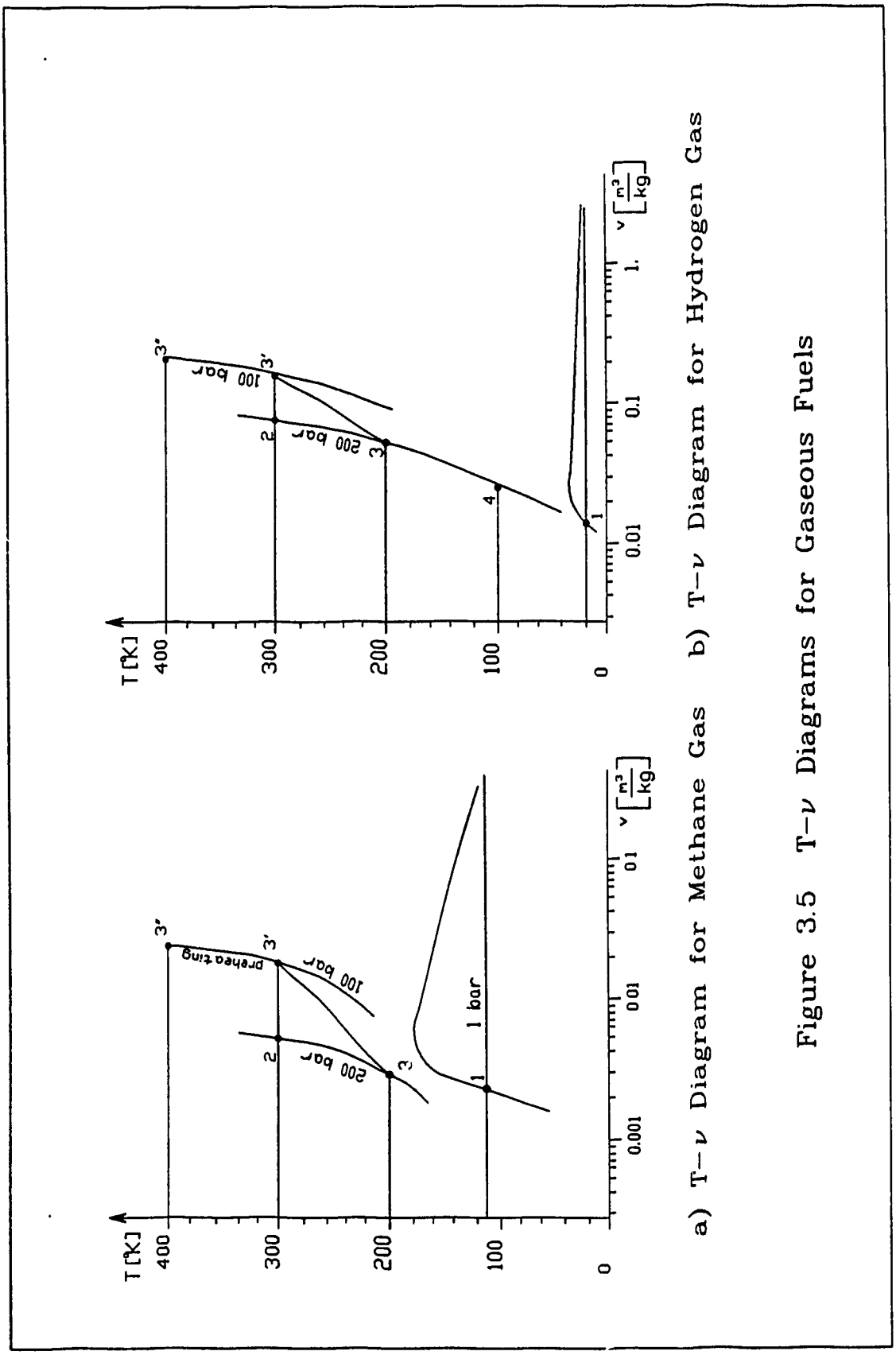

a) T–ν Diagram for Methane Gas b) T–ν Diagram for Hydrogen Gas

Figure 3.5 T–ν Diagrams for Gaseous Fuels

approximately. This system allows the user to extract more fuel from the tank (approximately three times more) [17] than in present CNG cylinders for the 200 to 100 bar pressure drop.

Storage for other gaseous fuels, such as Hydrogen, can also be explained in a similar way based on Figure 3.5 (b). Point 1 on the diagram for Hydrogen is at atmospheric pressure and at a temperature of 20 K; it corresponds to the cryogenic storage point. Point 2 shows the storage capabilities in present standardized cylinders, at a pressure of 200 bars and at atmospheric temperature. The graph indicates that there is five times more Hydrogen stored at point 1 than at point 2 [21]. Point 3 shows the proposed storage point at 200 bar pressure and at a temperature of 200 K. At this point, the amount of Hydrogen stored is approximately 1.5 times greater than in the standardized cylinders and about 3.5 times lower than in a cryogenic tank. Point 4 shows a more effective possible storage point for Hydrogen at 100 K. The respective storage values at this point are approximately three times higher and two times lower as compared to the standard pressurized cylinders and to cryogenic tank respectively.

In the case of Hydrogen stored at 200 bar pressure and 100 K temperature, the pressure must be regulated down to

100 bar. As the pressure in the tank drops due to fuel consumption, the temperature of the Hydrogen Gas in the tank can be raised, first to ambient temperature and then up to 400 K. This would be accomplished by controlling the amount of exhaust gases passing through the heat exchanger in the semi-cryogenic tank. This gas preheating system allows the user to extract almost five times more fuel for the 200 to 100 bar pressure drop, as compared to the amount provided by the standard pressurized cylinders [21].

The metering valve - injector system for gaseous fuels was first proposed by Krepec et al [15]. It relies on the use of a metering valve to throttle the gas mass flow rate to the injector during the injection process. The newly proposed multi-point injection system, in this research, for gaseous fuels, has one metering valve interfacing several injectors. However, it will be affected by the pressure waves which are present in the fuel supply line between the injectors and the metering valve during the injection period and the refilling period as well. Thus, the metering valve must be strategically located in order to produce the required discharge characteristics of the gas injection system. The effect of the gas throttling in the metering valve is a definite decrease of pressure in the injector during the injection period and a slow rise in pressure during the refilling period. The benefits from

such a pressure pattern are the shortening of the injector closing time due to the decrease in pressure under the injector needle, and the drop in fuel leakage from the injector due to the lower initial gas pressure and to the slower rise in pressure during the refilling period. This pressure pattern can be significantly changed by the presence of pressure waves. The difference, regarding the new system, lays also in the fact that two or more injectors are interfaced to one digitally controlled metering valve, as shown in Figure 3.6.

Thus, the main objective of this research will focus on the ability of the solenoid operated injectors and on the digitally controlled metering valve to deliver the appropriate fuel dose to the engine.

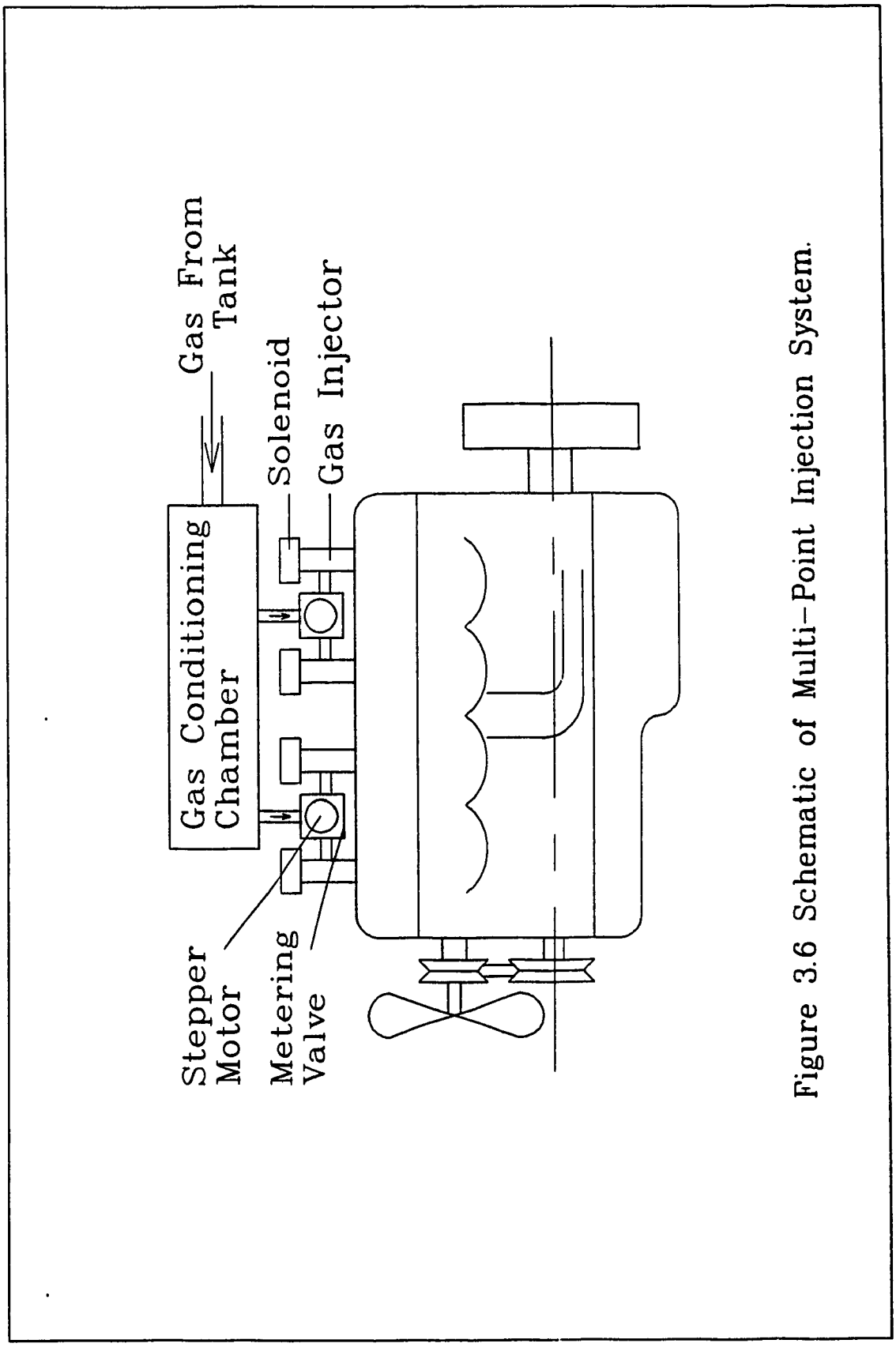

Figure 3.6 Schematic of Multi-Point Injection System.

3.3 GASEOUS FUEL INJECTION SYSTEM DESIGN

In the design of the gaseous fuel system there are two components which must meet certain specifications and these components are: the solenoid actuated injector and the metering valve.

3.3.1 Injector Design

The solenoid actuated injectors which are used in this research have been originally developed by Giannacopoulos [19,20] and have undergone some modifications for lower supply pressure. The design of such an injector relies on several engine parameters and fuel supply requirements, as well as on the ambient conditions. Engine parameters on which the design is dependent are: engine size, engine speed, and engine power, which depict the required fuel mass dose and the mass flow rate. The fuel parameters are: the supply pressure and temperature, which alter the properties of the gaseous fuel.

The engine for which the injectors were designed is a Peugeot Idenor high speed diesel engine for a passenger vehicle. It is a two litre, four cylinder, four stroke water cooled engine with a compression ratio of 22:1 and

with a Ricardo Comet Mark V swirl type combustion chamber, see Appendix A.

Some basic calculations for Hydrogen Gas dose and average discharge rate have been performed by Giannacopoulos [20]; thus, to complete the subject, the calculations for Natural Gas (Methane) will be performed in this investigation. The stoichiometric equation for the complete combustion of Methane Gas with Oxygen [23] is the following, as shown in equation (3.1).

$$CH_4 + 2O_2 \longrightarrow CO_2 + 2H_2O \qquad (3.1)$$

Since air is used as the oxidizer and consists of 79 percent Nitrogen and 21 percent Oxygen by volume [23] the chemical equation for air is the following:

$$O_2 + 3.762\ N_2 \longrightarrow 4.762\ Air \qquad (3.2)$$

and thus, the stoichiometric equation becomes the following:

$$CH_4 + 2(O_2 + 3.762N_2) \longrightarrow CO_2 + 2H_2O + 7.524N_2 \qquad (3.3)$$

The stoichiometric fuel/air ratio is calculated from the aforementioned reaction and is presented below for

Methane Gas.

$$FA_{stoich} = 0.05824 \frac{kg\ CH_4}{kg\ air}$$

Note that for a significant reduction of pollutants such as hydrocarbons (HC) and NO_x, it is necessary to use an equivalence ratio, ϕ, of less than 0.8, i.e. excess air. Thus, the actual FA ratio is written below.

$$FA_{actual} = 0.04659 \frac{kg\ CH_4}{kg\ air}$$

Assuming that the air pressure is 1 bar , the temperature is 295 K, and knowing that the volume per cylinder of the engine is 0.5 litres, the fuel dose can be calculated by using the equation of state and the above mentioned fuel/air ratio, as follows,

$$m_f = m_{air}\ FA_{actual} = \frac{P\ V}{R\ T}\ FA_{actual}$$

$$= \frac{1\ (10^5) * 0.5\ (10^{-3})}{287 * 295} * (0.04659)$$

$$m_f = 27.52\ mg\ CH_4$$

Maximum fuel mass flow through the injector occurs at maximum power at which the speed of the engine is assumed to be 2000 rpm. Assuming that the injection duration is to

last 30 degrees of the crank angle, the duration can be calculated in terms of time, by equation (3.4).

$$t = \frac{\psi}{6N} \qquad (3.4)$$

where ψ is the crank angle and N is engine speed in rpm. Substituting the previously mentioned values in equation (3.4), time t is found to be,

$$t = \frac{30}{6 * 2000} = 2.5\ (10^{-3})\ \text{sec.}$$

In order to calculate the required mean gas mass flow rate through the injector, the mass dose is divided by the time of injection duration calculated previously and the following average mass flow rate is obtained.

$$\dot{m}_{f_{av}} = \frac{27.52\ \text{mg}\ CH_4}{2.5\ \text{ms}} = 1.1008(10^{-2})\ \frac{\text{kg}}{\text{s}}$$

This mass flow rate will determine the injector nozzle orifice flow area in order to achieve the required power of a diesel engine operating on methane gas. The remaining fuel doses are summarized in Table 3.1 for Methane Gas as

well as for Hydrogen Gas. This is calculated by using the same scheme as mentioned above, and knowing the required doses as mentioned in Appendix A.

Table 3.1 Fuel Dose vs Engine Speed

Engine Speed (rpm)	Methane Gas dose (mg)	Hydrogen Gas dose (mg)
starting / 600	44.03	22.18
idle / 600	5.50	2.77
max. torque / 1600	35.78	18.02
max. power / 2000	27.52	13.86
max. idle / 2300	5.50	2.77

3.3.1.1 Nozzle Area

The fuel injector must be capable of discharging the fuel mass dose in the time required and at the gas supply pressure indicated. This states that the injector must have an orifice with the flow area sufficient to allow for the aforementioned flow rate at the given gas supply pressure. Assuming isentropic flow through the injector nozzle orifice and the fact that Methane Gas behaves as a perfect gas at the given conditions, the required discharge area can be calculated. Figure 3.7 demonstrates the original pintle and the modified injector needles and

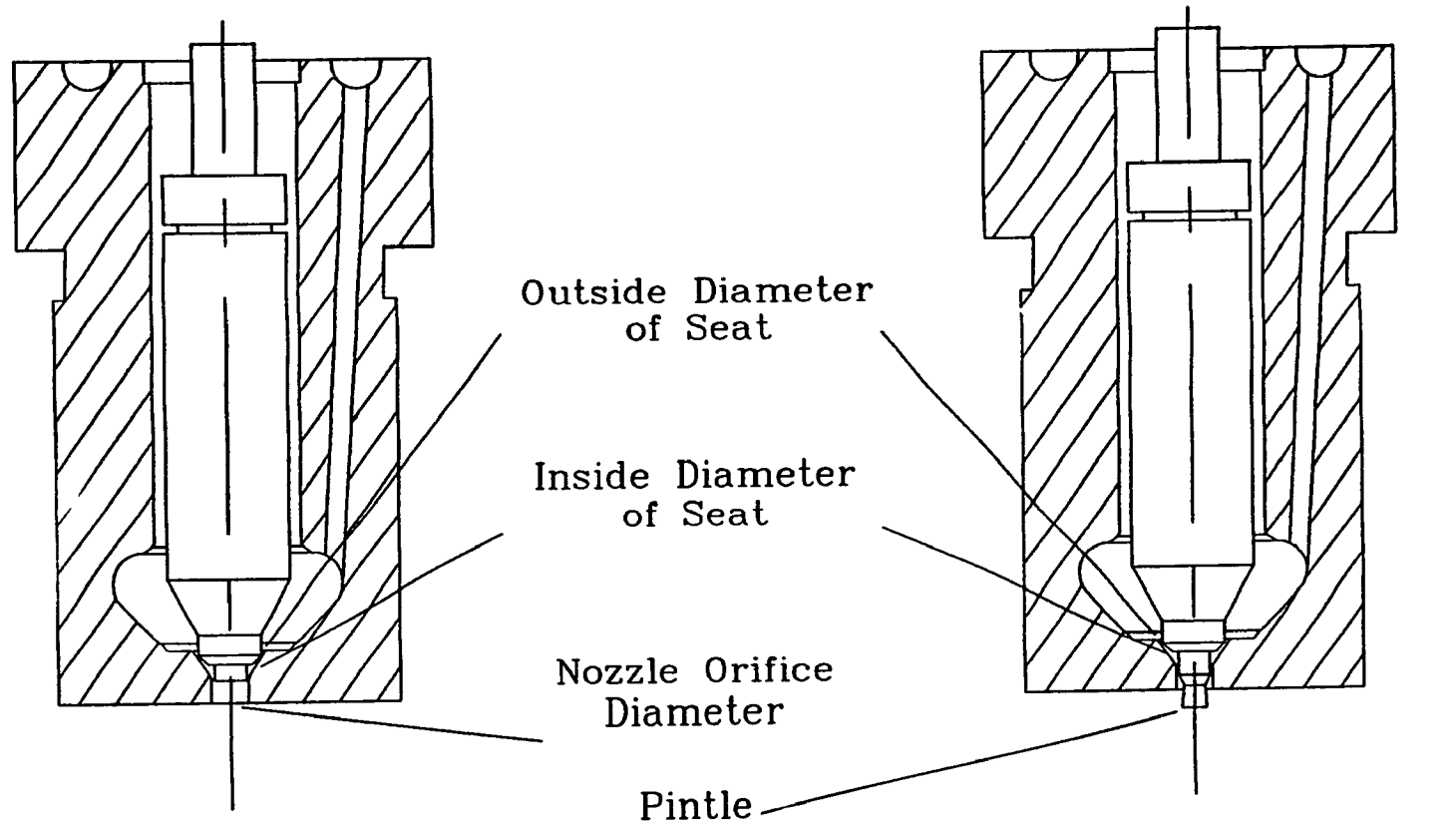

Figure 3.7. Diesel Engine Pintle Nozzles

nozzles.

Before finding the required discharge area it is vital to understand how the critical flow areas are formed in the pintle nozzle injector. In Figure 3.7 (b), the situation is first discussed for the original pintle nozzle. As the injector needle is lifted off its seat, the critical or minimum flow area is first formed in the seat at the outer diameter. As the needle continues to rise, the critical flow area shifts its location, to the inner diameter of the seat. Finally, as the injector's needle continues to rise to the maximum lift, the critical flow area shifts again and is formed by an annulus, at the pintle's circumference. In the next modified version of the needle, shown in Figure 3.7 (a), where the pintle has been partially removed, the last maximum critical flow area is formed at the nozzle orifice diameter, and has a greater flow area than in the original pintle nozzle. The equations describing the flow area characteristics are shown in Appendix B. Figure 3.8 b) shows a graph of the flow area versus needle lift of the modified pintle injector nozzle, while a) shows the flow area versus needle lift of the original injector nozzle.

The mass flow rate through a nozzle can be calculated by using the equation of continuity which can be expressed differently for compressible gases under isentropic conditions in equation (3.5) [24]. The following equations

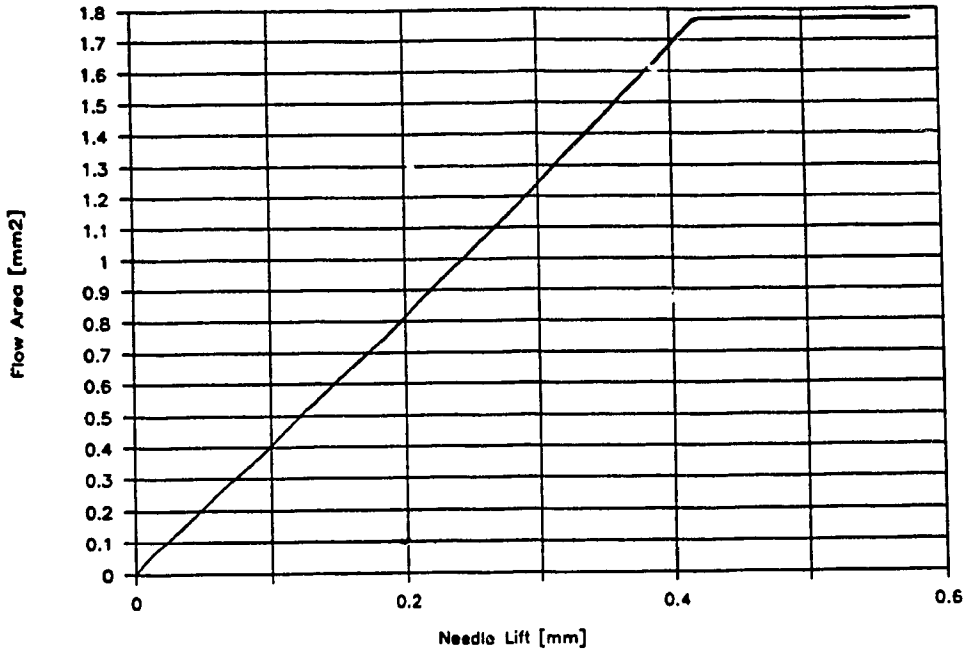

Figure 3.8 a) Modified Pintle Nozzle Flow Area versus Needle Lift.

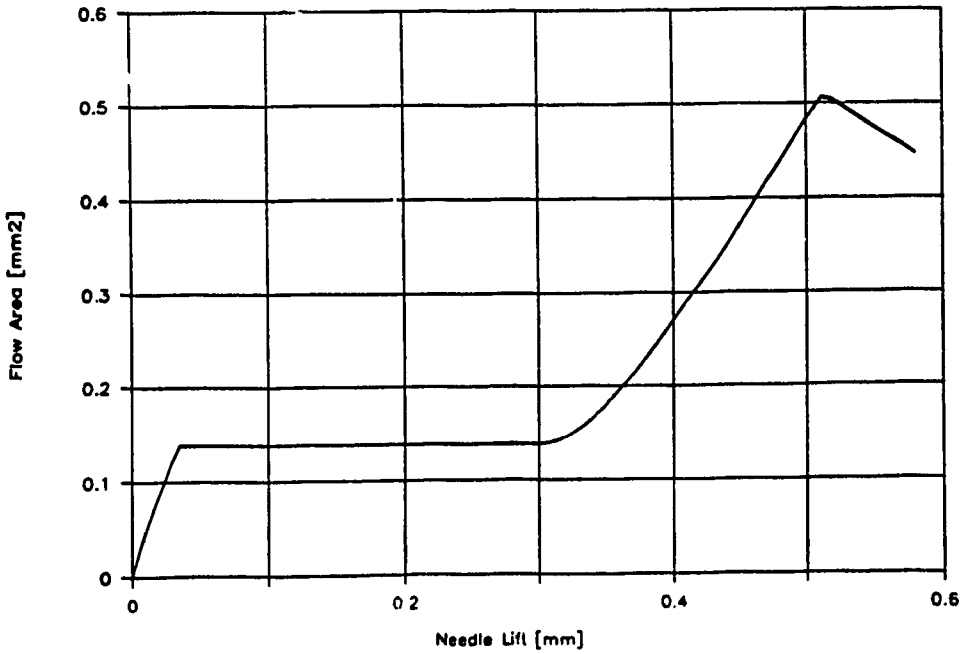

Figure 3.8 b) Pintle Nozzle Flow Area versus Needle Lift.

will be used to calculate the required nozzle flow area for the Natural Gas dose at maximum power.

$$\dot{m}_f = \frac{C_d \, C_m \, A_o \, P_i}{\sqrt{T}} \tag{3.5}$$

The discharge coefficient, C_d, depends on the shape of the nozzle orifice surface. Based on literature review, the coefficient lies between 0.60 and 0.80 [25]. Since the injector flow rate is considered turbulent and unsteady, a value of 0.65 will be used.

The mass flow coefficient, C_m, depends on the mass flow rate, through the injector orifice area, which can be choked or unchoked. The coefficient is dependent on the ratio of the downstream pressure to the upstream pressure. The following equation can be used to determine if the choked mass flow condition is reached [26],

$$\frac{P_3}{P_2} = \left(\frac{2}{\gamma + 1} \right)^{\frac{\gamma}{\gamma - 1}} \tag{3.6}$$

where P_3 is the downstream pressure, in this case combustion chamber pressure, and P_2 is the upstream pressure and γ is the isentropic constant for Methane Gas. Thus, if the pressure ratio is greater than 0.5457, then the flow is not choked and C_m can be calculated using

equation (3.7) [24].

$$C_m = \sqrt{\frac{2\gamma}{R(\gamma - 1)} \left[\left(\frac{P_3}{P_2} \right)^{\frac{2}{\gamma}} - \left(\frac{P_3}{P_2} \right)^{\frac{\gamma + 1}{\gamma}} \right]} \qquad (3.7)$$

If pressure ratio is less than 0.5457, then the mass flow is choked and C_m is calculated from equation (3.8) [24].

$$C_m = \sqrt{\frac{2\gamma}{R(\gamma + 1)} \left(\frac{2}{\gamma + 1} \right)^{\frac{2}{\gamma - 1}}} \qquad (3.8)$$

The engine cylinder maximum pressure at the end of the compression stroke is approximately 40 bars and the maximum injector pressure is 100 bar. Thus, the flow can alternate from choked flow to unchoked flow during the injection period. Values for C_m are shown below for both types of flow.

$$C_m \text{ unchoked} = 0.0260 \frac{s\sqrt{K}}{m}$$

$$C_m \text{ choked} = 0.0293 \frac{s\sqrt{K}}{m}$$

Thus, an average value for C_m will be used to calculate the average orifice area required for the mentioned mass flow

rate.

By rearranging equation (3.5) to solve for the required orifice area A_o and substituting the values for pressure, temperature, C_d, C_m, and the required mass flow rate, calculated before, the following answer for the required flow area is obtained:

$$A_o = 1.1397\ (10^{-6})\ m^2 = 1.1397\ mm^2$$

and in terms of nozzle orifice diameter d_o,

$$d_o = 1.205\ mm$$

This is the required nozzle diameter in order to achieve the mentioned flow rate and gas dose; however, with the conventional pintle nozzle injector needle it would be impossible to achieve the required area. By modifying the pintle, as shown in the Figures 3.7 and 3.8, the required flow area can be achieved with the available nozzle orifice diameter of 1.5 mm. After having cut the pintle from the needle of the present injector nozzle, the orifice diameter of 1.5 mm becomes the last critical flow area. With parallel calculations for Hydrogen Gas, the required nozzle orifice diameter is 1.418 mm; thus, for Hydrogen Gas the same modified nozzle can be used to satisfy the engine

requirements as with Methane Gas. Knowing that the most severe case has been dealt with, all other conditions of the engine's operational characteristic can be satisfied.

3.3.2 Metering Valve Design

The metering valve is an essential component of the gaseous fuel supply system which throttles the gas flow to reduce the pressure in the fuel injectors and; thus, shapes the gas discharge characteristic. Its distance from the injector has an impact on the gas discharge rate due to the change in volume and to the generation of pressure waves in the fuel line between the injectors and the metering valve. In order to throttle the gas flow, the metering valve must have a much smaller minimum flow area than the fuel supply line.

The metering valve flow area characteristics are given by the manufacturer in Appendix D. In Figure 3.9, shown are the graphs of C_v versus the number of revolutions and number of revolutions versus the metering valve flow area. The reasons for using the flow coefficient C_v for calculating the flow area, is due to that the producer is giving the flow area of the metering valve which has been obtained experimentally; to calculate it via theoretical

equations, as given in Appendix D, requires the knowledge of the datum position of the valve which is not given.

Knowing the flow of water across the metering valve and the pressure drop, the flow coefficient of the valve can be calculated via equation (3.9), from the manufacturer's data.

$$C_v = \frac{Q}{\sqrt{dP}} \tag{3.9}$$

where,

Cv = flow coefficient
dP = pressure drop across valve in psi
Q = water flow in Gallons per minute (GPM)

The full equation for water flow across a valve is given by equation (3.10) [26].

$$Q = C_d\, A \sqrt{\frac{2g\ dP}{\rho}}\ cf * 12\ \frac{in}{ft} \tag{3.10}$$

where cf is the conversion factor for changing GPM into ft^3/s, 448.93 GPM-s/ft^3. Equations (3.9) and (3.10) can be combined to solve for the flow area A, as shown in equation (3.11).

$$A = \frac{C_v}{C_d} \sqrt{\frac{\rho}{2g}}\ \frac{1}{cf}\ \frac{1}{12} \tag{3.11}$$

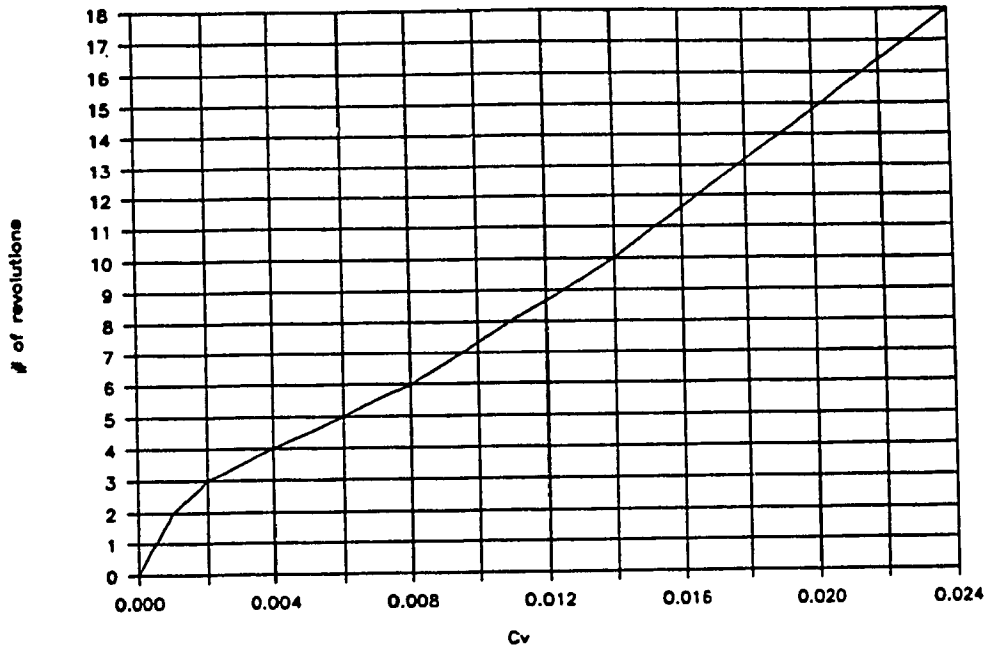

Figure 3.9 a) Metering Valve Thimble Revolutions versus C_v.

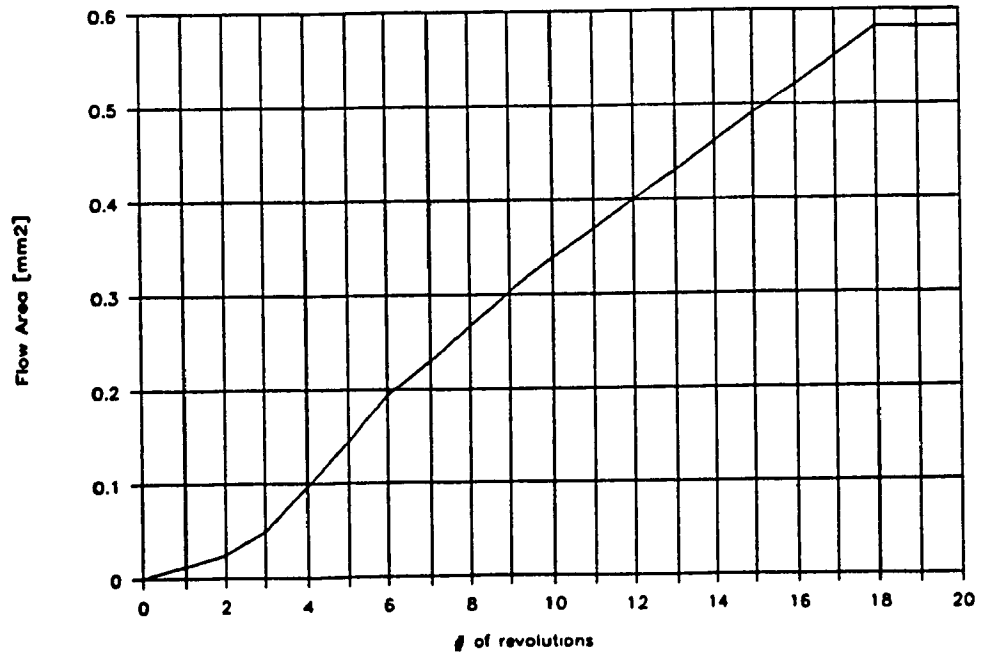

Figure 3.9 b) Metering Valve Flow Area versus Metering Valve Thimble Revolutions.

Assuming that the discharge coefficient , C_d, for the open valve is 0.70 and that the flow coefficient, C_v for 18 revolutions of the metering valve handle, is 0.024 and knowing that the density of water is 62.4 lb/ft^3, the flow area for the fully open metering valve is found to be 6.2647 (10^{-6}) ft^2 or 0.58201 mm^2. Figure 3.10 shows the direction of flow in the metering valve which is opposite to the injector nozzle. It is a poppet type valve, whose C_d can be approximated to 0.85 [25], i.e considerably higher than for the injector nozzle, since there are no sharp edges.

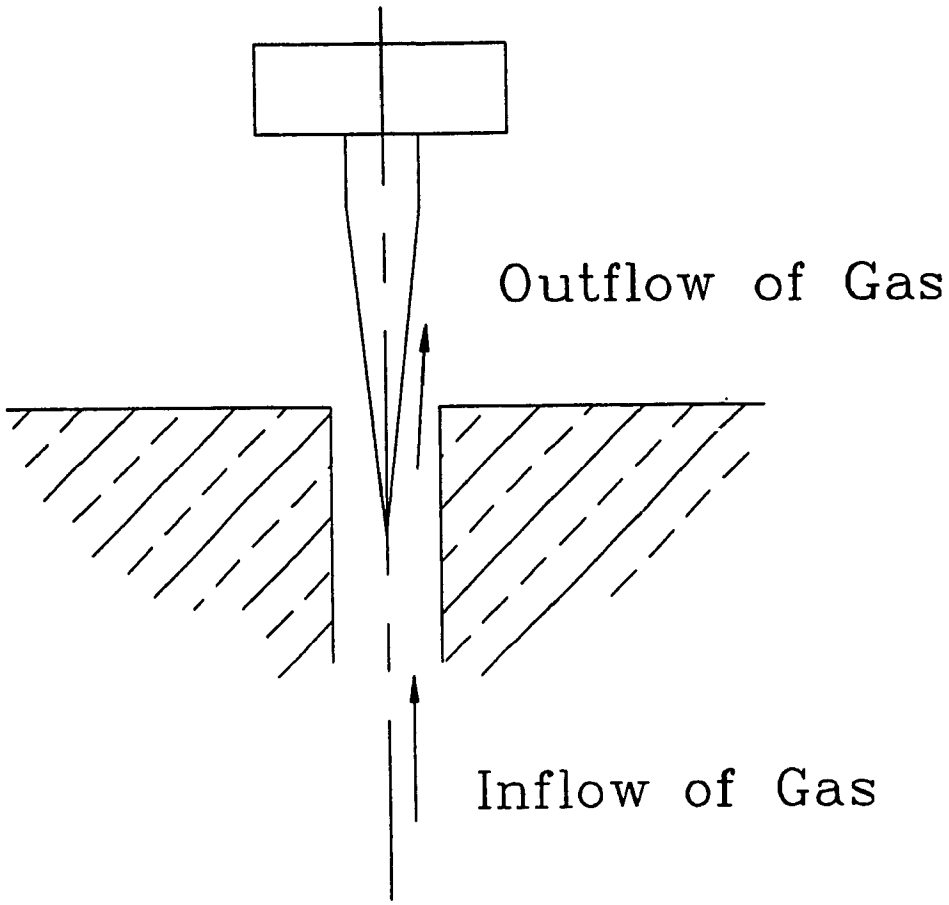

Figure 3.10. Direction of Flow in Metering Valve

3.4 ELECTRONIC INJECTION SYSTEM

3.4.1 Electronic Controller

The electronic controller developed for the gaseous multi-point direct injection system, as it has been used for the fuel system investigation, is shown schematically in Figure 3.11. The system configuration consists of an IBM microcomputer, a Lab Master data acquisition and control system, and in house built circuits: a control circuit, two switching circuits for the solenoid operated injectors, an actuating circuit for the stepper motor, amplifiers, and finally, the converters for the analog sensors.

The computer is interfaced with the electronic circuits via the data acquisition and control card, which is located inside the computer on the 62 pin IBM PC bus. The acquisition and control system has input/output (I/O) ports which are connected to the electronic circuits. The computer executes the control program and accesses the I/O ports of the acquisition and control system to read or write bytes in order to acquire information about events external to the program, or to perform some action required by the control program.

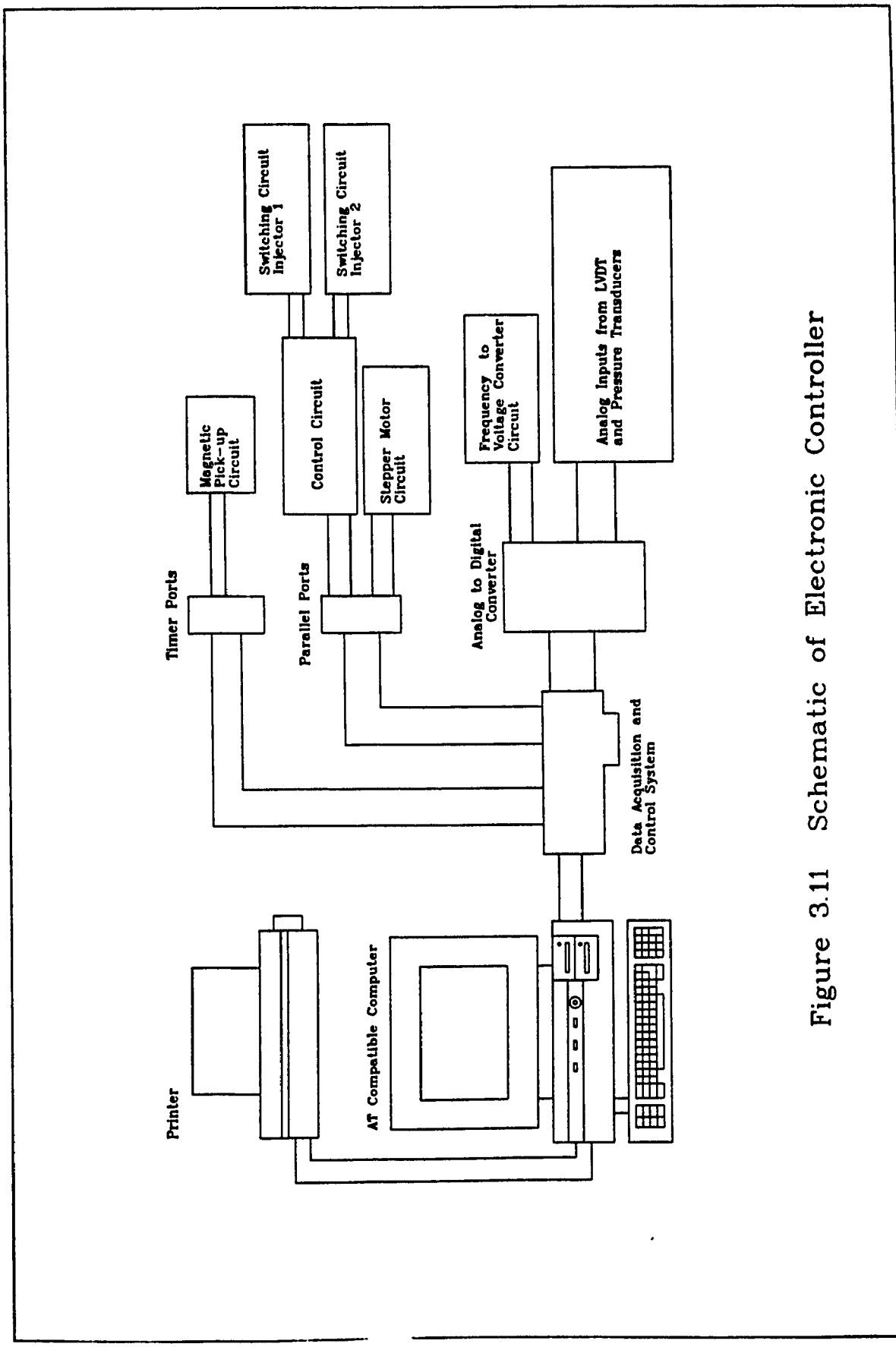

Figure 3.11 Schematic of Electronic Controller

The computer's main functions in the controller are to synchronize the injectors opening with the engine cycles, to calculate the required fuel dose; thus, timing and duration of injection, to adjust the metering valve flow area due to the engine speed changes and to energize and de-energize the solenoid injectors.

The data acquisition and control system used is the Lab Master made by Scientific Solutions Incorporated. The system consists of a motherboard, installed on the 62 pin bus inside the computer, and a daughterboard, external to the computer; the two boards are connected by a 50 pin cable. The system contains four basic I/O ports: the parallel ports, the timer ports, and the analog to digital (A/D) and digital to analog (D/A) ports. The parallel ports are originating from the Intel 8255 chip on the Lab Master motherboard in the computer. This chip has three 8 bit parallel ports, which can also be divided into two twelve bit ports, and can be used for bidirectional data transmission. The timer ports are located on the motherboard and the chip is AMD's 9513 Timer chip. The main features of this chip is that it contains five 16 bit independently programmed timers which can be cascaded to form two 32 bit counters and one 16 bit counter. The counts can be hexadecimal or binary coded decimal (BCD). The counters can count forwards or backwards. The counting

source is either an external signal or an internal signal, with an integrated frequency divider. Also, the chip can output a terminal count when the count is over, which is ideal for interrupts. The A/D module is mounted in the daughterboard and has 12 bit resolution with a conversion rate of 30 KHz. The A/D module is equipped to handle 16 single-ended or 8 true differential analog inputs and can be multiplexed to handle 256 single-ended and 128 true differential inputs. The D/A also has 12 bit resolution with a 5 microsecond settling time. There are two independent D/A chips, of type ADDAC80, with jumper selectable output ranges.

The controller uses a total of 5 analog input ports, 2 digital output ports and one timer input port. The entire controller circuitry is shown in Figures 3.12 and 3.13, as well as in Figures 3.2 and 3.3.

3.4.2 Control Circuits

The control circuit for the solenoid injectors is shown in Figure 3.3. The main purpose of this circuit is to latch the data which were sent out by the computer, through the parallel port of the Lab Master, to energize or de-energize the selected solenoid injector. The circuit

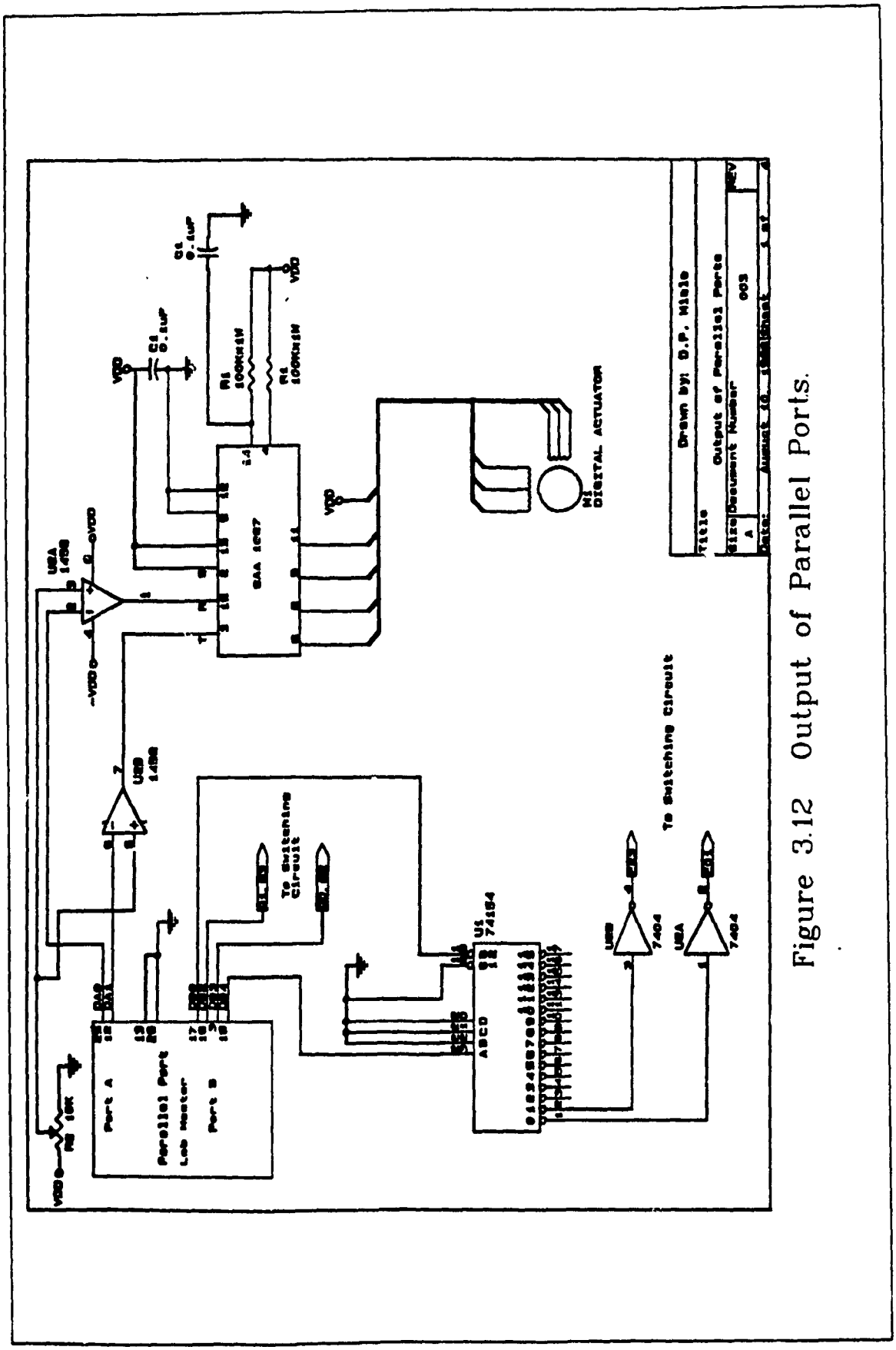

Figure 3.12 Output of Parallel Ports.

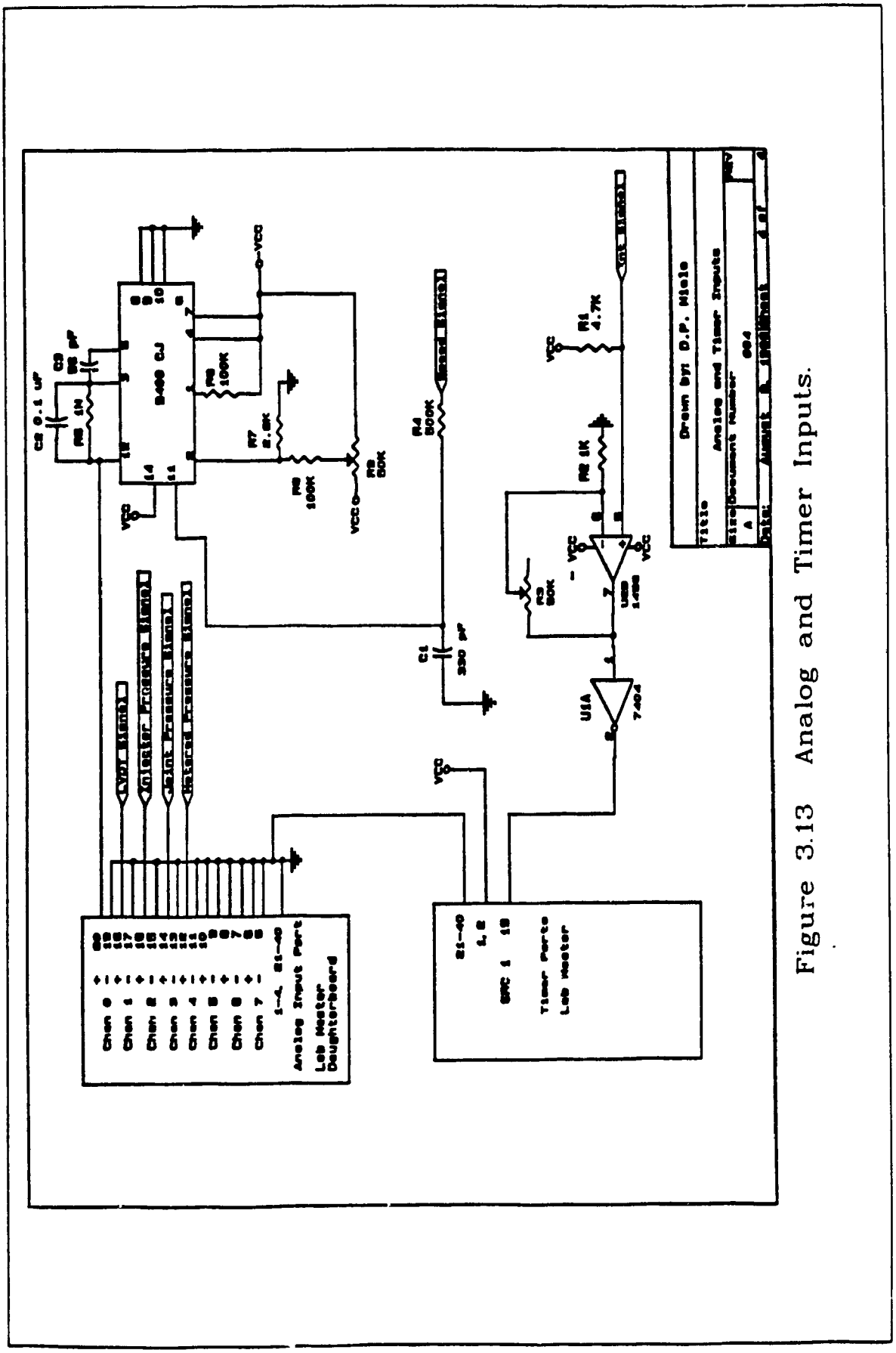

Figure 3.13 Analog and Timer Inputs.

consists of TTL (transistor-transistor-logic) chips for the latching and buffering of inputs. This circuit is similar to the one used by Giannacopoulos [19,20] in his experiments; however, he used a less powerful, Z-80 based, MicroProfessor Controller which limited his data acquisition potential.

There are 6 inputs to the control circuit and they come from the parallel port of the Lab Master, shown in Figure 3.12. The inputs Q0 and Q2 to the control circuit have the value of bit 3 of the control word, while inputs Q1 and Q3 have the value of bit 2. Bits 0 and 4 select which injector, E01 or E23, will be chosen to latch the output data of bits 2 and 3 . The inputs Q0, Q1, Q2, and Q3 represent whether the injector selected is energizing, de-energizing or off, while inputs E01 and E23 select which injector is in operation. When E01 is high and E23 is low (because of bit 4), injector 1 is in operation and when E01 and E23 are high, injector 2 is in operation. The TTL 74154, 4 to 16 demultiplexer, is used to determine which injector is to be selected with the changes in bits 0 and 4 of the parallel port. No injector is selected when bit 0 is high. But when bit 0 is low, bit 4 determines which injector is selected, i.e. injector 1 when low; thus, E01 high, and injector 2 when high; thus, E23 high.

When an injector is selected, Q0 and Q1 are latched by

the 7475, a bistable latch, when E01 is high, assuming injector 1 is selected. Q0 and Q1 are then processed through a logic circuit and 4 outputs, D1, D2, D3, and D4, are obtained. These 4 outputs are then sent to the solenoid switching circuit, Figure 3.2, where, in turn, they activate and de-activate the solenoid actuator. As mentioned previously, Q0 and Q1 are determined by the value of bits 3 and 2 respectively and, in turn, determine the state of the injector solenoid actuator. Table 3.2 summarizes the 8 bit control words in hex format, the bit values of bits 4, 3, 2, and 0, injector selection, and the state of the selected solenoid actuated injector.

Table 3.2 Summary of Control Words for Solenoid Injectors

Control Word	Bit Status 4	3	2	0	Injector States Injectors 1 & 2
0CH	0	1	1	0	Injector 1 De-energize
1CH	1	1	1	0	Injector 2 De-energize
08H	0	1	0	0	Injector 1 Close
18H	1	1	0	0	Injector 2 Close
04H	0	0	1	0	Injector 1 Energize
14H	1	0	1	0	Injector 2 Energize
09H	0	1	0	1	Both Injectors Disabled

3.4.3 Solenoid Switching Circuit

The solenoid switching circuit is used to energize and de-energize the injector solenoid; thus, the circuit affects the performance of the solenoid actuators. In this investigation, the switching circuit was duplicated twice to operate the multi-point injection system, see Figure 3.2 for the schematic of the switching circuit. It was also adapted for operation with the Lab Master data acquisition board.

The inputs to the switching circuit actuate the high power transistors to release the high current required by the solenoid. The switching circuit functions as follows: when the control word to open injector 1 is transmitted by the computer through the Lab Master parallel port and the control circuit, transistors T1 and T2 are actuated and current, from a 12 Volt battery, is applied across the solenoid actuator circuit which is then energized. When the injection period is terminated, the control word to turn "off" transistors T1 and T2 is sent. In order to de-energize the solenoid and to decrease the closing time of the injector, a control word to open transistors T3 and T4 is transmitted and the current flow is reversed through the magnetic core of the solenoid. This action decreases the residual current and allows for a faster closing of the

injector. The transistors T3 and T4 are "on" for a very short period of time, i.e. << 0.5 millisecond, and then turned "off" so that one injection could be completed.

The solenoids used in the fuel injectors are quite powerful and require a high amount of current to develop the magnetic flux required to move the solenoid armature and overcome the spring preload force. In order to generate the necessary current, Giannacopoulos [19,20] used a 12 Volt battery and high power transistors. These transistors required some time in order to saturate and to switch the current to the solenoid. The switching circuit was also found successful in the present investigations. The solenoid also requires some time to generate the magnetic flux to move the armature; the proof of this was found when the control program requested a 6 millisecond solenoid energizing period and only a 2.5 millisecond injection period was recorded on the oscilloscope, without achieving full needle lift. When longer injection periods were requested, an inherent 3.5 to 4 millisecond time delay was encountered, as can be seen from Figure 3.14, which confirms the delay from the initial current rise to the initial needle lift.

Faster and more powerful solenoids seem becoming readily available as new concepts in solenoid design are emerging [20]. These new concepts can be seen in the

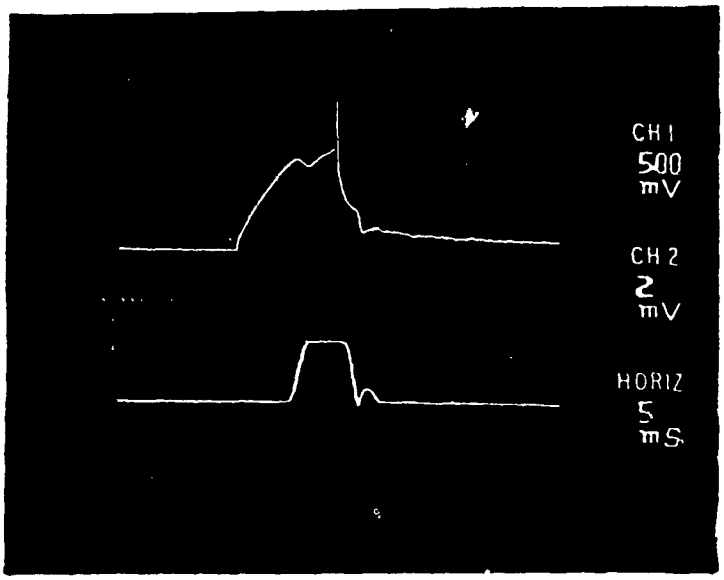

a) 6 ms injection

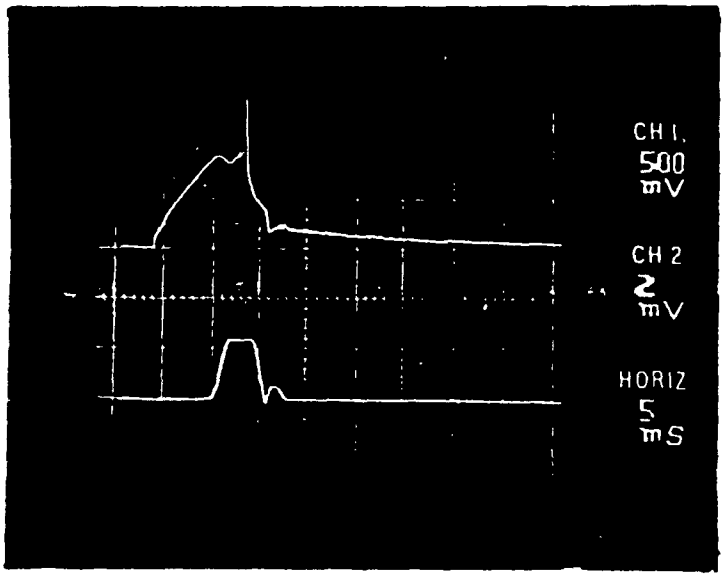

b) 5 ms injection

Figure 3.14 Needle Lift and Solenoid Current Demand.

design of the HELENOID and COLENOID type solenoids, as described by Seilly [27,28]. Similar solenoids have been used in diesel engine injectors for liquid fuels and for electronically controlled spill valves in diesel engines [29,30,31,32]. They have proven themselves in terms of speed and force, and should be scrutinized for future applications in electronically controlled gaseous fuel injectors.

3.4.4 Input and Digital Actuator Circuits

The inputs to the controller and the digital actuator circuits are shown in Figures 3.12 and 3.13. There are 6 input signals in all: a speed signal, an interrupt signal, a needle lift signal from an LVDT, and three pressure signals from strategically located pressure transducers, required for testing. All signals are in the form of analog voltage, except for the interrupt signal, which has been digitized. The analog signals are fed to the analog input ports on the Lab Master daughterboard. The digital actuator circuit is a single chip circuit with two outputs from the Lab Master parallel port which are being used to control the actions of the actuator.

The speed signal is actually a sine wave generated

from a magnetic pick-up and a multi-toothed gear located on the engine crankshaft. This signal is first filtered and is then fed to a frequency to voltage converter chip, Teledyne 9400CJ. The input frequency is converted to an analog voltage and this output voltage is input to the analog port of the data acquisition system. The operating range of this circuit is between 500 and 3500 rpm (see Appendix C for the calibration curve) with an output voltage between 0 and 4.14 volts. This analog input is converted to a digital value by the A/D converter and the control program converts this digital value into engine speed in rpm. This speed value is used to determine injection timing and duration, as well as metering valve opening.

The interrupt signal is generated from a single tooth rotating against a magnetic pick-up on the engine crankshaft. This signal is filtered and amplified to generate a square wave and is then inverted, by a TTL 7404 chip, in order to resemble a clock pulse. This pulse is fed into a ti ort of the Lab Master. Since the engine operates on a stroke cycle, an injection occurs in the first cylinder o every second revolution. Thus, after the second pulse to the timer, the timer reaches a terminal count and generates an interrupt on line IRQ3 of the computer, interrupt number 3. This interrupt is

acknowledged by the computer and an interrupt routine is executed. The interrupt routine recalls the injection timing and injection period and the time difference between the closing of injector 1 and the opening of injector 2 and then waits for the correct moment to open injector 1. When the correct moment has arrived, injector 1 is opened for a certain period of time and is then closed; at this point the computer counts down the time to open the second injector. Once the second injection is finished, the interrupt routine outputs a signal to the interrupt controller to signify that the interrupt has been serviced and the control program is executed from the line where it was interrupted.

The signals from the lift transducer and the pressure transducer are converted to digital signals and recorded into a file which is to be compared later with simulated data.

The digital actuating circuit's purpose is to drive the actuator so that the metering valve flow area can be varied according to the changes in engine speed and torque requirements. The circuit consists of several resistors and capacitors, as well as a SAA 1027 driver chip and a K82954-M1 Airpax stepper motor. The stepper motor is capable of attaining 48 steps per revolution, 7.5 degrees per step, at a maximum speed of 125 Hz. Two signals are

required to operate the stepper motor, a trigger signal and a rotation signal. Both signals are the outputs of the Lab Master parallel port. Both signals are amplified to give a high of 12 volts, while retaining a low of 0 volts, or ground. The amplification is necessary due to the operating voltage of the stepper motor driver chip.

The trigger signal is basically a group of square wave pulses, with a high of 5 volts and a low of 0 volts. The number of pulses represents the number of steps to be executed by the stepper motor.

The rotation signal is either a high signal, which causes the stepper motor to rotate in the clockwise direction, or a low signal, to rotate in the counterclockwise direction.

4. COMPUTER SIMULATION OF THE ELECTRONICALLY CONTROLLED GASEOUS FUEL INJECTION SYSTEM MODEL

The objective of this chapter is to develop a mathematical model for the gaseous injection system and simulate its behavior on a computer to verify the experimental data. The need for such a mathematical model is to reduce the number of experiments required to investigate all the engine operating characteristics, so that only some essential points will be verified experimentally.

The mathematical model of the gaseous fuel injection system allows for the following: a) computer aided design (CAD) of the injection system, b) optimization of the present design and of newer and more efficient designs, as well as c) reduction of the costs of running many experiments for each design alteration.

No such mathematical model has been found, in the literature, to be developed for a multi-point gaseous fuel injection system consisting of multiple injectors, a single metering valve, and a fuel pipeline between the mentioned components. However, many mathematical models have been developed for liquid injection systems and some consideration has been given to the methods already used in order to develop the mathematical model for the gaseous injection system.

In this chapter, the main objectives and assumptions pertaining to the mathematical model will be presented. Then, the transient flow equations will be described, as well as the steady state equations and the method of solution to these equations. Then, the boundary conditions in the gaseous injection system will be discussed, as well as the development of the method of solution to a particular boundary condition, i.e to the gaseous fuel injector. Finally, the total system model will be reviewed and a computer simulation will be performed. But first, some background literature review on previous mathematical models developed for liquid and gaseous fuel injection systems will be presented.

4.1 OVERVIEW OF MATHEMATICAL MODELS OF LIQUID AND GASEOUS FUEL INJECTION SYSTEMS

Mathematical modeling is vital for the optimization of any type of system which can be improved. Many researchers have successfully modeled liquid fuel injection systems for diesel engines, but not many researchers have modeled or attempted to model a gaseous fuel injection system. As mentioned in the literature review, most researchers were using direct fuel injection of Hydrogen Gas, and this direct injection was achieved through modified in-line diesel fuel pumps or by rocker arm and cam actuated injectors. Only Giannacopoulos [19,20] developed a simple mathematical model for a gaseous fuel injection system, consisting of a single solenoid actuated injector, without the interfacing metering valve.

Wylie et al [33,34,35] developed a mathematical model for an entire diesel fuel injection system. The model takes into account wave propagation in the fuel pipeline and the friction in the system. The model was simulated on a computer, by solving the equations via the method of characteristics in the pipeline and a modified predictor-corrector method for the boundary conditions, i.e. for fuel injectors and delivery valves. The mathematical model was successfully validated through the experimental results of the actual fuel injection system.

Scullen and Hames [36] developed a mathematical model for the GM Unit Injector, and they too were able to validate their model by the experimental results. However, to solve for the system equations, a fourth-order Runge Kutta procedure was used with no error checking. Goyal [37] also developed a mathematical model similar to Wylie et al [33,34,35], but he simplified the simulation by using a modular approach. The modular approach divided the fuel injection system into several subsystem models, and in turn each model was turned into a subroutine. The subroutines were then linked together to simulate the entire model. Goyal also used a fourth-order Runge Kutta method to obtain a solution for his mathematical model. Smith and Spinweber [38] developed a mathematical model for an electronic fuel injector for spark ignition engines. In this model, even the solenoid properties were physically simulated. The model successfully retraced the experimental data. Marcic and Kovacic [39] developed a similar model as Wylie et al [33,34,35]; however, with less simplifications. The transient conditions were solved by the method of characteristics in the fuel pipeline and a fourth-order Runge Kutta procedure was used for the boundary conditions, i.e. fuel injectors and delivery valves.

The mathematical model developed by Giannacopoulos [20] for a single gaseous fuel injector is very simple;

however the model was validated with the data obtained experimentally. The method of solution that he used was a fifth and sixth-order Runge Kutta subroutine, that was obtained from the International Mathematical and Statistical Library (IMSL). This is the only available model for a gaseous fuel injector simulation. The model to be developed in this investigation will consist of multiple injectors, a metering valve and the fuel pipeline connecting these two components.

4.2 MATHEMATICAL MODEL FOR THE MULTI-POINT GASEOUS FUEL INJECTION SYSTEM

As mentioned in the previous section, mathematical modeling is the key factor to the optimization of any system. The model of the injection system will be divided into three sections. The first section includes the unsteady flow equations in the fuel pipeline, which describe the pressure wave propagation. The second section consists of the boundary conditions to the transient flow equations. The third section will discuss the entire mathematical model of the gaseous fuel injection system. But first, the objectives and assumptions of the mathematical model will be discussed.

4.2.1 Objectives and Assumptions

The objectives of formulating the mathematical model for the gas injection system, is to obtain a reasonable computer generated simulation of the actual injection process and needle valve motion, which will be used to optimize the gaseous injection system.

The governing equations of the gas injection system consist of the equation of continuity and the equation of motion. However, before proceeding with the actual

modeling of the gaseous injection system, it is necessary to make several assumptions in order to simplify the mathematical model to a certain extent. The assumptions are as follows:

1) The gaseous fuel behaves as a perfect gas.
2) The mass flow within the pipeline is isothermal.
3) The mass flow through the orifices is isentropic.
4) The pressure underneath the needle valve has uniform distribution.
5) One-dimensional flow equations will be used.

These assumptions will be used throughout the entire modeling procedure.

4.2.2 Transient Flow Equations

The transient flow equations are actually the equation of continuity and the momentum equation in the fuel pipeline between the metering valve and the injectors. Recall that isothermal conditions exist in the pipeline. Thus, the equation of state for the gaseous fuel [40] is as follows,

$$P = \rho RT \tag{4.1}$$

and the speed of sound in the gaseous fuel is expressed below in equation (4.2) [40].

$$a = \sqrt{\frac{P_1}{\rho}} = \sqrt{\gamma RT} \qquad (4.2)$$

These two equations are to be taken into account for the next two subsections.

4.2.2.1 Equation of Continuity

The equation of continuity states that the rate of change of mass in a control volume must be equal to the rate of mass that crosses the control surface. Knowing that the control surface is the pipeline cross sectional area and that the control volume is the cross sectional area times the length dx, as seen in Figure 4.1, the equation of continuity can be written as follows:

$$\frac{\partial(\rho\ A\ u)}{\partial x}\ dx = -\frac{\partial}{\partial t}(\rho\ A\ dx) \qquad (4.3)$$

Knowing the equation of continuity in its simplest form which is the following, $\mathring{m} = \rho AU$, and recalling equation (4.2), equation (4.3) can be rearranged to obtain the following:

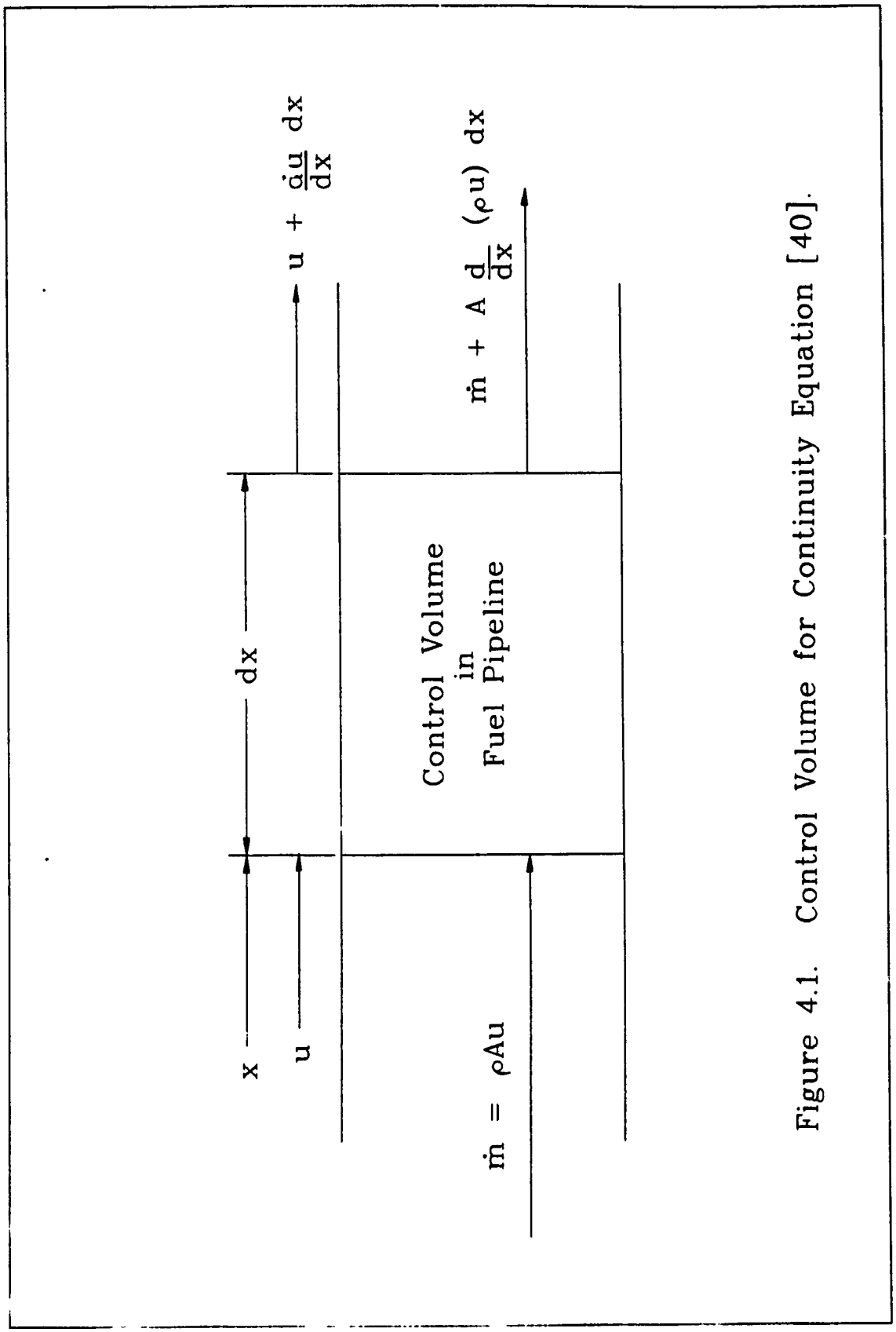

Figure 4.1. Control Volume for Continuity Equation [40].

$$\frac{A}{a^2}\frac{\partial P}{\partial t} + \frac{\partial \dot{m}}{\partial x} = 0 \qquad (4.4)$$

This equation is the continuity equation for unsteady flow in the pipeline.

4.2.2.2 Momentum Equation

The momentum equation for a given length of pipe, from Figure 4.2, is the following:

$$PA - A\left(P + \frac{\partial P}{\partial x}\,dx\right) = \frac{\partial}{\partial t}\,(\rho A dx\ u) + \tau_o \pi D_p dx + \int_{cs} \rho u^2 dA \qquad (4.5)$$

The last term on the right hand side is the momentum of the gas entering and exiting the control volume via the control surface, and since the flow area is constant the term can be neglected.

From Wylie [40], the shear stress, τ_o, can be expressed in terms of the Darcy-Weisbach equation as,

$$\tau_o = \frac{\rho\ f\ u^2}{8} = \frac{\rho f\ \dot{m}^2\ a^4}{8P^2 A^2_{pipe}} \qquad (4.6)$$

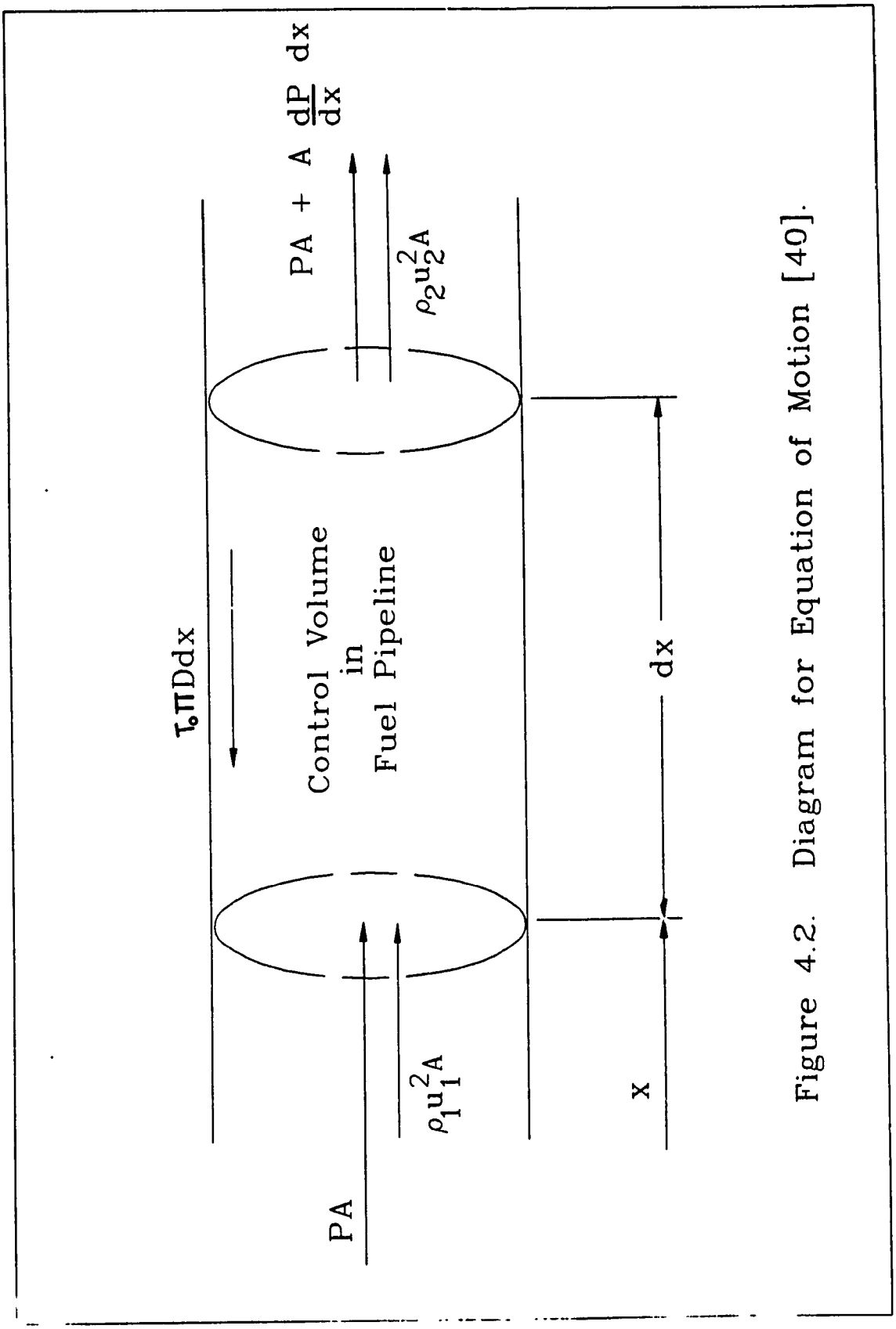

Figure 4.2. Diagram for Equation of Motion [40].

By recalling equation (4.2) and substituting τ_o, equation (4.5) is transformed into the following:

$$A\frac{\partial P}{\partial x} + \frac{\partial \dot{m}}{\partial t} + \frac{f\dot{m}^2a^2}{2PAD} = 0 \qquad (4.7)$$

Equation (4.7) is the momentum equation for the gaseous fuel in the pipeline between the injectors and the metering valve.

4.2.2.3 Method of Solution

The method of solution to be used in the case of the transient flow equations is the method of characteristics. By recalling equations (4.4) and (4.7), and combining and rearranging the two equations and letting λ be an unknown multiplier, the following equation is obtained.

$$\lambda\left(\frac{\partial P}{\partial t} + \frac{1}{\lambda}\frac{\partial P}{\partial x}\right) + \left(\lambda a^2\frac{\partial \dot{m}}{\partial x} + \frac{\partial \dot{m}}{\partial t}\right) + \frac{f\dot{m}^2a^2}{2PA^2D} = 0 \qquad (4.8)$$

Knowing that the first term is the total derivative for the pressure with respect to time and that the second term is the total derivative for mass flow with respect to

time, λ can be solved for. The two equations for the total derivatives are shown below as:

$$\frac{DP}{Dt} = \frac{\partial P}{\partial t} + \frac{\partial P}{\partial x}\frac{dx}{dt} \tag{4.9}$$

$$\frac{D\mathring{M}}{Dt} = \frac{\partial \mathring{M}}{\partial t} + \frac{\partial \mathring{M}}{\partial x}\frac{dx}{dt} \tag{4.10}$$

Thus, in equation (4.9), $1/\lambda$ is equal to the value of dx/dt, and in equation (4.10), λa^2 equals the value of dx/dt. In summary, dx/dt is equal to two results which must be equal.

$$\frac{dx}{dt} = \frac{1}{\lambda} = \lambda a^2 \tag{4.11}$$

By solving for λ, it is found through equation (4.11) that λ equals $\mp 1/a^2$ and thus, dx/dt equals $\mp$ a. Recalling equation (4.8) and by substituting λ and the total derivatives, the following two sets of equations are obtained:

$$\frac{1}{a}\frac{dP}{dt} + \frac{1}{A}\frac{d\mathring{m}}{dt} + \frac{f\,\mathring{m}^2\,a^2}{2\,PA^2\,D} = 0 \tag{4.12}$$

when dx/dt = + a, and,

$$-\frac{1}{a}\frac{dP}{dt} + \frac{1}{A}\frac{d\mathring{m}}{dt} + \frac{f\,\mathring{m}^2\,a^2}{2\,PA^2\,D} = 0 \tag{4.13}$$

when dx/dt = - a.

Equation (4.12) is the characteristic equation for the gas propagating in the positive direction , from high pressure to low pressure,and equation (4.13) is the characteristic equation for the gas propagating in the negative direction, from low pressure to high pressure. Figure 4.3 shows the method of specified time intervals and how the wave propagation corresponds to the aforementioned equations and the ensuing equations below. The positive waves are denoted by C+ and the negative waves are denoted by C-.

The following equations are obtained by rearranging equation (4.12) in finite difference form and by multiplying through with dx = a dt, and then integrating from point x to point z, along the C+ characteristic. Similarly for equation (4.13) along the C- characteristic.

C+

$$P_z = P_x - \frac{a}{A}(\mathring{m}_z - \mathring{m}_x) - \frac{fa^2\Delta x\,(\mathring{m}_z + \mathring{m}_x)}{(P_z + P_x)\,4DA^2}|\mathring{m}_z+\mathring{m}_x| \qquad (4.14)$$

C-

$$P_z = P_y + \frac{a}{A}(\mathring{m}_z - \mathring{m}_y) - \frac{fa^2\Delta x\,(\mathring{m}_z + \mathring{m}_y)}{(P_z + P_y)\,4DA^2}|\mathring{m}_z+\mathring{m}_y| \qquad (4.15)$$

These equations are the solution to the transient flow equations, and since steady state flow is a special case of

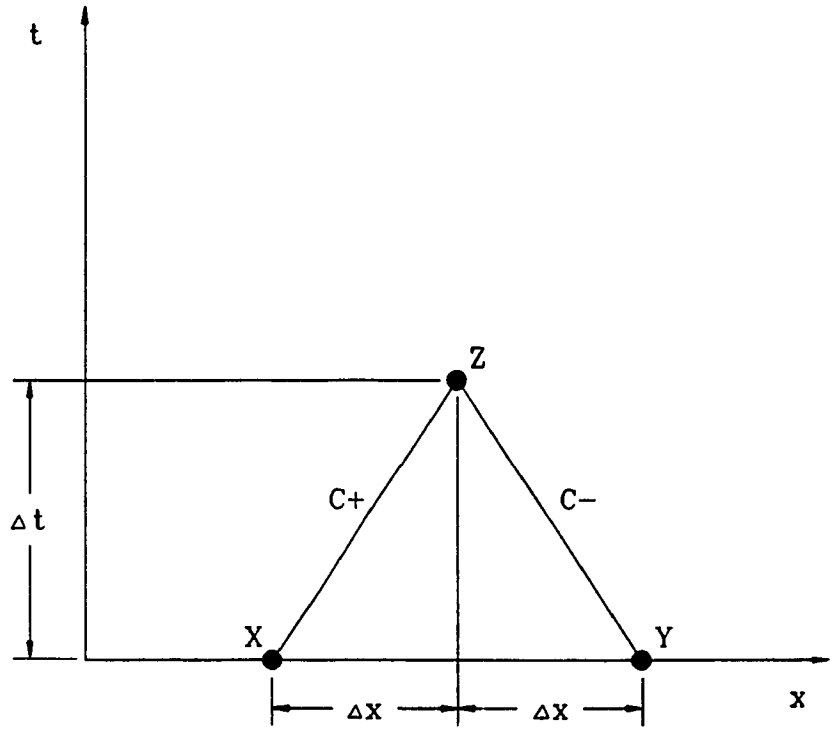

Figure 4.3 Method of Specified TIme Intervals [40].

transient or unsteady flow, steady state flow can be solved for as well. These equations are used for the internal pipe sections and the ends or boundary conditions are necessary to complete the mathematical model of the gaseous fuel injection system.

4.2.3 Boundary Conditions

Having solved for the equations describing the transient and steady state flows in the fuel pipeline, the next step in the procedure is to solve for the boundary conditions. As mentioned before, there are two boundary conditions: the metering valve and the gaseous fuel injectors.

4.2.3.1 The Metering Valve

The metering valve represents a passive boundary condition to the transient flow equations. The metering valve's only function is to throttle the fuel flow from the supply to the fuel pipeline.

The mass flow through the metering valve is dependent on the pressure ratio between the supply pressure, or

upstream pressure, and the fuel pipeline pressure immediately following the throttling area of the metering valve, or downstream pressure. The mass flow can either be choked or unchoked, and the equation which determines the choking condition is equation (3.5). From Zalmanzon [26], when the pressure ratio is less than 0.5457, the mass flow is choked and the equation which describes the choked mass flow is shown below as:

$$\dot{m}_{12} = C_d A_{12} \sqrt{\frac{2P_1^2}{RT} \frac{\gamma}{(\gamma + 1)} \left(\frac{2}{\gamma + 1}\right)^{\frac{2}{\gamma-1}}} \qquad (4.16)$$

where C_d is the discharge coefficient of the metering valve, A_{12} is the throttling area of the metering valve, as calculated in Chapter 3, using the manufacture's data given in Appendix D and P_1 is the supply pressure. In the case of the pressure ratio being greater than 0.5457, the mass flow is considered to be unchoked and the formula describing the mass flow is:

$$\dot{m}_{12} = C_d A_{12} \sqrt{\frac{2P_1{}^2}{RT} \frac{\gamma}{(\gamma-1)} \left[\left(\frac{P_x}{P_1}\right)^{\frac{2}{\gamma}} - \left(\frac{P_x}{P_1}\right)^{\frac{\gamma+1}{\gamma}}\right]} \qquad (4.17)$$

where P_x is the downstream pressure immediately following the throttling area of the metering valve.

This boundary condition is to be applied to the transient flow equations, after the internal points or the

mass flow and the pressure are solved for each pipe increment. The metering valve condition is applied only then to find out if the mass flow through the metering valve is moving towards the fuel injectors or if it is returning to the supply source , due to the pressure waves, and their magnitude.

4.2.3.2 Gaseous Fuel Injector

The second boundary condition is the gaseous fuel injector. The injector is considered as an active boundary condition, since the flow area varies with respect to time. There are several equations used to model the effects of the injector on the entire fuel injection system. The basic equations describing the behavior of the injector are the equation of continuity and the equation of motion.

4.2.3.2.1 Equation of Continuity for a Fuel Injector

The control volume is considered as the injection chamber. There are three different mass flows which affect the quantity of gas in the chamber, i.e. the injector pressure. The three mass flows are: a) the mass flow into

the chamber, $\dot{m}_{n-1}$, b) the mass flow into the combustion chamber of the engine, $\dot{m}_{23}$, and c) the mass flow out of the injector into the atmosphere, leakage flow, $\dot{m}_{24}$. Figure 4.4 demonstrates the three mass flows affecting the injector chamber pressure. Thus, the equation of continuity for the change of mass in the injector volume is:

$$\frac{dm_2}{dt} = \dot{m}_{n-1} - \dot{m}_{23} - \dot{m}_{24} \qquad (4.18)$$

where $\frac{dm_2}{dt}$ is the change in mass with respect to time in the injection chamber. The mass flow $\dot{m}_{n-1}$ is the quantity of gas entering the chamber from the fuel pipe. The value is obtained from the previous iteration of the time interval method (Method of Characteristics).

The mass flow $\dot{m}_{23}$ is the rate of gas mass entering the combustion chamber of the engine, or the discharge characteristic of the injector. This accumulated flow results in the fuel dose delivered to the engine for combustion. The mass flow is definitely turbulent, and the equations describing this flow are similar to those found for the metering valve modeling, as seen in equations (4.16) and (4.17). The equations are shown below for the injector:

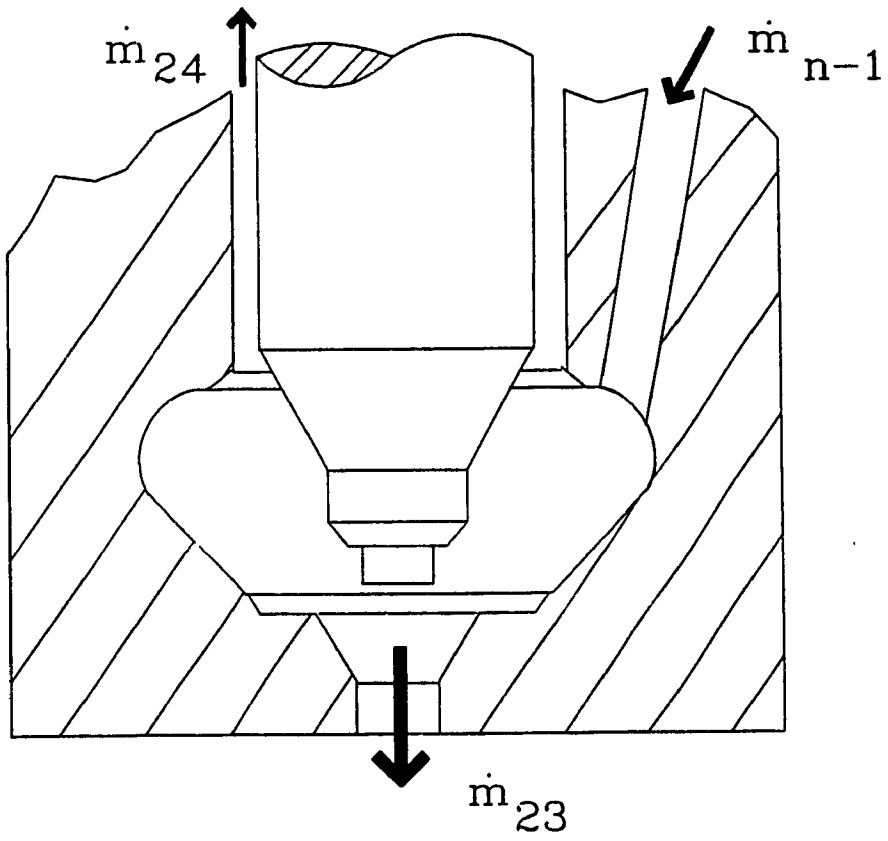

Figure 4.4 Mass FLows in the Injector

-for choked flow

$$\dot{m}_{23} = C_d A_{23} \sqrt{\frac{2P_2^2}{RT} \frac{\gamma}{(\gamma + 1)} \left(\frac{2}{\gamma + 1}\right)^{\frac{2}{\gamma-1}}} \qquad (4.16)$$

-for unchoked flow

$$\dot{m}_{23} = C_d A_{23} \sqrt{\frac{2P_2^2}{RT} \frac{\gamma}{(\gamma-1)} \left[\left(\frac{P_3}{P_2}\right)^{\frac{2}{\gamma}} - \left(\frac{P_3}{P_2}\right)^{\frac{\gamma+1}{\gamma}}\right]} \qquad (4.17)$$

where the C_d for $\dot{m}_{23}$ is much lower than the C_d for $\dot{m}_{12}$. A_{23} is the injector flow area, which is dependant on the injector needle lift. Calculations of the flow area are given in Appendix B.

The mass flow $\dot{m}_{24}$ represents the amount of gas that is leaked to the atmosphere. The leakage flow can be represented as flow between two parallel plates [26], as seen in equation (4.19).

$$\dot{m}_{24} = \frac{\Pi \delta^3 \left(P_2^2 - P_4^2\right) D_T}{24 \mu R T L} \qquad (4.19)$$

The mass flow in this case is considered laminar due to the small clearance, δ, of 0.5 μm and its interactive length, L, of 20 mm. D_T is equivalent to the diameter of the needle plus the clearance, δ. See Figure 4.5.

Now that the mass fluctuation model has been

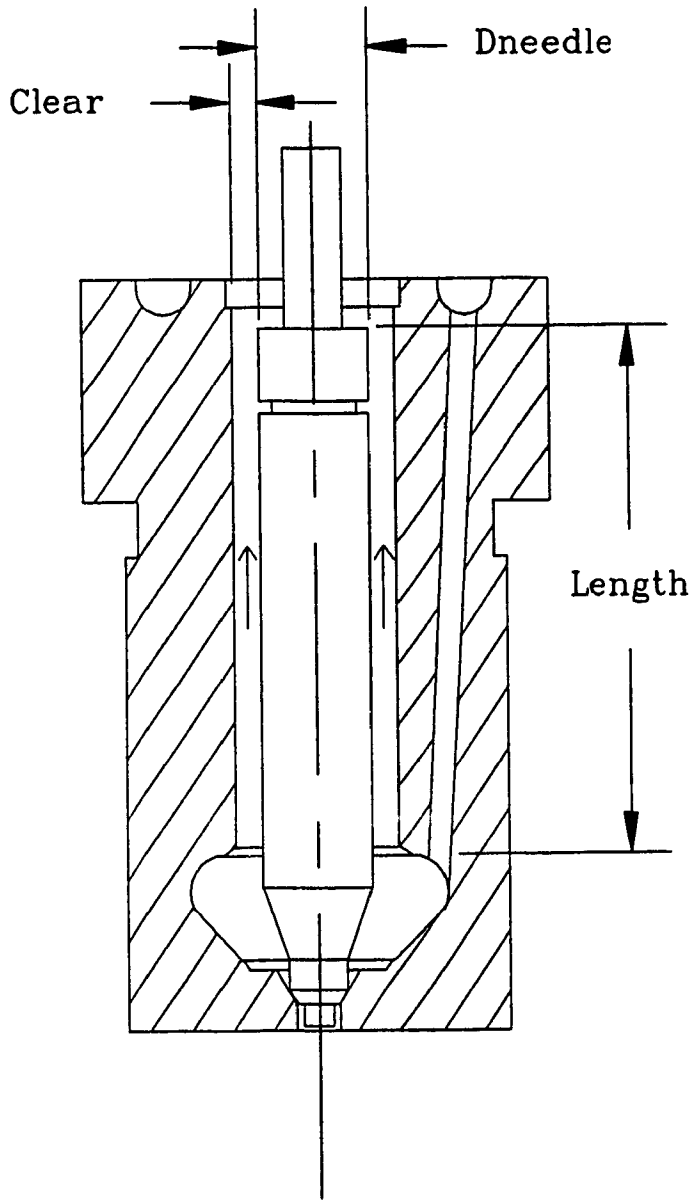

Figure 4.5 Leakage Flow

developed, by use of the continuity equation, the pressure fluctuations in the injector chamber must be accounted for. Using the equation of state, the mass of gas in the injector chamber is solved for as such,

$$m_2 = \frac{P_2 \, V_2}{R \, T} \tag{4.20}$$

However, the mass m_2 in the injector chamber is calculated by the use of the continuity equation, equation (4.18); multiplying the net mass flow change by the time increment and adding it to the initial mass in the chamber as shown by equation (4.21).

$$\dot{m}_{2f} = \dot{m}_{2i} + \frac{dm_2}{dt} \, dt \tag{4.21}$$

Thus, by knowing that the mass changes in time and that the gas constant and the temperature are constant, the pressure and the volume also change in time as invoked by the equation of state.

The injector volume changes due to the injector needle motion, i.e. needle lift h. The equation describing the volume of the injector chamber is shown in equation (4.22) [41].

$$V_{2f} = V_{2i} + \frac{dV_2}{dt}\,dt \qquad (4.22)$$

where,

$$\frac{dV_2}{dt} = \frac{dh}{dt}\,\frac{\Pi}{4}\left(d^2_{needle} - d_{se}^{\,2}\right)$$

Finally, by rearranging equation (4.20) and solving for the pressure, P_2, in the chamber after each iteration and substituting m and V with their iterative values, the pressure is solved for.

$$P_2 = \frac{\dot{m}_{2f}\,R\,T}{V_{2f}} \qquad (4.23)$$

This is how the above mentioned equations will be utilized in the simulation program to solve for the changes in the injection chamber. Note that for the change in volume, the value of dh was necessary and it will be obtained from the equation of motion of the injector needle.

4.2.3.2.2 Equation of Motion of the Injector Needle

Many of the researchers in this chapter's overview have modeled an injector by a physical approach, i.e. mass-damper-spring model; thus, indicating a similarity amongst all liquid fuel injector models. A model of

complex injector is shown in Figure 4.6 (a) and that of a simplified model, which will be used in this case, is shown in Figure 4.6 (b) [42].

The equation describing such a system is a second order differential equation. The equation for the model in Figure 4.6 (b) is as follows;

$$\text{mass}\ \frac{d^2h}{dt^2} + D_f\ \frac{dh}{dt} + K_s h = F_{eff} \qquad (4.24)$$

where mass is for all the moving parts of the injector, D_f is the damping coefficient, K_s is the spring force, and F_{eff} is the total sum of the forces acting on the moving injector mass. The values of d^2h, dh, and h describe the moving mass acceleration, velocity, and displacement (needle lift).

The total mass of the injector is considered to be the sum of the injector needle, the spring holder and the solenoid armature, plus one-third ($\frac{1}{3}$) the mass of the spring [42]. Thus, the equation for the total moving mass is:

$$\text{mass} = \text{mass}_{needle} + \text{mass}_{armature} + \frac{1}{3}\ \text{mass}_{spring} \qquad (4.25)$$

The total mass involved in this case resulted in 0.094 kg.

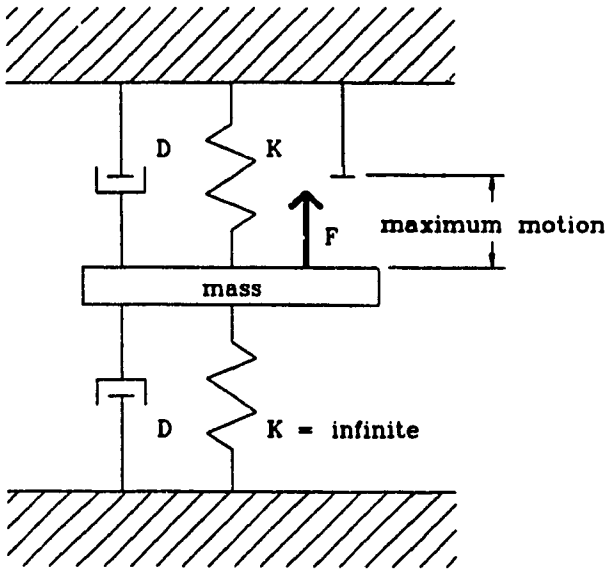

Figure 4.6 a) Complex Physical Model

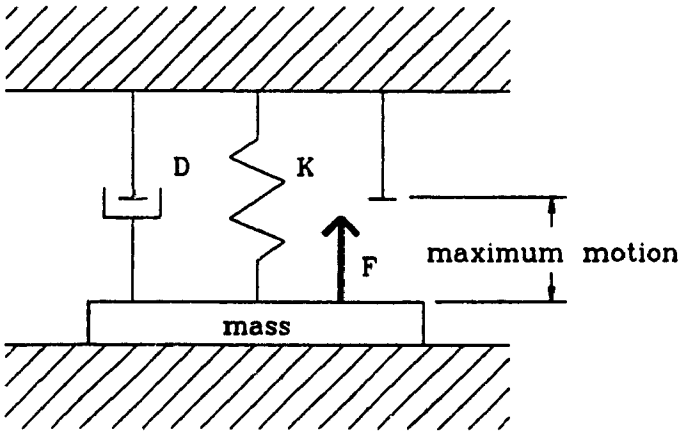

Figure 4.6 b) Simplified Physical Model

The derivation of the damping coefficient, D_f, is given in more detail in Appendix E, and the spring force, K_s, was already discussed in Chapter 3, with the calibration curves for the springs given in Appendix C.

The effective force, F_{eff}, represents the total sum of the forces acting on the moving mass. The forces which act upon the mass are the following: a) the solenoid (electric) force , F_{elec}, which lifts the injector needle of its seat. b) the spring preload force, F_{pre}, which maintains a constant force to return the needle to its seated position. c) the Coulomb friction force [19], F_{fric}, which is the friction between the surfaces of the injector needle and the injector housing and d) the gaseous force, F_{gas}, which is the force of the gas acting upon the injector needle. The manner in which the forces affect needle movement are shown in Figure 4.7, and the sum of the forces is shown in equation (4.26).

$$F_{eff} = F_{elec} + F_{gas} - F_{pre} \pm F_{fric} \qquad (4.26)$$

Note that the friction force is dependent on the direction of the moving mass.

Thus, the equation of motion can be expanded, using equations (4.24) and (4.26), in order to model the motion of the injector needle.

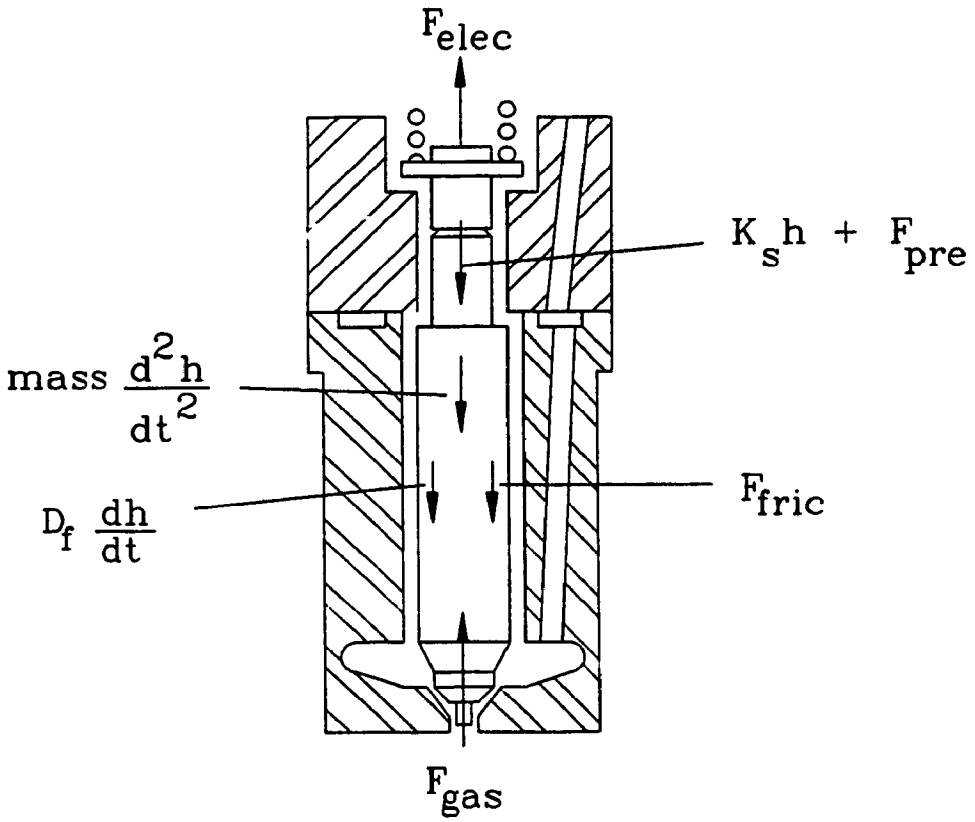

Figure 4.7 Simplified Free Body Diagram

$$\text{mass}\ \frac{d^2h}{dt^2} + D_f\ \frac{dh}{dt} + K_s h = F_{elec} + F_{gas} - F_{pre} \pm F_{fric} \qquad (4.27)$$

where $D_f\ \frac{dh}{dt}$ is the damping force acting upon the needle, (see Appendix E). Thus the modeling of the injector needle motion is complete and what remains is to solve for this equation.

4.2.3.2.3 Method of Solution

The method of solution for the equation of motion of the injector needle is by the use of a fourth-order Runge-Kutta approximation. This numerical method was used by many of the investigators and modelers mentioned in the overview. A self starting routine was an essential factor in choosing a numerical method to solve for the injector needle motion. Even though higher order (fifth and sixth order) Runge Kutta routines are available, a fourth order routine provides enough accuracy and flexibility. Another factor involved in the solution was the size of the time step; however, the time step for this method of solution is dependent on the gaseous fuel properties as depicted by the method of characteristics, i.e. speed of sound of the gas.

The Runge Kutta equations were taken from James et al

[43], and this method can be considered as a typical Runge Kutta method of solution.

In order to begin the simulation, some initial value must be assumed for the forces acting upon the injector needle.

$$F_{gas} = P_2(A_{needle} - A_{nozzle}) + P_3 A_{nozzle} = 233.36 \text{ N}$$

$$F_{pre} = P_x (A_{needle} - A_{nozzle}) = 264.51 \text{ N}$$

$$F_{fric} = 0.5 \text{ N}$$

To start the injector needle movement, the electrical force, F_{elec}, must overcome all forces opposing the upward motion of the needle.

$$\begin{aligned} F_{elec} &= F_{pre} + F_{fric} - F_{gas} \\ &= 264.51 + 0.5 - 233.36 \\ &\cong 32 \text{ N} \end{aligned}$$

Thus, the solenoid must provide a minimum force of 32 N in order to start the needle motion. In order for the needle to reach its full height off its seat, the solenoid must also overcome the additional spring force, which increases with needle displacement, h. The additional force is a product of the spring force and needle displacement; thus, the total electrical force required is the sum of this additional force due to the needle displacement and the force required to start the needle motion.

$$F_{elec} = 32 + K_s h = 32 + 321 * 0.55$$
$$\cong 209 \text{ N}$$

Now, after some preliminary values have been found in order to commence the Runge Kutta routine, these parameters must be upgraded so that a more accurate simulation of the injector needle motion can be obtained. From all the above mentioned equations, a computer code for the model was developed and parameters optimized so that the model of the needle motion would closely match the preliminary displacement diagrams shown in Figures 3.14 a) and b).

4.2.3.3 Multi-Point Injectors

In the case of multi-point injection system, for example a twin injector system, the second injector and feeder pipe act as an accumulator in the fuel system. At the point where the tee joint exists, an exclusion is made in the model in order to account for the larger volume of gas, which affects the pressure and mass flow fluctuations in the fuel pipe. The following equations are inserted into the model to account for the accumulator effect:

a) volume of accumulator

V_{acc} = length of pipe * cross-sectional area of pipe

$= l_{pipe} * A_{pipe}$

b) equation of continuity

$$\frac{dm_{acc}}{dt} = \dot{m}_{acc+1} - \dot{m}_{acc-1} \qquad m_{acc} = m_{acc} - \frac{dm_{acc}}{dt}\, dt$$

c) equation of state

$$P_{acc} = \frac{m_{acc}\ R\ T}{V_{acc}}$$

These three equations are the only difference between a multi point-injection system and a single-point injection system model. The effect of the additional volume will be definitely noticed in the pressure wave effects of the discharge characteristics.

4.3 SIMULATION RESULTS

The four major components of the mathematical model of the fuel injection system have been discussed. The method of solution for the pressure wave traversing is solved by the method of characteristics. The boundary conditions of this solution method have been discussed; these are the metering valve and the gaseous fuel injector. Whereby the fuel injector represents an active boundary condition with an always changing flow area, the metering valve represents a passive boundary condition with a constant flow area for one particular engine operating condition. Recall that the fuel injector was also modeled, with a fourth order Runge Kutta method of solution to solve its equation of motion, (a second order differential equation). Finally, the second injector was discussed on how it affects the fuel discharge characteristics.

Having defined the model, initial simulations of the injector can begin to assist in fine tuning of the parameters in order to obtain a more accurate model of the entire gaseous fuel injection system.

Following are shown the results of simulations of a single point gaseous injection system with a 125 mm pipe connecting the injector and the metering valve. The system operates on Natural Gas and Hydrogen Gas. The first graph,

in Figure 4.8, shows the pressure drop and pressure waves within the pipe, and the second graph, in Figure 4.8, shows the gas mass flow out of the injector and through the metering valve. Figure 4.9 shows similar results for Natural Gas at a different metering valve opening and Figure 4.10 shows a simulation using Hydrogen gas. The simulation will be discussed further in Chapter 6, when the comparison between experimental values and the analytical values are discussed, in order to validate the model.

As a note of interest, a finite difference approach was also considered, the equations to be solved for were parabolic. Using such a numerical method, one has to restrict the time increment for stability considerations. A very small Δt will require more computations which results in increased computer time. Therefore, in order to obtain one cycle of the injection process required a very small time increment which was much greater than 1000 times that of the used numerical method. The time increment was decreased in order to maintain stability rather than to improve on the accuracy of the method. Thus, the reasoning behind the rejection of this method.

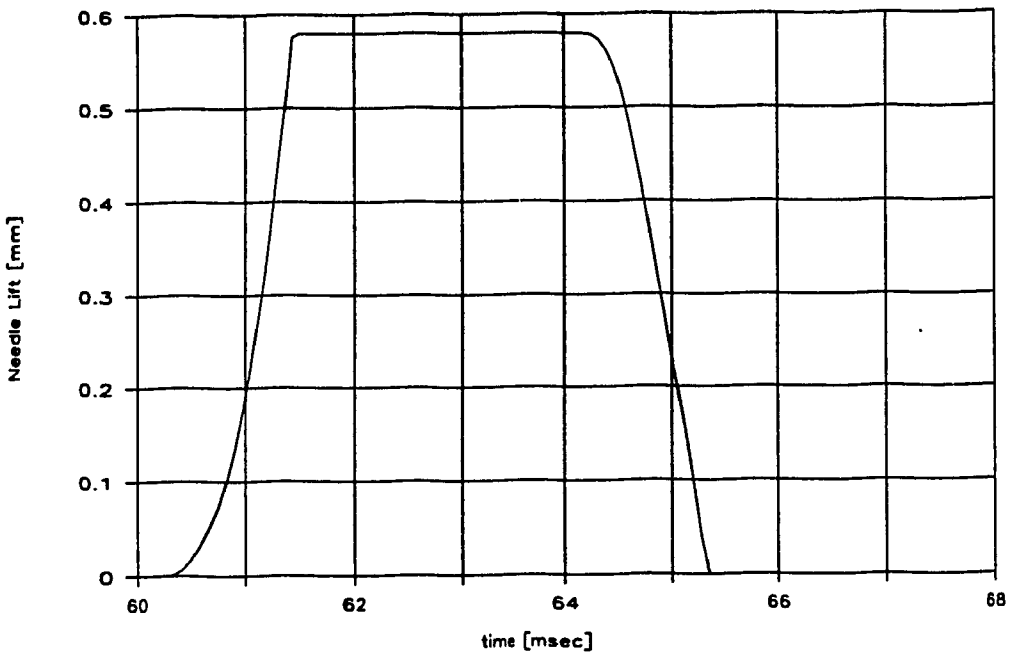

Figure 4.8 a) Simulated Needle Lift versus Time for Natural Gas, with y = 4.2 and x = 125 mm.

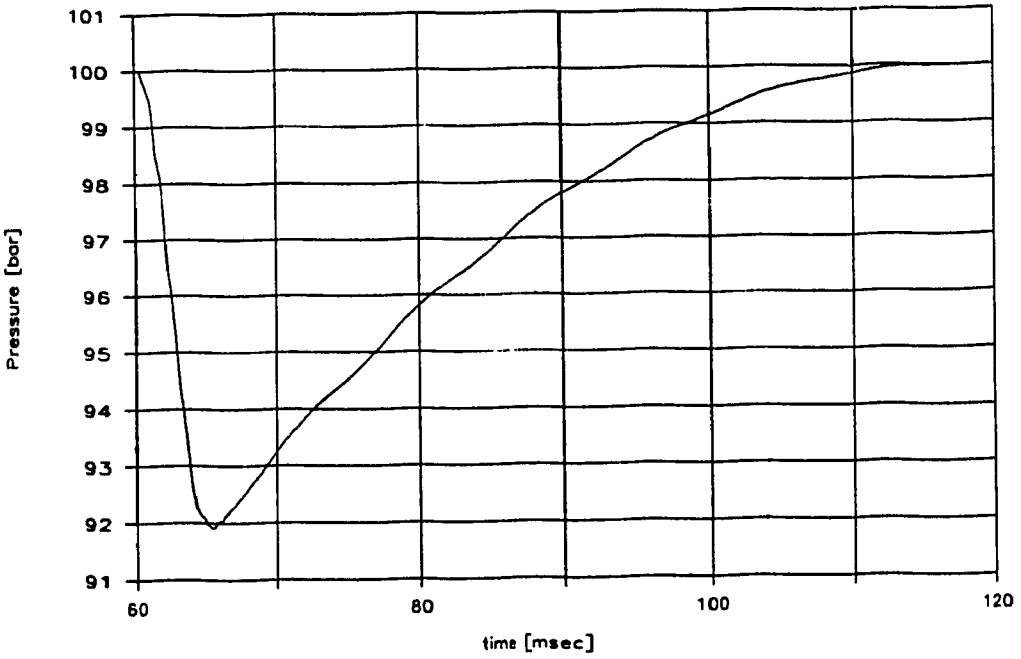

Figure 4.8 b) Simulated Pressure versus Time for Natural Gas, with y = 4.2 and x = 125 mm.

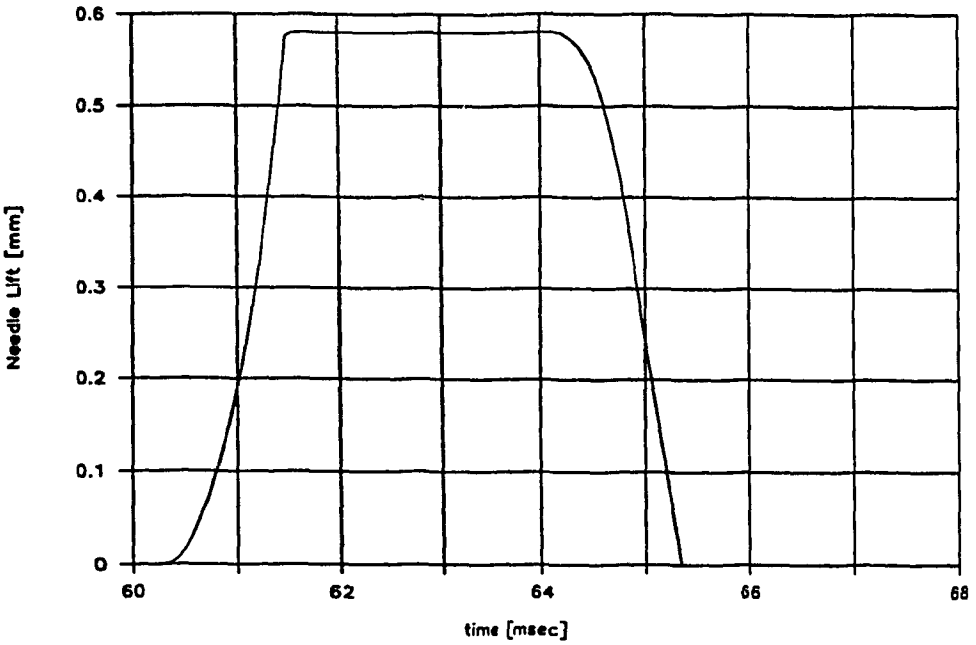

Figure 4.9 a) Simulated Needle Lift versus Time for Natural Gas, with y = 10.0 and x = 125 mm.

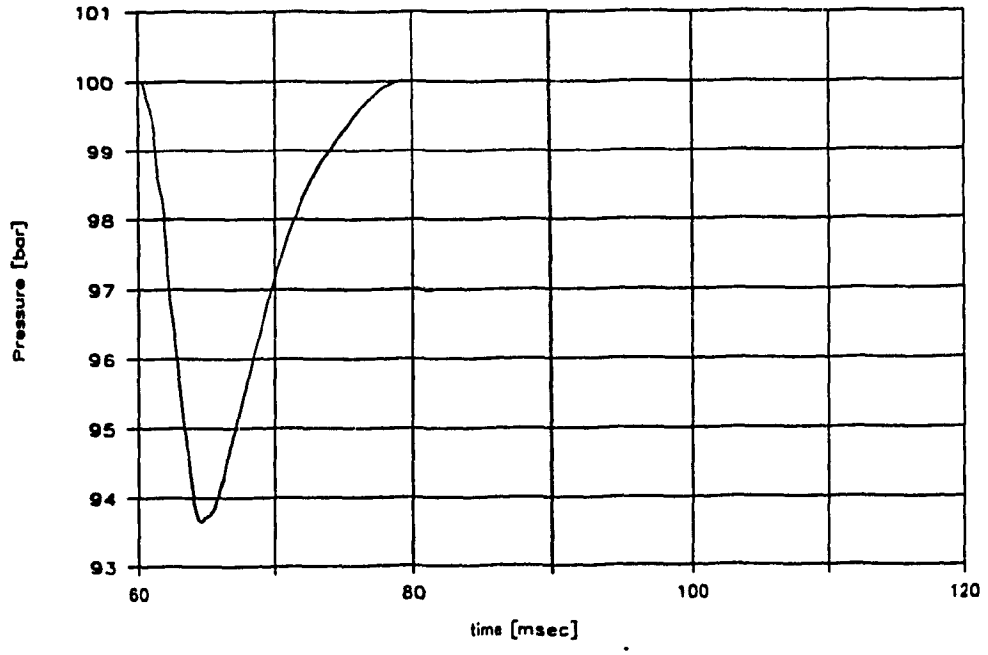

Figure 4.9 b) Simulated Pressure versus Time for Natural Gas, with y = 10.0 and x = 125 mm.

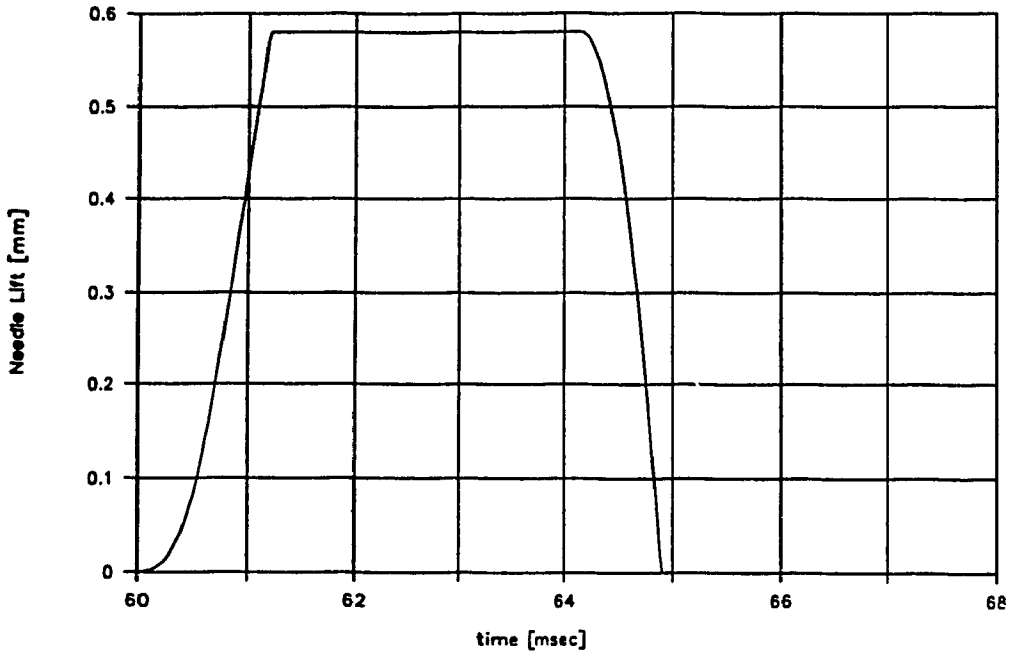

Figure 4.10 a) Simulated Needle Lift versus Time for Hydrogen Gas, with y = 5.0 and x = 125 mm.

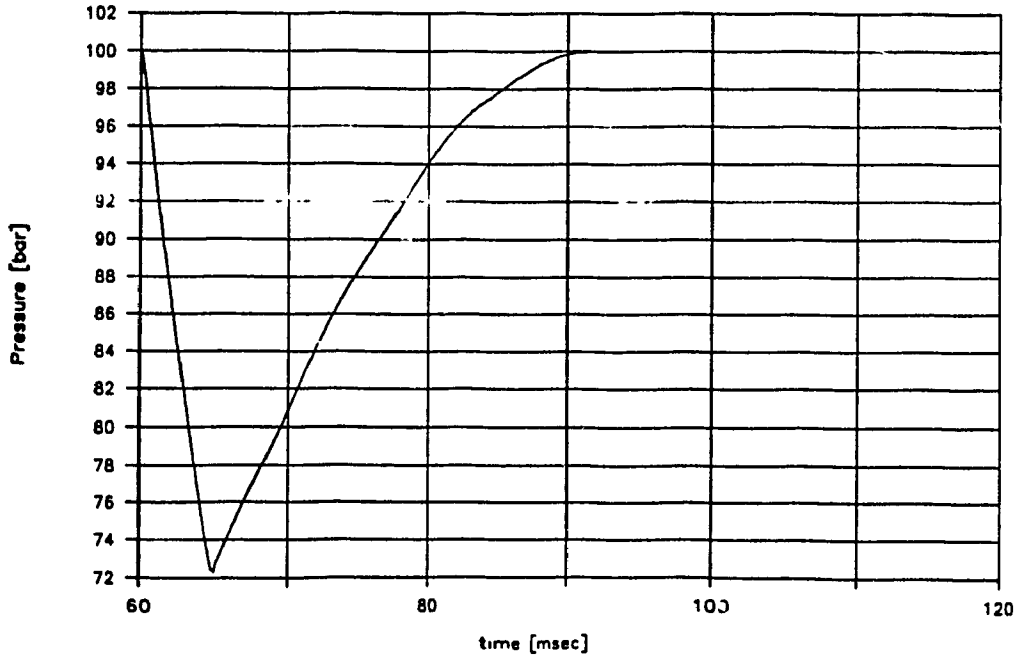

Figure 4.10 b) Simulated Pressure versus Time for Hydrogen Gas, with y = 5.0 and x = 125 mm.

5. EXPERIMENTAL INVESTIGATION

This chapter deals specifically with the experimental investigation of the electronically controlled gaseous injection system. The main focus of this investigation is to ensure that both injection systems, single point and multi-point, can match the operating characteristics of the given diesel engine, as outlined in Chapter 3, using gaseous fuels, Hydrogen and Natural Gas. Thus, the discharge characteristic and the injected fuel dose will determine if the injection systems can satisfy those characteristics.

In the ensuing subsections, the test set-up and experimental procedure will be first discussed, followed by the experimental results of the injection systems, using the gaseous fuels aforementioned. During the tests, the injection system will be subject to various parameter changes in order to obtain the appropriate fuel discharge characteristic and delivery curves. Then, a discussion will follow in order to draw conclusions and make recommendations.

5.1 TEST SET-UP AND PROCEDURE

A test set-up is required in order to measure and to analyze the capabilities of the injection systems under investigation. This set-up was developed specifically to deal with gaseous fuels. It can be seen schematically in Figure 5.1.

The test set-up consists of the following components: a) bottle of compressed gaseous fuel, i.e Hydrogen or Natural Gas. b) pressure regulator to bring the gaseous fuel pressure to the required operating pressure level of 100 bars. c) metering valve operated by a linear digital actuator. d) modified diesel injector fitted with a solenoid actuator. e) gas dose measuring chamber. f) computer interface. g) microcomputer with a data acquisition system and h) oscilloscope and other required instrumentation for signal acquisition.

The metering valve configuration consists of a metering valve, Hoke 1315M4B with a 3° taper, and a pipe leading to the injector. This configuration can be altered by varying the pipe length and pipe diameter. The solenoid equipped injector, a modified CAV BKB - 40S5146V diesel injector, can be altered by varying the spring stiffness and also by altering the exit flow area of the nozzle by either changing the injector nozzle or by modifying the

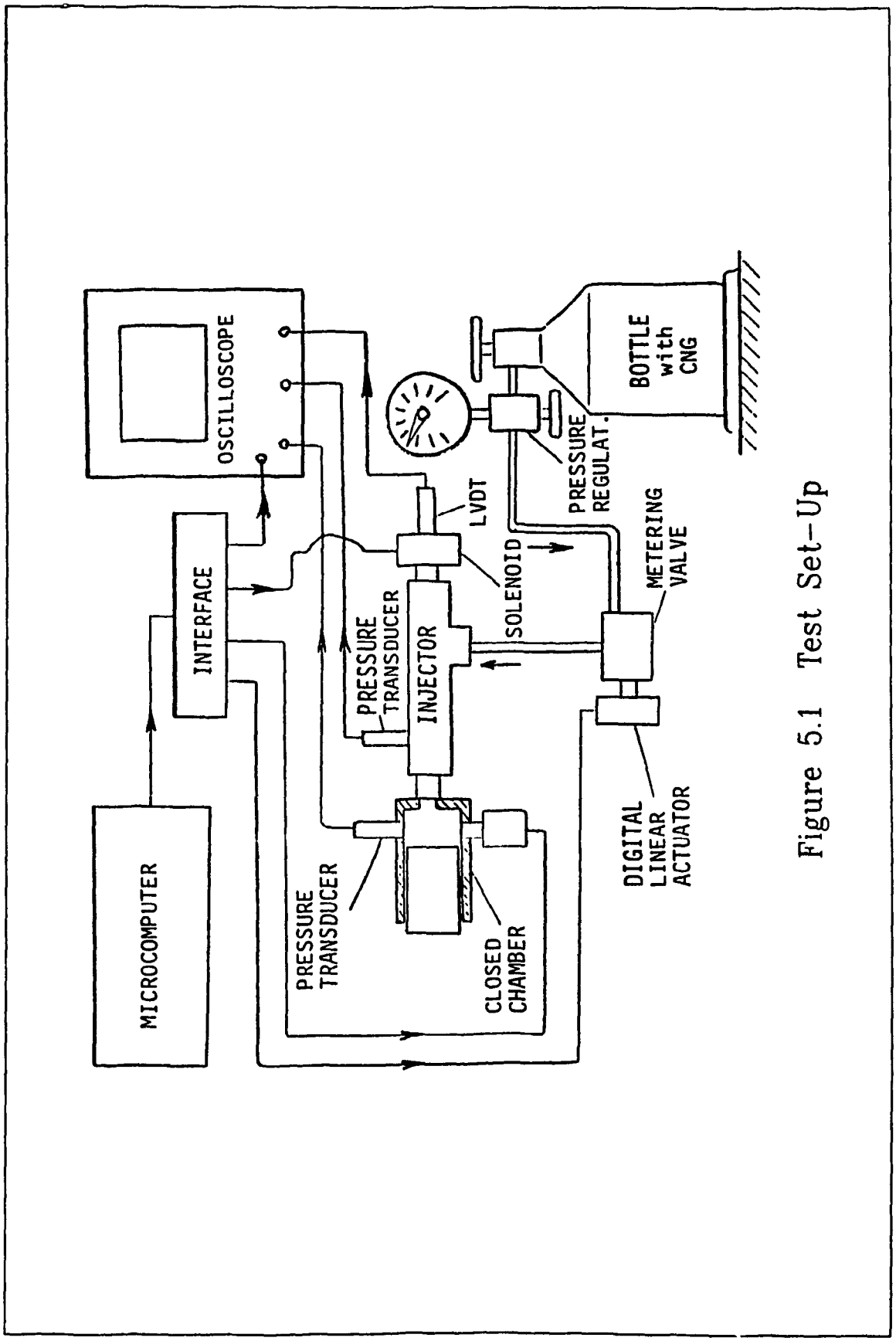

Figure 5.1 Test Set-Up

pintle, as mentioned in Chapter 3. The computer interface has been discussed in detail in the preceding chapter and will not be repeated here. The last two items of importance in the test set-up are the instrumentation and the fuel dose measuring chamber. Tables 5.1 and 5.2 show the different configurations for the experiments performed with Hydrogen and Natural Gas. The configurations can also be seen in Figure 5.2.

Table 5.1 Gaseous Fuel Injector Configurations

Injector Configuration No. 1

Injector Housing	CAV BKB - 40S5146V
Injector Nozzle	CAV BDN4SD508W
Spring Constant	143 kN/mm
Needle Lift Limit	0.58 mm

Injector Configuration No. 2

Injector Housing	CAV BKB - 40S5146V
Injector Nozzle	CAV BDN4SD508W*
Spring Constant	321 kN/mm
Needle Lift Limit	0.55 mm

* The injector needle had a modified pintle as noted in Chapter 3.

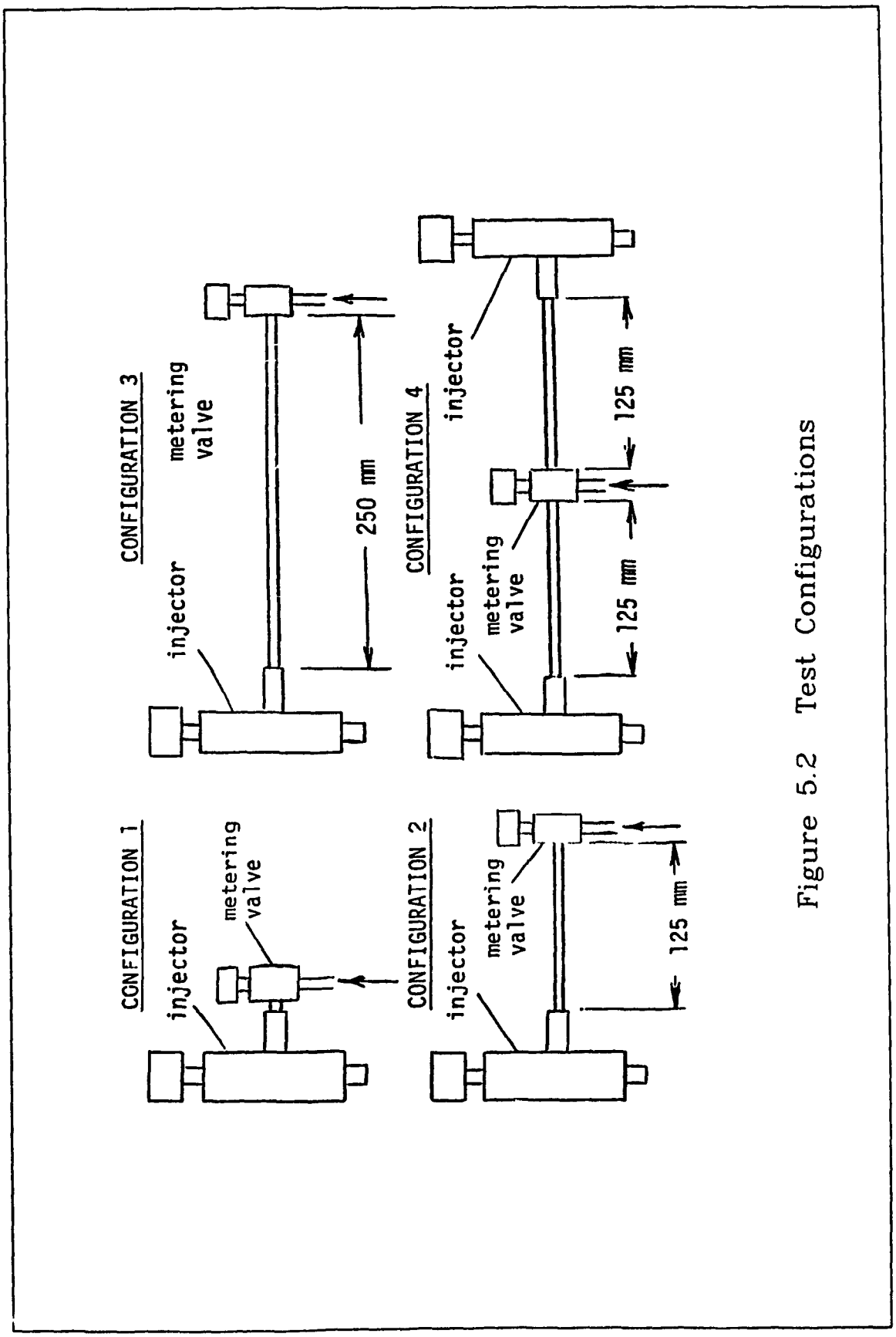

Figure 5.2 Test Configurations

Table 5.2 Metering Valve Configurations

Metering Valve Type	Hoke - S/N 1315M4B 3° taper 1.19 mm diameter
Pipe Lengths Pipe Diameters nominal	125 mm, 250 mm 3.0 mm, 4.5 mm
Configuration # 1	no pipe, metering valve only
Configuration # 2	125 mm pipe of 4.5 mm dia., between metering valve and gaseous injector
Configuration # 2b	same as # 2,with 3.0 mm dia.
Configuration # 3	250 mm pipe of 4.5 mm dia., between metering valve and gaseous injector
Configuration # 3b	same as # 3,with 3.0 mm dia.
Configuration # 4	metering valve attached to a tee separating two injectors connected by two 125 mm pipes of 4.5 mm diam.
Configuration # 4b	same as # 4,with 3.0 mm dia.

The instrumentation used for signal acquisition on the injection system consists of two pressure transducers and a linear variable displacement transducer (LVDT). The pressure transducers are situated in the injector and in the dose measuring chamber. They are both KISTLER piezoelectric quartz transducers model 603B2. The one located in the injector is used to collect data about the fuel pressure variations in the injection chamber, which

are vital in analyzing the discharge characteristics of the injection system. The second transducer is located in the fuel dose measuring chamber and is being used to measure the pressure rise in the chamber, which determines the gas fuel dose injected. This will be discussed further in the next paragraph specifically describing the fuel dose measuring chamber. The calibration curves for these two pressure transducers are given in Appendix C. The LVDT, an AVL 3075 - A02 transducer, is used to measure the travel of the injector needle during the injection process. This is essential in evaluating the effective spring constant, the spring preload, and the nozzle exit flow area, to avoid post-injection and chattering of the injector needle. The calibration curve of the LVDT is also given in Appendix C.

The dose measuring system consists of a closed steel chamber of fixed volume, a pressure transducer, a relief valve, and an injector. The dose measuring chamber principle is based on the perfect gas assumption; thus, having a fixed volume at a constant temperature, the pressure rise in the chamber should be proportional to the mass change in the chamber, i.e. to the fuel dose. The change in mass due to the change in pressure can be calculated from the equation of state as follows [1]:

$$\Delta m = \frac{\Delta P V}{R T} \qquad (5.1)$$

where, Δm = the mass of gas injected
ΔP = the pressure rise in the chamber after the injection process
V = volume of the chamber
T = absolute temperature of the gas in the chamber
R = the gas constant of the gaseous fuel

Figure 5.3 shows an oscillogram of the pressure increase during consecutive fuel injections into the dose measuring chamber. The step-like pressure increases correspond to single injections and they are directly proportional to the mass dose of injected fuel. The chamber also provides the required back pressure, and is regulated through a relief valve. The relief valve serves a dual purpose; first it acts as a safety valve so that not too high pressure could built up in the chamber and second, it limits the maximum pressure level in order to avoid too high pressure variations where the change in the gas compressibility should be taken into account.

The procedure for investigating the electronic gaseous fuel injection system is as follows: First, the appropriate fuel doses are calculated for the key points of the engine operating characteristic, as seen in Appendix A. The main objective is to satisfy the 5 different doses of the characteristic, which are: 100% or nominal dose, better known as maximum power dose, 130% or maximum torque dose,

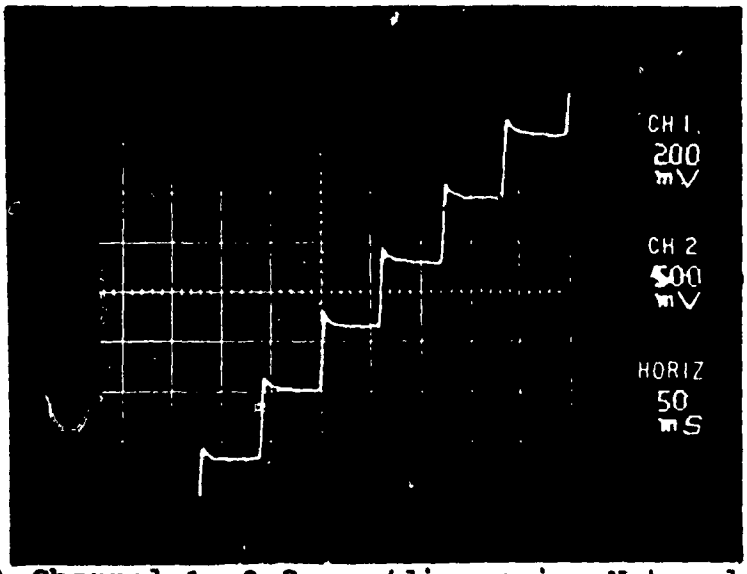

a) Channel 1, 3.2 mg/div using Natural Gas

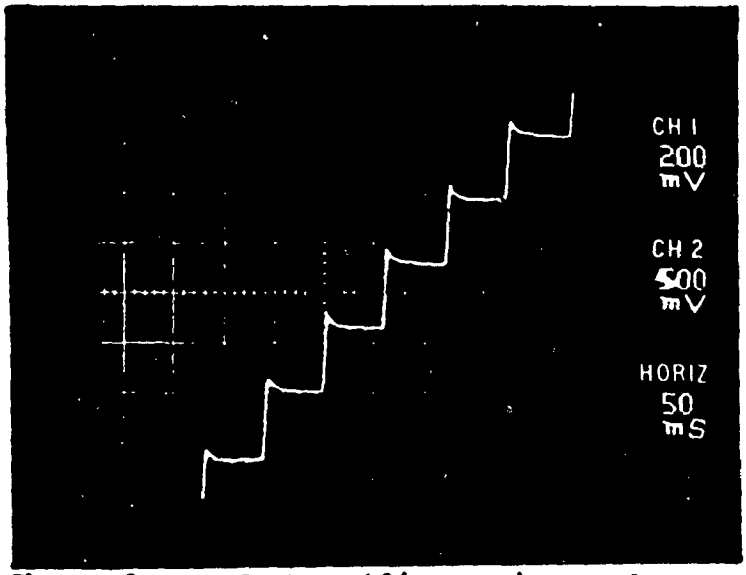

b) Channel 1, 25.5 mg/div using Hydrogen Gas

Figure 5.3 Dose Measurement Calibration Curves.

20% or minimum idle dose, 20% or maximum idle dose, and 160% or starting dose. Then, the pipes of various lengths and diameters are cut, as required, to match the injection configurations to be tested, as shown in Figure 5.2. These configurations have been selected according to the possible location of these components on an engine as seen in Figure 3.6. Thirdly, the injector is selected with the required spring constant and preload to produce adequate needle lift and to avoid post-injection problems, as well as to provide the correct fuel discharge rate in order to assure a large enough flow area through the injector nozzle. Once this last step has been accomplished, the tests can be performed for both gaseous fuels used for this investigation, Hydrogen and Natural Gas. It was found that, at particularly low doses, the injector needle has a tendency to seize due to two factors which are the small clearance between the needle and the nozzle body and the limited lubricating properties of gaseous fuels. Thus, in order to avoid this problem the needle was lubricated with diesel fuel during testing. This procedure proved successful for tests with Natural Gas; however, with Hydrogen, some needle sticking still occurred during lower frequency operations.

The four configurations, as shown in Figure 5.2, were tested for each gaseous fuel, Natural Gas and Hydrogen. Along with the four configurations, the pipe diameters were varied from 3.0 mm to 4.5 mm, and the pipe lengths from 125

mm to 250 mm. This was in order to demonstrate the effects of the pipe flow area change and volume increase between the injector and the metering valve on the pressure waves traversing the pipe, the fuel discharge characteristics and the final fuel dose output from the injection system. The results were recorded on oscillograms and are discussed in the ensuing subsections.

5.2 DISCHARGE CHARACTERISTICS

The intent of this section is to discuss the results of the experimental investigation on the gaseous injection system in the different configurations presented previously, using both Natural Gas and Hydrogen as fuels.

All tests were conducted at the gas supply pressure of 100 bars, and the injector spring preload was set at 120 bars; however, the injector underwent two parameter changes with Hydrogen as compared to Natural Gas. These changes consisted of a stiffer spring and a larger nozzle exit area, as mentioned previously and in Appendices C and B respectively. Injector configuration 1 was used for Natural Gas and injector configuration 2 was used for Hydrogen Gas. The fuel dose measuring chamber was close to atmospheric pressure at the beginning of the injections and was drained after each test run.

The following four key points were observed for the given diesel engine characteristics which are described in Appendix A: maximum power (nominal dose) @ 2000 rpm, maximum torque dose (130% of nominal dose) @ 1600 rpm, minimum/maximum idle (20% of nominal dose) @ 600/2300 rpm, and starting dose (160 % nominal dose) @ 600 rpm. These four points were investigated for both gases in all the configurations tested. See Figure 5.1 for the test set-up.

The two subsections following are showing the test results and include the discussions of the discharge characteristics records when using Natural Gas and Hydrogen, for all four configurations aforementioned.

5.2.1 Natural Gas Discharge Characteristics

The gas discharge characteristics for Natural Gas from the four different configurations will be discussed; however for only one pipe diameter of 4.5 mm. It was found that the pressure wave amplitudes in the 3.0 mm diameter pipe were too high and were disturbing the operation of the injection system, i.e. the system could not operate correctly and post-injection was always present. Thus, the 3.0 mm diameter pipe was no longer considered for the investigation using Natural Gas.

The test results for the first configuration are shown in Figure 5.4. As can be seen from the records, the changes in flow area of the metering valve resulted in variations of the fuel delivery characteristics, while the solenoid remained energized for the same amount of time. Notice that for the maximum torque and for the starting conditions, the pressure rose quickly in the injector. This was due to the high flow area in the metering valve

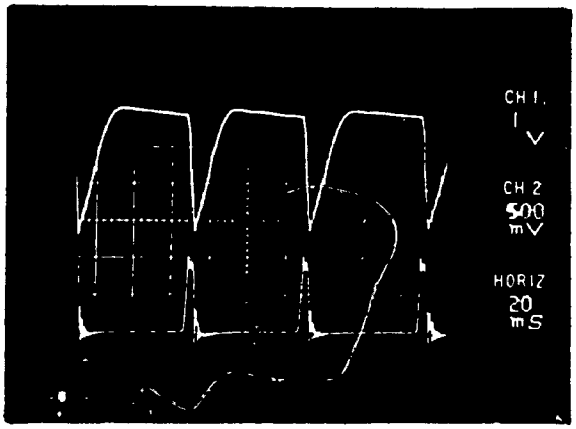

a) Engine Speed at 2000 rpm and y = 3.5

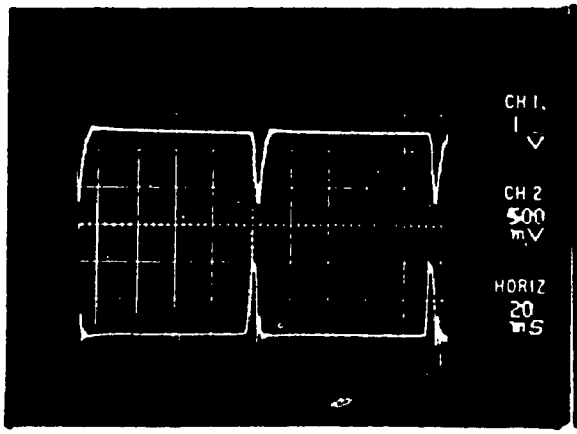

b) Engine Speed at 1600 rpm and y = 3.5

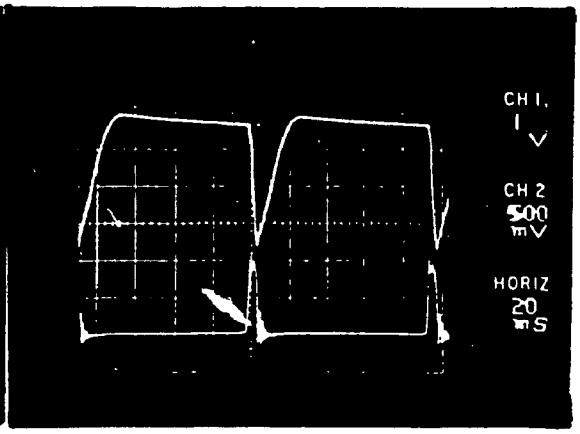

c) Engine Speed at 1600 rpm and y = 10.0

Figure 5.4 Injection Cycles for Configuration 1 using Natural Gas.

and to the fact that there was very little volume of gas between the metering valve orifice and the injector orifice. Figure 5.4 a) shows the discharge characteristics for the injection frequency at 2000 rpm, and Figure 5.4 b) represents the injection frequency at 1600 rpm with the same metering valve position as for the injection frequency at 2000 rpm. However, the fuel dose achieved at that point was not 30 % greater than at nominal dose, as required for the nominal torque. In Figure 5.4 c), the 30 % increase in fuel dose was achieved by increasing the metering valve flow area. It can be concluded from these tests that the first configuration is not providing the required 30 % increase in fuel dose from the nominal fuel dose at maximum power (at 2000 rpm) to 130 % of nominal dose at maximum torque (at 1600 rpm) without altering the metering valve position. The main factor in the first injection system configuration that can contribute to this fact is the small volume between the injector and the metering valve.

Figure 5.5 shows the difference in the injection characteristics between a partly open metering valve and a fully open metering valve for the first configuration. In the latter case, the injector pressure returns to the system pressure immediately after injection, while in the case of the partly open metering valve, the rise is much slower. The quick pressure rise is much affected by the

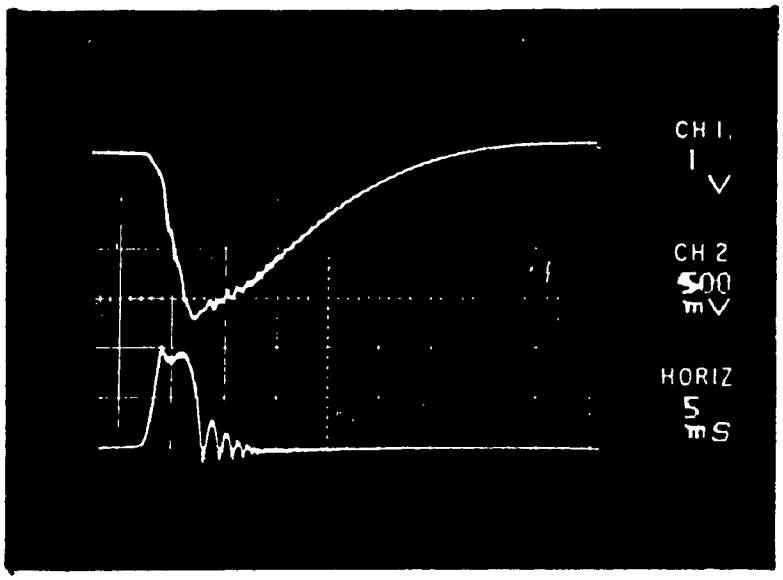

a) Partially Open

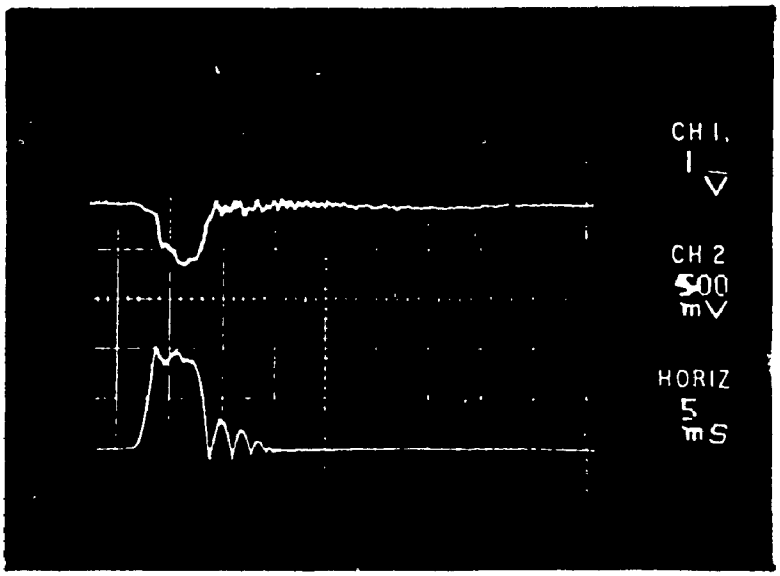

b) Fully Open

Figure 5.5 Effect of Metering Valve Flow Area on Pressure in the Injector.

small volume of tubing between the metering valve and the injector.

Figure 5.6 shows the fuel discharge characteristics resulting in different gas doses for configuration 1, that is with no pipe separating the fuel injector and the metering valve. The doses achieved for this configuration for the 4 observed points, maximum power, maximum torque, idle, and starting dose, are as follows:

Table 5.3 Configuration 1 results for Natural Gas

Engine Point	Fuel dose (mg)	M. Valve (rev)
max. power	27.86	3.5
max. torque	35.98	10.0
idle	5.22	0.98
starting	44.11	10.0

In each of the oscillograms in Figure 5.6, the upper curve represents the gas fuel pressure in the injection chamber and the lower curve is the injector needle displacement. Note the small oscillations on the pressure curve after minimum injection pressure has been reached. These fluctuations result from the pressure waves generated at high frequency between the injector and the metering valve critical flow areas, which are very close to each other. In the case of Figure 5.6 a), b) and d) the

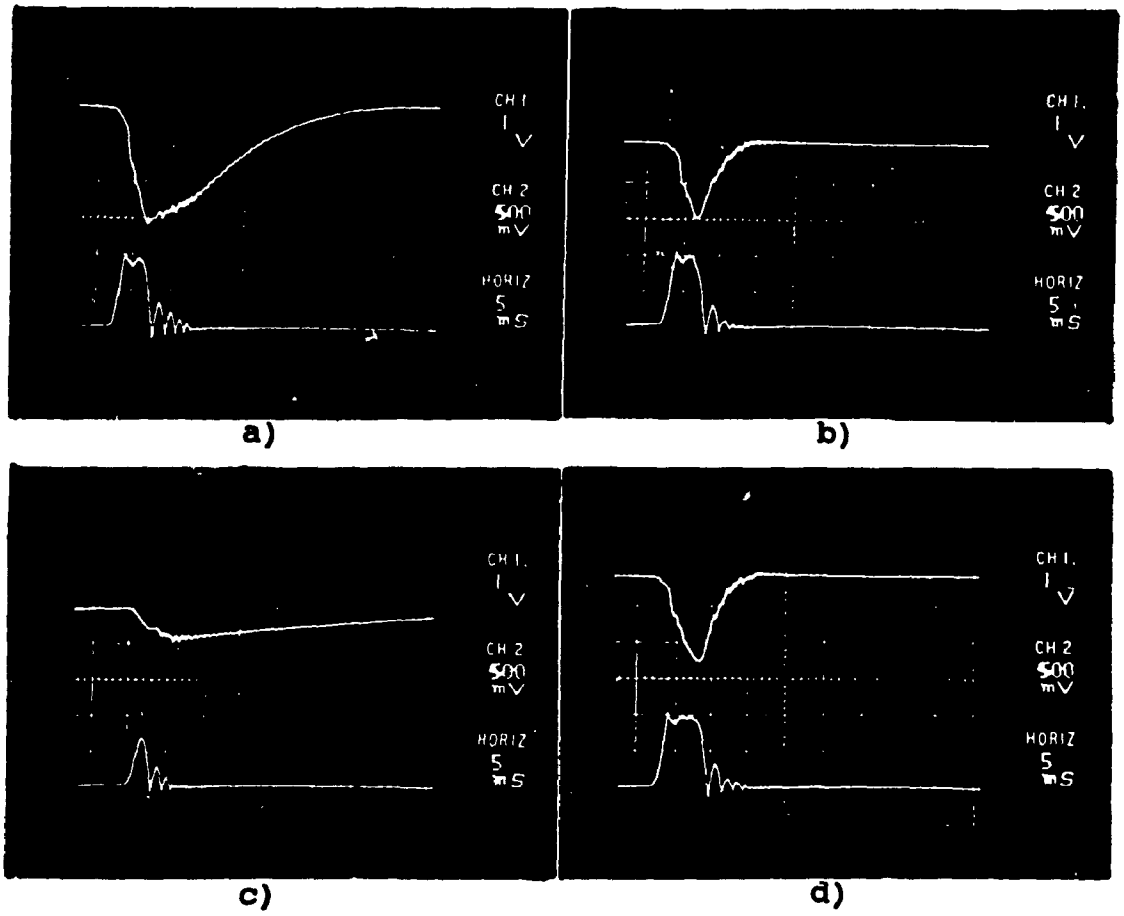

Figure 5.6 Oscillograms of Needle Lift and Pressure Drop for Configuration 1 using Natural Gas.
a) maximum power dose
b) maximum torque dose
c) maximum/minimum idle dose
d) starting dose
Calibration for pressure curve, 6.9 bar/div.
Calibration for needle lift, 0.3 mm/div.

injector needle achieves full lift, while for the idle engine point, the needle is not reaching the stop.

Figure 5.7 represents the test results of fuel discharge characteristics for configuration 2 with Natural Gas. Now a pipe of 125 mm in length has been inserted between the metering valve and the gaseous fuel injector. The results achieved for this test are presented below in Table 5.4.

Table 5.4 Configuration 2 results for Natural Gas

Engine Point	Fuel dose (mg)	M. Valve (rev)
max. power	27.86	2.85
max. torque	35.98	3.5
idle	5.22	0.98
starting	44.11	4.0

Notice how much more evident are the pressure waves in this configuration, as compared to the previous configuration, with no pipe between the metering valve and the injector. Also, the pressure drop is significantly lower due to the larger volume of gas that has been added between the injector and the metering valve. By comparing the metering valve openings with those of the previous configuration, a considerable difference can be seen for all engine operation ranges, except for the idle dose,

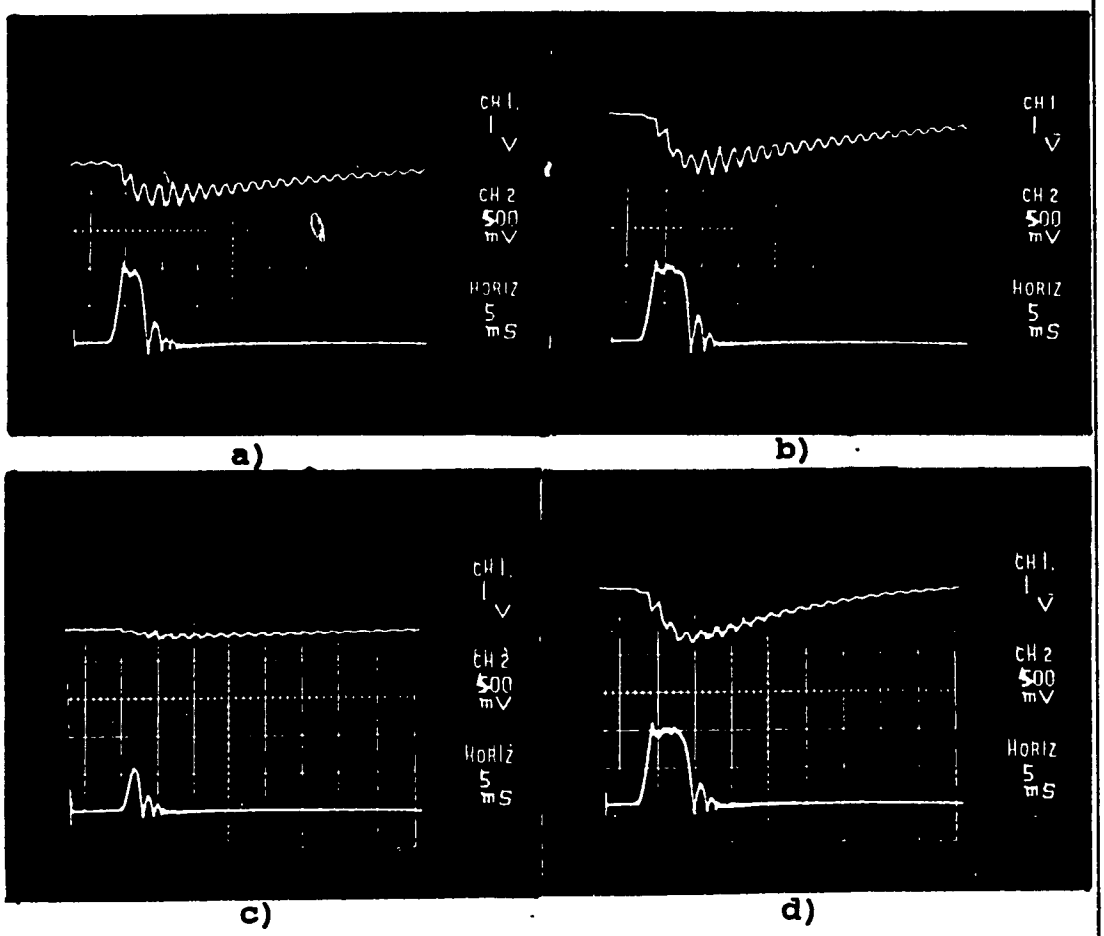

Figure 5.7 Oscillograms of Needle Lift and Pressure Drop for Configuration 2 using Natural Gas.
a) maximum power dose
b) maximum torque dose
c) maximum/minimum idle dose
d) starting dose
Calibration for pressure curve, 6.9 bar/div.
Calibration for needle lift, 0.3 mm/div.

which happen to have identical flow area but with different pressure drop. This can be, also in part, due to the inaccuracies of the metering valve positioning during the tests and will be discussed, in greater detail, later.

Figure 5.8 shows the oscillograms for the fuel discharge characteristics for configuration 3 with a 250 mm pipe length inserted between the metering valve and the injector. The test results are summarized in the following table.

Table 5.5 Configuration 3 results for Natural Gas

Engine Point	Fuel dose (mg)	M. Valve (rev)
max. power	27.86	2.0
max. torque	35.98	2.0
idle	5.22	0.95
starting	44.11	N.A.

The effects of the pressure waves in this configuration seem to be smaller as compared with configuration 2. This can be attributed to the only two changes added to the system, the increased volume and the increased distance between the injector and the metering valve. Notice that the pressure drop for idle dose is almost negligible, which indicates that there is almost enough fuel stored in the pipe to supply the minimum engine

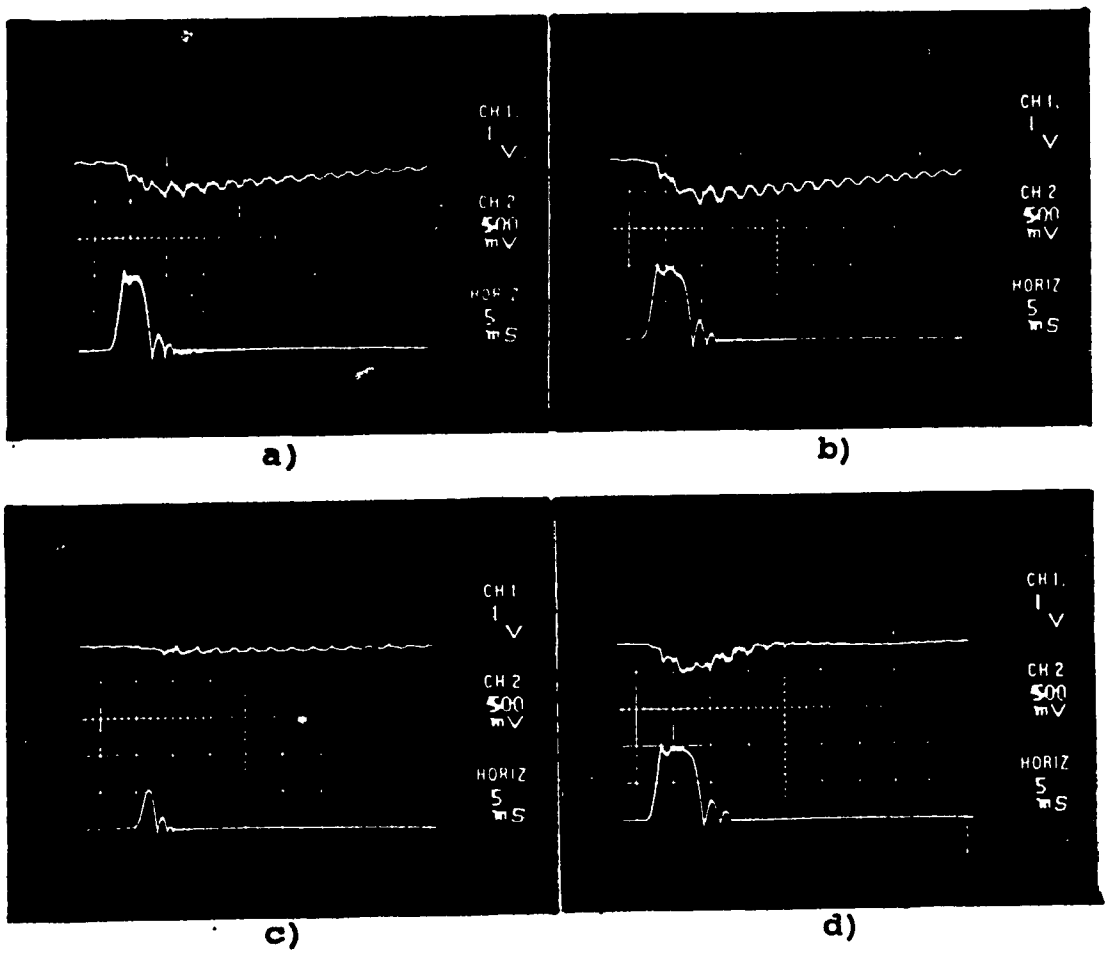

Figure 5.8 Oscillograms of Needle Lift and Pressure Drop for Configuration 3 using Natural Gas.
a) maximum power dose
b) maximum torque dose
c) maximum/minimum idle dose
d) starting dose
Calibration for pressure curve, 6.9 bar/div.
Calibration for needle lift, 0.3 mm/div.

requirement at idle speeds. For this configuration, the metering valve position for both, maximum power and maximum torque was found to be identical, i.e driveability of the engine, is assured without the metering valve position changing. The pressure drop and the metering valve flow area for this configuration have decreased by a large increment as compared to the values obtained for configuration 2.

Figure 5.9 shows the discharge characteristics for configuration 4 for Natural Gas. This configuration is for the multi-point injection system and the results are shown in Table 5.6.

Table 5.6 Configuration 4 results for Natural Gas

Engine Point	Fuel dose (mg)	M. Valve (rev)
max. power	27.86	2.0
max. torque	35.98	2.5
idle	5.22	0.98
starting	45.27	4.0

The volume in this configuration is identical to the one in configuration 3. but the length of the pipes between the metering valve and the injectors is identical to configuration 2. Notice how more evident the pressure waves are regarding the pressure drop curve, as compared

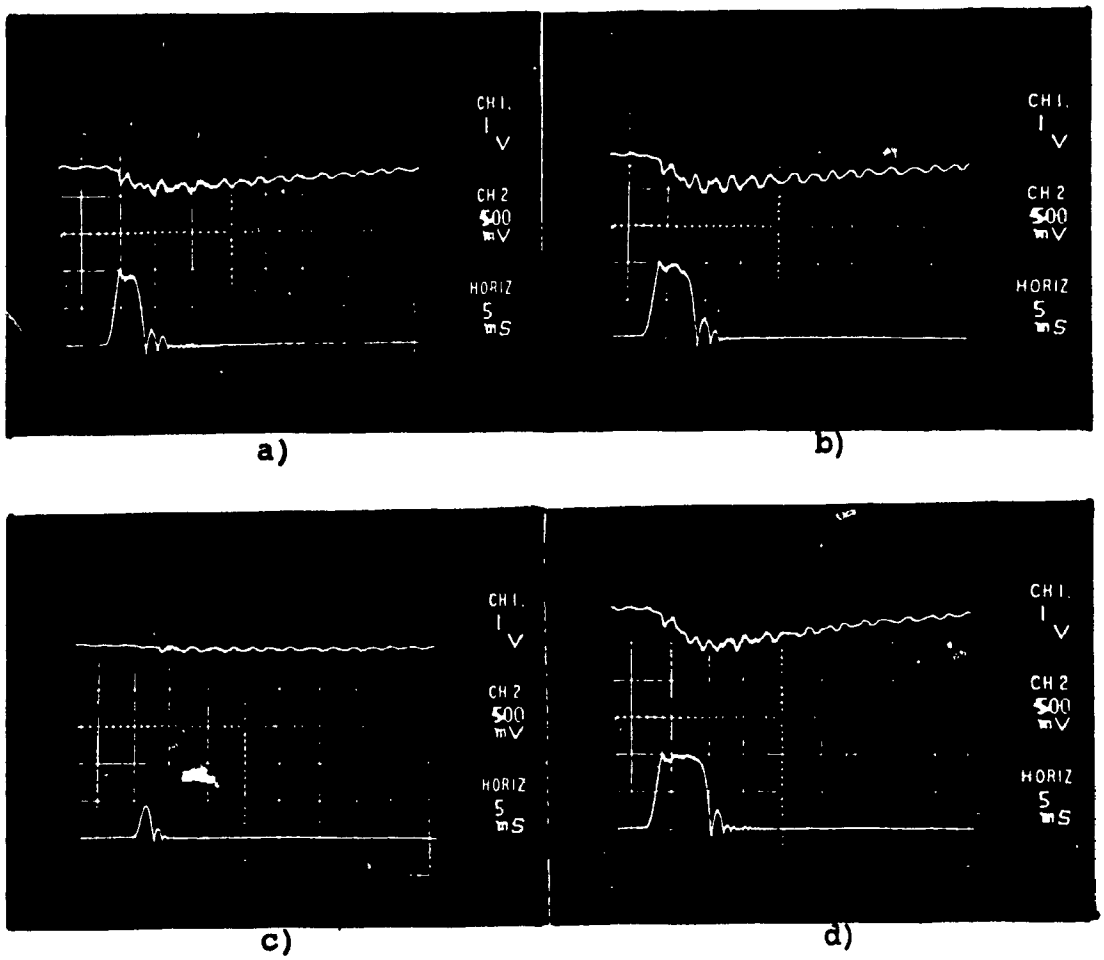

Figure 5.9 Oscillograms of Needle Lift and Pressure Drop for Configuration 4 using Natural Gas.
a) maximum power dose
b) maximum torque dose
c) maximum/minimum idle dose
d) starting dose
Calibration for pressure curve, 6.9 bar/div.
Calibration for needle lift, 0.3 mm/div.

to those in configuration 3. The waves are dampened due to the accumulator effect caused by the volume of the second injector in the pipeline between the metering valve and the first injector; thus, the effects on the pressure drop are minimized, as can be seen from the pressure curves and doses. However, the metering valve position for maximum torque has changed as compared to those observed in configuration 3, no longer maintaining the desired driveability factor found in configuration 3.

From observations made with the four configurations, it can be concluded that there was reduced nozzle chattering and less post-injection in the configurations with higher fuel volume between the metering valve and the injector.

5.2.2 Hydrogen Gas Discharge Characteristics

The tests of the gas discharge characteristics for hydrogen gas were performed for all the configurations mentioned in Table 5.3. The pressure wave amplitudes during the tests were not as disruptive as those found during the tests for Natural Gas. The injector configuration number 2 was used due to the required flow area for Hydrogen gas as calculated in Chapter 3.

Figure 5.10 contains the oscillograms obtained for the fuel discharge characteristics for configuration 1, i.e. with no connecting pipe. Table 5.7 summarizes the fuel doses and metering valve positions. Notice that the effect of the metering valve on throttling of the incoming supply gas is negligible. The pressure rise is almost immediate and leads to higher amounts of leaked gas due to sustained higher pressure in the injector.

Table 5.7 Configuration 1 results for Hydrogen Gas

Engine Point	Fuel dose (mg)	M. Valve (rev)
max. power	13.87	7.5
max. torque	18.25	13.0
idle	3.00	1.05
starting	22.63	8.0

Figure 5.11 are showing the resultant oscillograms of the tests performed with configuration 2 of Table 5.3. Table 5.8 summarizes the results obtained.

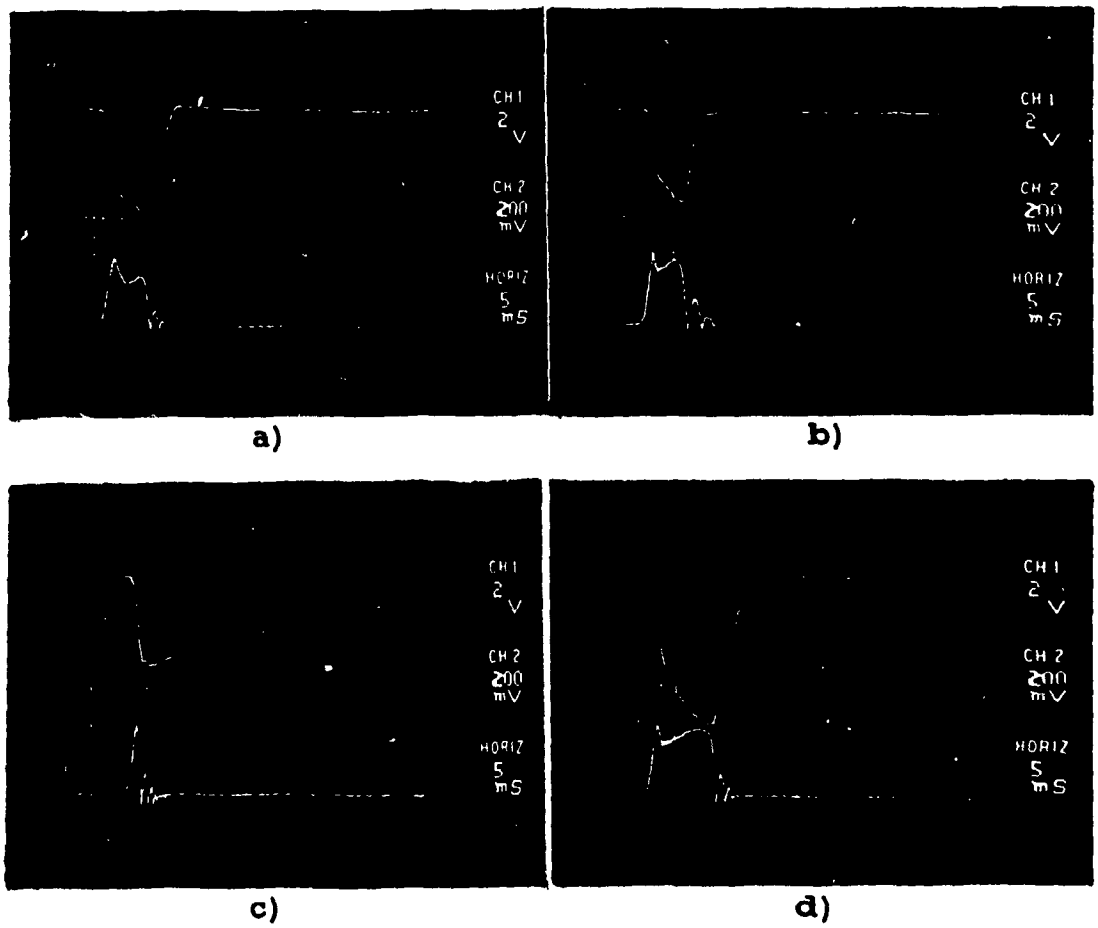

Figure 5.10 Oscillograms of Needle Lift and Pressure Drop for Configuration 1 using Hydrogen Gas.
a) maximum power dose
b) maximum torque dose
c) maximum/minimum idle dose
d) starting dose
Calibration for pressure curve, 13.8 bar/div.
Calibration for needle lift, 0.3 mm/div.

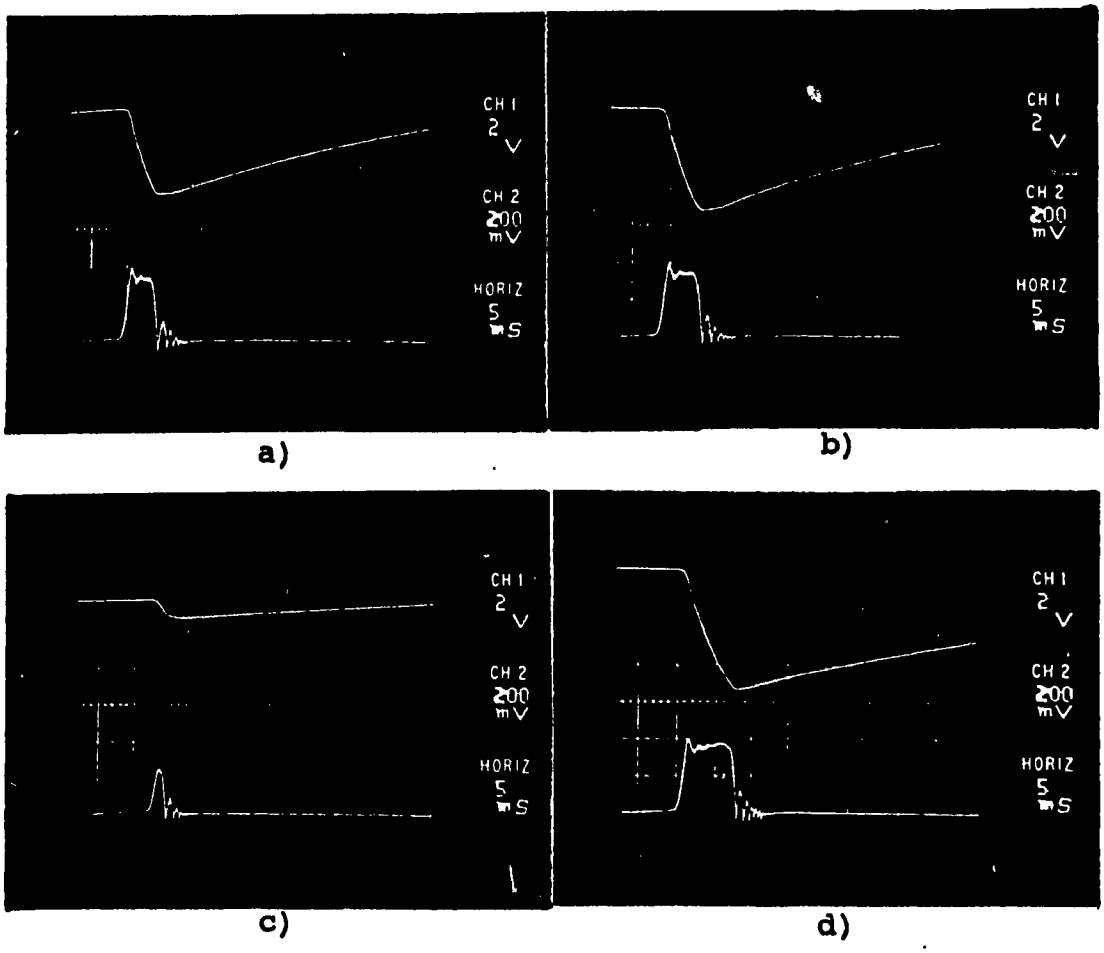

Figure 5.11 Oscillograms of Needle Lift and Pressure Drop for Configuration 2 using Hydrogen Gas.
a) maximum power dose
b) maximum torque dose
c) maximum/minimum idle dose
d) starting dose
Calibration for pressure curve, 13.8 bar/div.
Calibration for needle lift, 0.3 mm/div.

Table 5.8 Configuration 2 results for Hydrogen Gas

Engine Point	Fuel dose (mg)	M. Valve (rev)
max. power	13.87	1.9
max. torque	18.25	1.9
idle	3.00	1.03
starting	23.56	1.25

A large impact of the metering valve opening and additional volume inserted between the metering valve and the injector can be shown by comparing this figure to Figure 5.10. The pressure wave effect is also seen in this series of oscillograms; however, is less disturbing than found previously for Natural Gas.

Figure 5.12 shows the results from tests of configuration 2b. Table 5.9 summarizes the essential values of the test results. Configurations 2 and 2b differ by a cross sectional flow area and a different volume. The first observation is that the metering valve positions are not very different and that there is a definite difference in pressure drop in order to obtain the required doses. The difference is approximately 6 bars at maximum power between the two configurations.

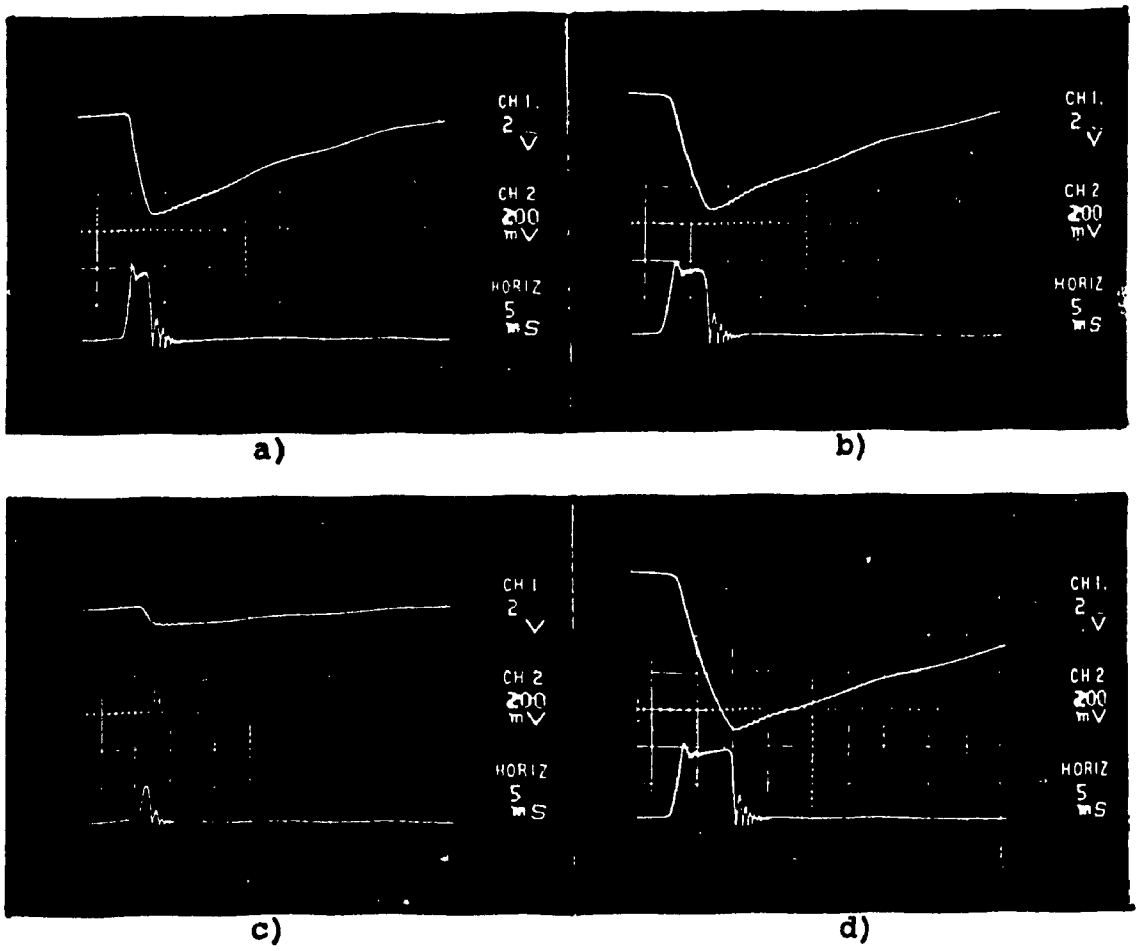

Figure 5.12 Oscillograms of Needle Lift and Pressure Drop for Configuration 2b using Hydrogen Gas.
a) maximum power dose
b) maximum torque dose
c) maximum/minimum idle dose
d) starting dose
Calibration for pressure curve, 13.8 bar/div.
Calibration for needle lift, 0.3 mm/div.

Table 5.9 Configuration 2b results for Hydrogen Gas

Engine Point	Fuel dose (mg)	M. Valve (rev)
max. power	13.87	2.0
max. torque	17.55	2.0
idle	3.00	1.08
starting	22.63	1.5

Figure 5.13 shows the results of test on configuration 3. Table 5.10 summarizes the metering valve positioning and fuel doses achieved. The pressure waves have been dampened more due to the larger gas volume inserted between the injector and the metering valve and the pressure drop has been reduced in half as compared to that in Figure 5.11.

Table 5.10 Configuration 3 results for Hydrogen Gas

Engine Point	Fuel dose (mg)	M. Valve (rev)
max. power	13.87	1.85
max. torque	18.25	1.85
idle	3.00	1.05
starting	23.36	1.3

Figure 5.14 shows the results of configuration 3b tests. The ensuing table summarizes the results.

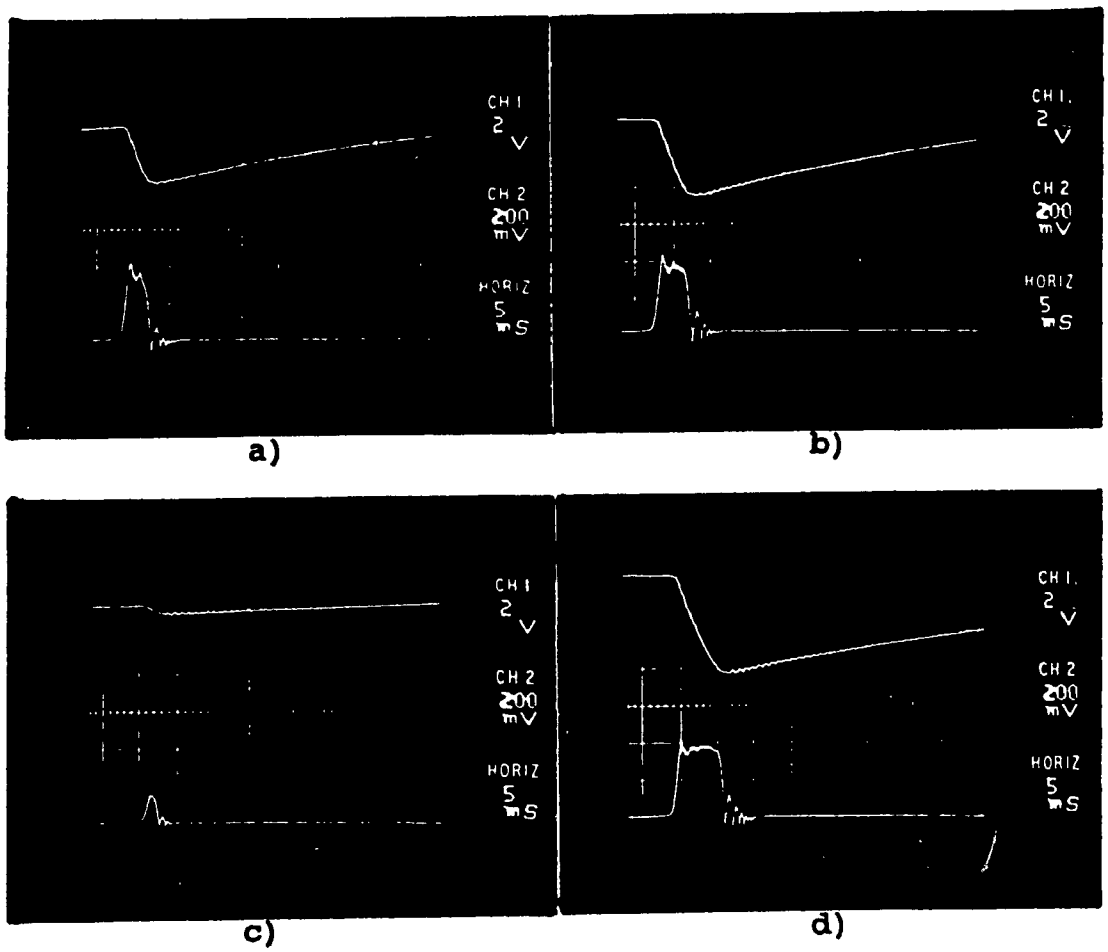

Figure 5.13 Oscillograms of Needle Lift and Pressure Drop for Configuration 3 using Hydrogen Gas.
a) maximum power dose
b) maximum torque dose
c) maximum/minimum idle dose
d) starting dose
Calibration for pressure curve, 13.8 bar/div.
Calibration for needle lift, 0.3 mm/div.

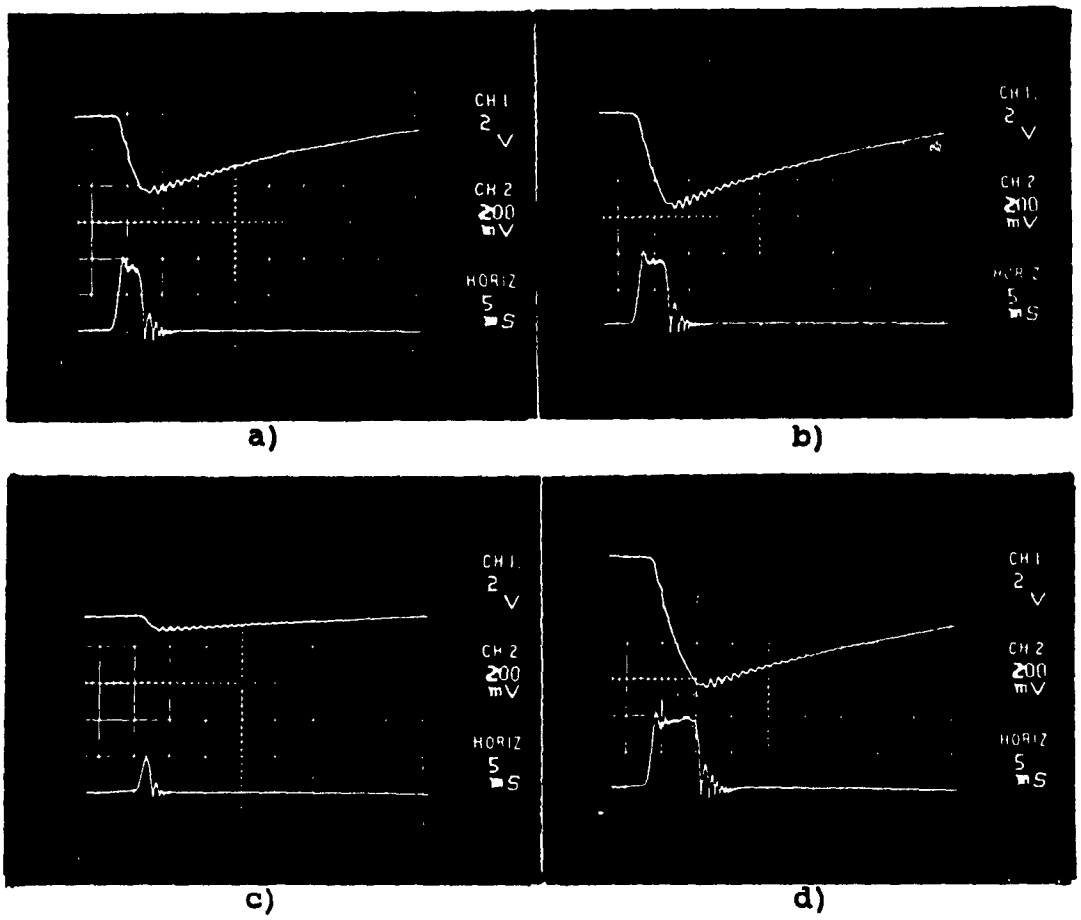

Figure 5.14 Oscillograms of Needle Lift and Pressure Drop for Configuration 3b using Hydrogen Gas.
a) maximum power dose
b) maximum torque dose
c) maximum/minimum idle dose
d) starting dose
Calibration for pressure curve, 13.8 bar/div.
Calibration for needle lift, 0.3 mm/div.

Table 5.11 Configuration 3b results for Hydrogen Gas

Engine Point	Fuel dose (mg)	M. Valve (rev)
max. power	13.87	1.9
max. torque	17.89	1.9
idle	2.63	1.04
starting	23.36	1.4

The results in Figure 5.14 are very similar to those in Figure 5.13, for configuration 3. The only exception is that in this case, the pressure waves are more evident than in configuration 2b. The amplification of these waves is probably due to the larger distance that the pressure wave must travel and that there is a more restrictive cross-sectional area as compared to configuration 2b and 3 respectively.

Figure 5.15 and 5.16 are the test results of configurations 4 and 4b respectively. These tests are for the multi-point injection system, which are the pinnacle for this entire investigation. Table 5.12 and 5.13 summarize the results respectively. In both cases the pressure wave amplitude has been dampened; however, a little less in configuration 4b. All doses have met the requirements and once again, the metering valve positioning is quite similar as is the pressure drop. This can help to determine what direct relation the metering valve position

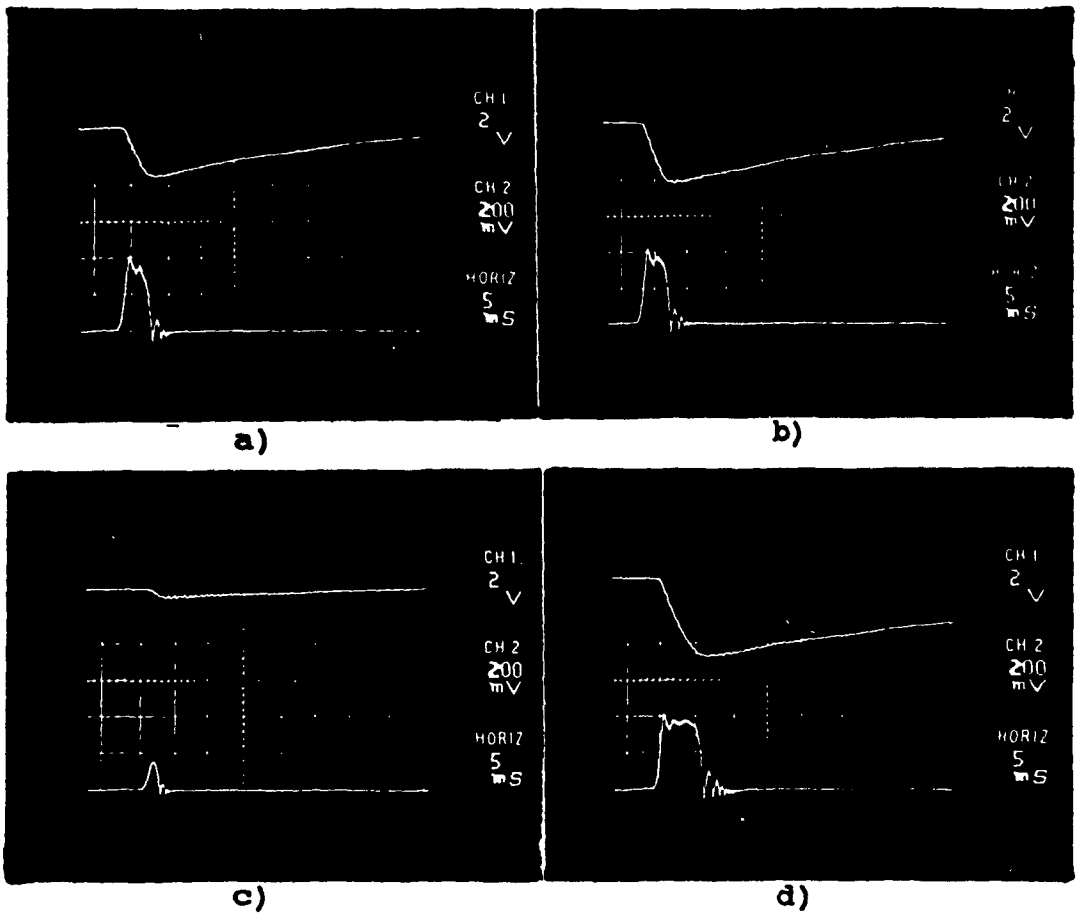

Figure 5.15 Oscillograms of Needle Lift and Pressure Drop for Configuration 4 using Hydrogen Gas.
a) maximum power dose
b) maximum torque dose
c) maximum/minimum idle dose
d) starting dose
Calibration for pressure curve, 13.8 bar/div.
Calibration for needle lift, 0.3 mm/div.

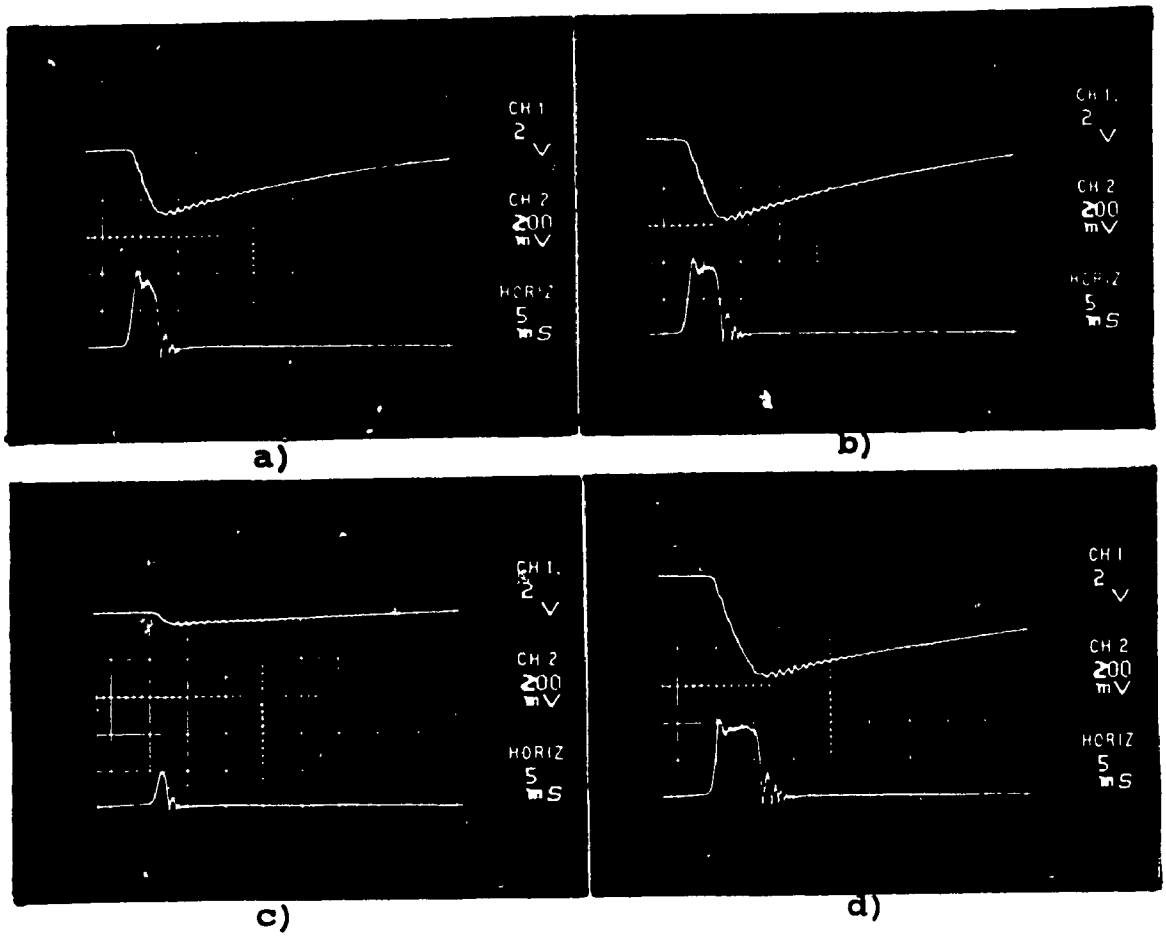

Figure 5.16 Oscillograms of Needle Lift and Pressure Drop for Configuration 4b using Hydrogen Gas.
a) maximum power dose
b) maximum torque dose
c) maximum/minimum idle dose
d) starting dose
Calibration for pressure curve, 13.8 bar/div.
Calibration for needle lift, 0.3 mm/div.

has on the pressure drop, given a known volume between the injector and the metering valve. Furthermore, the pressure drop difference between these two configurations has decreased significantly as compared to the difference in pressure drop between configurations 2 and 2b.

Table 5.12 Configuration 4 results for Hydrogen Gas

Engine Point	Fuel dose (mg)	M. Valve (rev)
max. power	13.87	1.9
max. torque	17.52	1.9
idle	3.00	1.1
starting	22.63	1.3

Table 5.13 Configuration 4b results for Hydrogen Gas

Engine Point	Fuel dose (mg)	M. Valve (rev)
max. power	13.87	1.97
max. torque	17.89	1.97
idle	2.92	1.05
starting	22.63	1.3

Notice that out of all configurations tested, seven of the configurations have met the desired driveability parameter of the engine and that only the first configuration did not. By comparing with Natural Gas, it

seems that there is definitely an effect of the molecular weight and molecular size of the gaseous fuel used during the tests.

5.3 DISCUSSION OF RESULTS

The intent of this discussion is to summarize the experimental results and to outline the key parameters that affect the gaseous injection systems in question. There are several conclusions which can be drawn from the test results with Natural Gas and Hydrogen Gas. Some of the key parameters to analyze are the following: pipe diameter, pipe length, injector configuration and gas dose size to satisfy the engine characteristics, including driveability.

The pipe diameter and pipe length have a definite effect on the pressure wave amplitudes in the injection system and can cause instability in the system, i.e. reasons for which the 3.0 mm pipe was not used in the Natural Gas injection system tests. The smaller the pipe diameter and the longer the length, the higher are the pressure wave amplitudes. This can be shown by comparing Hydrogen Gas tests of configuration 2 and 2b and then comparing 2b and 3b, respectively. This is true for the Natural Gas configurations as well.

The gaseous injection system was tested in different configurations in order to establish the best possible design, when delivering the required fuel doses. It was shown that the larger the volume between the injector and the metering valve, the easier it was to meet the required

fuel doses at higher speeds; however, much more difficult to achieve the required dose at low speeds.

In the case of the multi-point injection system, there were several points observed. The points are: a) It maintained a higher volume, such as configurations 3 and 3b. b) It fed multiple injectors; thus, decreasing costs of piping and metering valves required in an engine. And c) it met all the required engine characteristics and met the driveability requirements.

6. ANALYTICAL MODEL VALIDATION

The objective of this investigation is to develop a new type of injection system for gaseous fuels. In order to develop such a system, there are certain steps that must be performed. An experimental investigation is required to find out, what possible characteristics the injection system possess and whether it can meet the requirements of an engine's operating characteristics. Then, a method of prediction and optimization for such a system must be developed which is necessary to achieve desired improvements of the existing gas injection system. Thus, in order to predict the behavior and to optimize the injection system, a mathematical model must be developed, as was presented in Chapter 4, and it must be validated by comparing to the actual test results, such as the experimental results discussed in Chapter 5.

This comparison determines how close the gas injection system can be simulated for a given injection system on a particular engine. First, several simulation results will be shown plotted against the experimental results for both Natural Gas and Hydrogen. This will be followed by a discussion on the sources of error or discrepancies between the simulation results and the test results.

6.1 ANALYTICAL AND EXPERIMENTAL RESULTS COMPARISON

The following configurations were simulated, on the computer via simulation code in Appendix G, and plotted against the experimental results. Configurations 1 and 2 were chosen for Natural Gas, and configurations 2 and 4 were chosen for Hydrogen to be simulated. These configurations were chosen to reflect all the possible configurations described in Chapter 5. The validation of the model is performed not only on the gas dose value, but also on two additional parameters, pressure in the injector, and injector needle displacement.

Figures 6.1 and 6.2 compare the simulated results and the experimental results of configuration 1 and configuration 2 for Natural Gas, while Figures 6.3 and 6.4 show the comparison for configurations 2 and 4 for Hydrogen. While the injector pressure and needle motion is compared in the figures, the dose values are tabulated in the following table with the metering valve position and pressure drop for both experimental and simulated results.

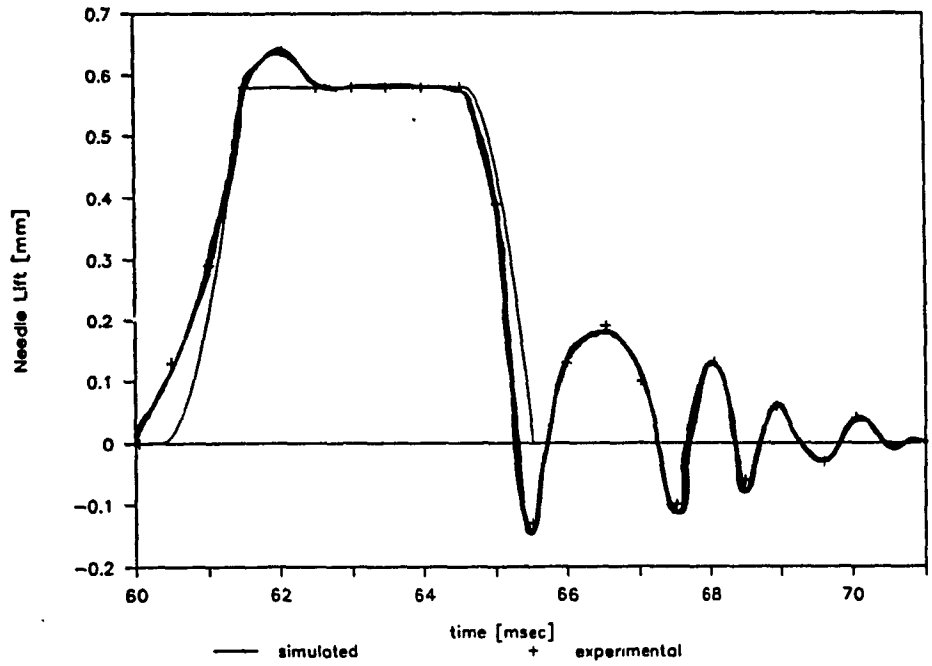

a) Needle Lift versus Time

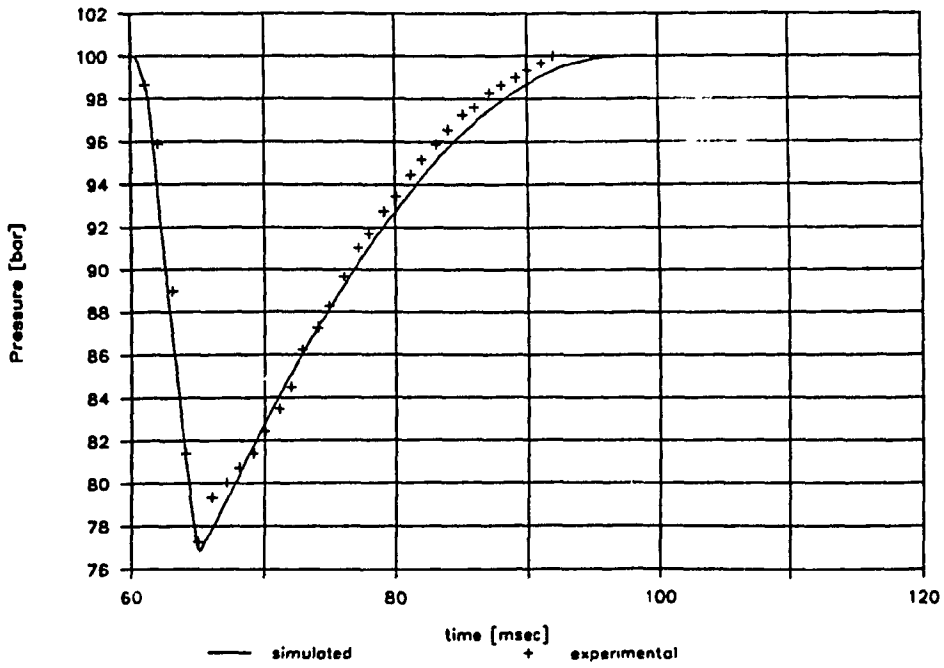

b) Pressure versus Time

Figure 6.1 Comparison of Experimental and Simulated Results for Configuration 1 using Natural Gas.

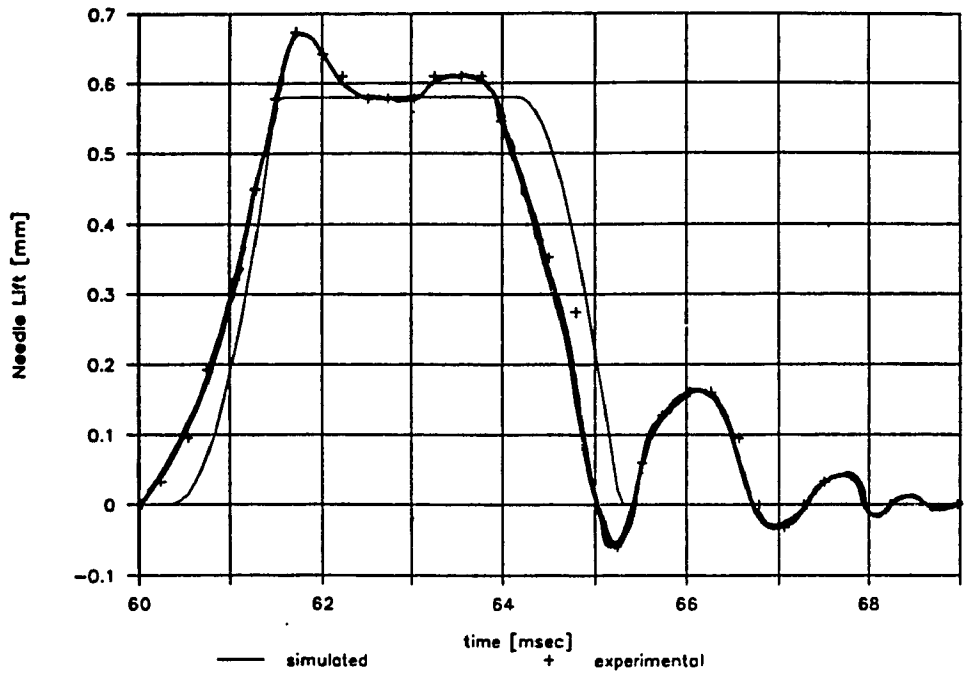

a) Needle Lift versus Time

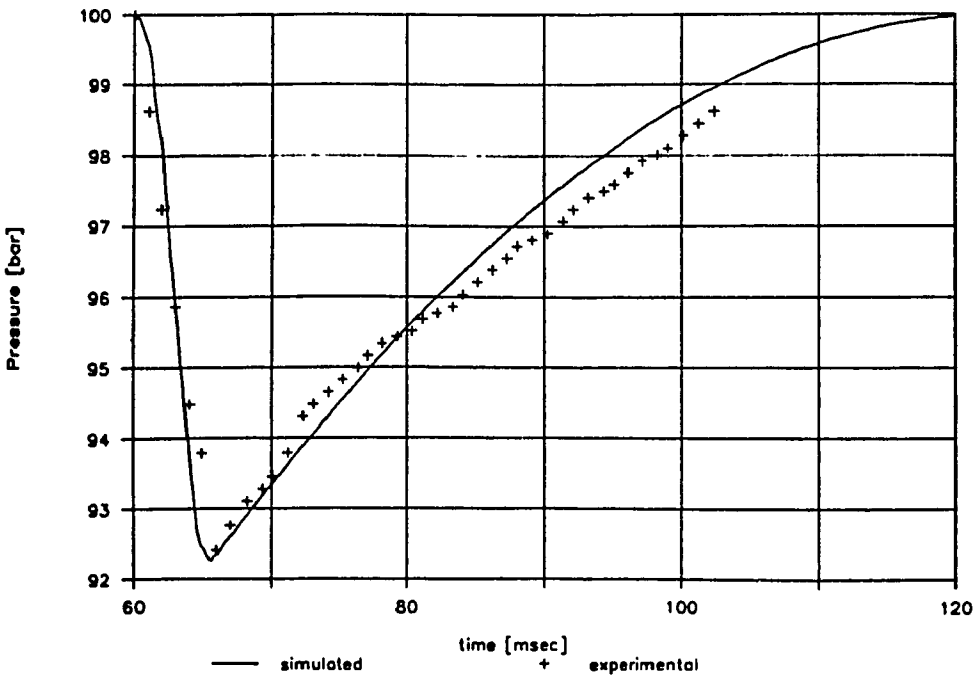

b) Pressure versus Time

Figure 6.2 Comparison of Experimental and Simulated Results for Configuration 2 using Natural Gas.

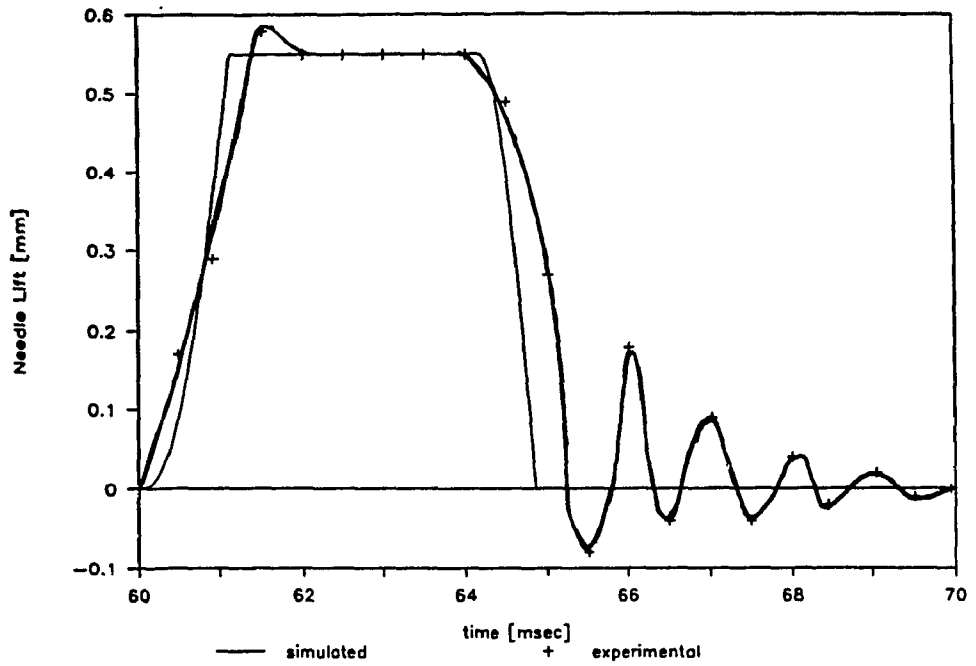

a) Needle Lift versus Time

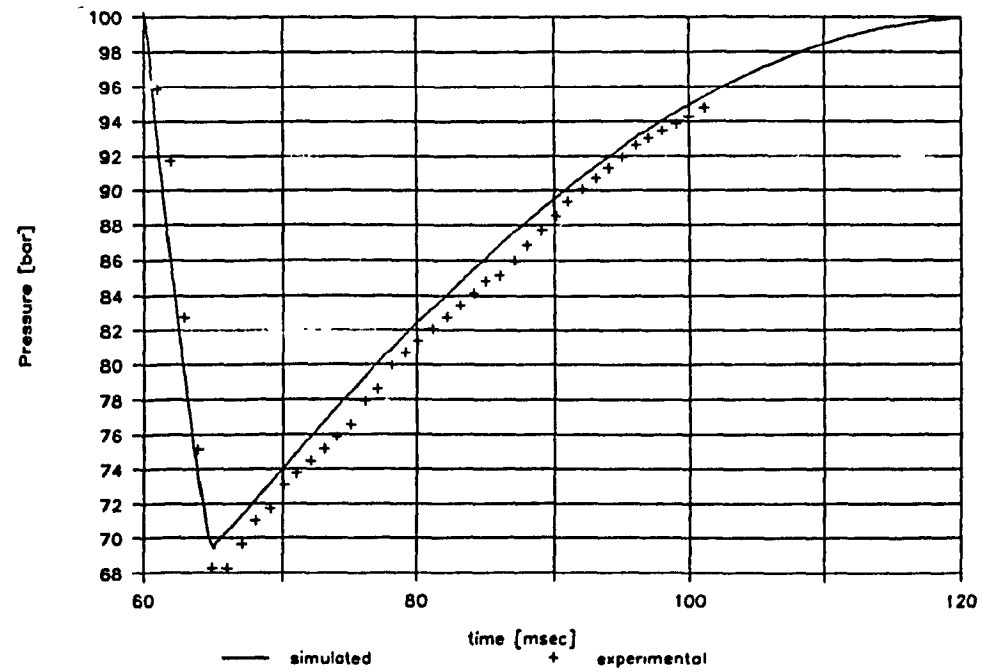

b) Pressure versus Time

Figure 6.3 Comparison of Experimental and Simulated Results for Configuration 2 using Hydrogen Gas.

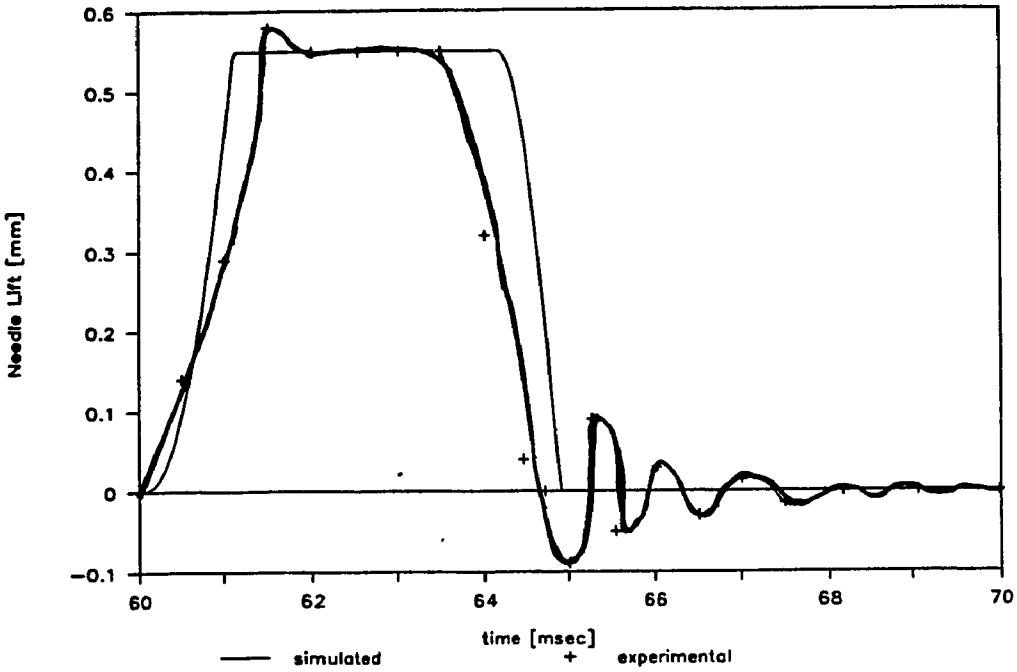

a) Needle Lift versus Time

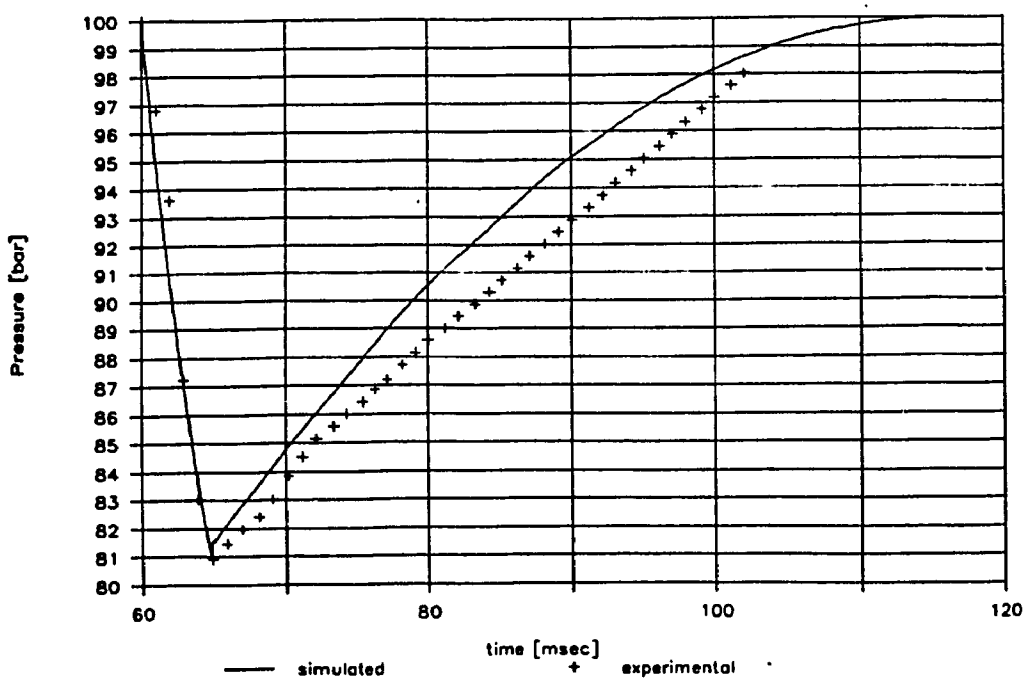

b) Pressure versus Time

Figure 6.4 Comparison of Experimental and Simulated Results for Configuration 4 using Hydrogen Gas.

Table 6.1 Summary of Experimental and Simulated Results

Conf.	Gas	Press. drop		M.V. revs.		Gas dose	
		sim.	exp.	sim.	exp.	sim.	exp.
1	CH_4	23.0	22.8	4.0	3.5	25.8	27.9
2	CH_4	7.82	7.59	4.2	2.85	28.2	27.9
2	H_2	30.4	31.7	3.5	1.90	12.8	13.9
4	H_2	19.3	19.1	4.3	1.90	14.1	13.9

Notice that for the pressure drop and the gas dose, the percentage difference between the experimental and simulated results is within a range of 10 %. The only variables that can be changed in the simulation code is the injector timing, ψ, which is adjusted in degrees of the crank, and the metering valve opening, y. The only larger discrepancy found in the entire comparison is the metering valve positioning. The sources of possible errors in the metering valve opening will be discussed in the ensuing section.

The overall result of the comparison is that the simulation results quite closely match the experimental results; thus, validating the mathematical model developed in Chapter 4. Furthermore, it will be shown that a simplified model can be developed which excludes the pressure wave effects and; therefore, requires less time to simulate the injection process; this will be discussed further in Chapter 7.

6.2 ERROR ANALYSIS

There are three different possible causes of error for the discrepancy between the experimental results and the simulated results. The three possibilities are the following: 1) reading of the oscillograms, 2) metering valve positioning and 3) volumetric calculations.

The oscillograms, as shown in Chapter 5, were quite difficult to interpret correctly. A millimeter of error on the curve for the pressure drop could result in a 1.5 bar difference. Note also that the pressure transducer was not located in the injector chamber, but at a distance of some 40 mm away from the actual point of observation; this was another source of error. The same could be said for the LVDT which was not located exactly on the injector needle, but was attached to the solenoid armature. Thus, the needle could move separately while the solenoid was still dissipating its energy field. This possible source of error from the LVDT is the evidence of overshoot and bouncing in the oscillograms; the measurements could be a little out of phase from the actual needle motion. Also, the bouncing has the effect of adding additional fractions of thefuel dose to the experimental values, while in the simulation code bouncing is omitted. Another source of error could be anticipated for the pressure transducer in

the dose measuring chamber; it may have deviated from the calibration regime, even though it was recalibrated after each experiment for a particular fuel dose.

The largest source of discrepancy results from the evaluation of the metering valve position. In the model simulation for the metering valve, the first attempt was to use the theoretical approach and to calculate the flow area; however, a larger discrepancy was observed when matching the experimental results to the analytical ones. Thus, the manufacture's data, Appendix D, was taken into account, as discussed in Chapter 3. Knowing the C_v, flow coefficient for water, the metering valve flow area was calculated, using water as the medium and with the use of basic flow equations given by the manufacturer. Thus, the metering valve flow area found was corresponding to the flow coefficient of the metering valve and then the flow area was matched to the notches on the thimble of the metering valve. This relationship of metering valve flow area to the notches permitted the correction of the major part of the discrepancy in metering valve positioning, and allowed the validation of the injection process, shown previously.

The last source of error to be discussed was the inaccuracies in determining the volumes in the pipes, connections, in the injector and metering valve. In the case of the pipe diameter it was assumed without production

tolerances, stating it at nominal value of 4.5 mm diameter when the real diameter was 5.5 mm. Also, some tees and bends have been omitted, which have caused a lower estimation of the actual volume in the system and it may have also been reflected on the pressure wave simulations. The injection chamber volume was easy to measure, but the pressure transducer was more difficult to measure, what would add to the inaccuracy of the volume estimation.

In summary, after all corrections, the simulated results quite closely matched the experimental results. With a little more parameter tuning and more precise assumptions and measurements, the simulated results could even more closely match the experimental results. Some of the parameters to tune are the effective solenoid force, the injection duration, the discharge coefficients for the metering valve and the injector, the gas flow friction in the pipe and the addition of some minor losses in the conduits. Also, with more attention being paid to the metering valve positioning and to the calibration of pressure transducers and LVDTs, the results would be more reflective of the actual process.

7. IMPACT OF SYSTEM DESIGN PARAMETERS ON THE INJECTED GAS DOSE

The intent of this chapter is to use a simplified model, as compared to that described in Chapter 6, and to use it in order to optimize the design and to predict the functioning of the electronically controlled gas injection system.

The present problem existing with the detailed model, is the long time required to complete one simulation cycle which amounts to approximately one half hour to perform all the iterations and to reach non-zero flow conditions within the fuel pipeline. Thus, the objectives of the simplified model are to decrease the number of iterations required to attain the steady engine operating state, while maintaining a sufficient degree of accuracy.

The test results presented in Chapter 5, are showing that there is not a big impact of the system volume distribution on the injected gas dose and that the most important factor affecting the dose is the total system volume, included behind the metering valve critical flow area. The latter is throttling the flow of the gas to the injection system and is providing some kind of barrier which isolates the system from the gas supply line. Therefore, a lumped volume assumption in making a simulation model of the injection system has its

justification; however, it would be limited rather to the injection systems for lower speed engines, as in large truck diesel engines. In some cases of high speed diesel engines, the injection system time would become shorter and the impact of the pressure waves on the injected gas dose will be more significant.

The proposed [illegible] gaseous fuel injection [illegible] shown in Figure 7.1, should be evaluated regarding its ability to inject a particular dose of gas within the required time limit. To control the gas dose, the design parameters of the gaseous injection system should be altered. There are two groups of design parameters: a) incorporated design parameters, which are included into the system components, and b) variable design parameters, which can be altered during the operation of the gaseous fuel injection system.

The incorporated design parameters for the gaseous fuel injection system are:

1) injector nozzle orifice flow area: A_o
2) injection system total volume : V_2
3) injector system supply pressure : P_1

The variable design parameters for the gaseous injection system are:

1) the metering valve flow area : A_{12}
2) the injection duration time : t_{inj}

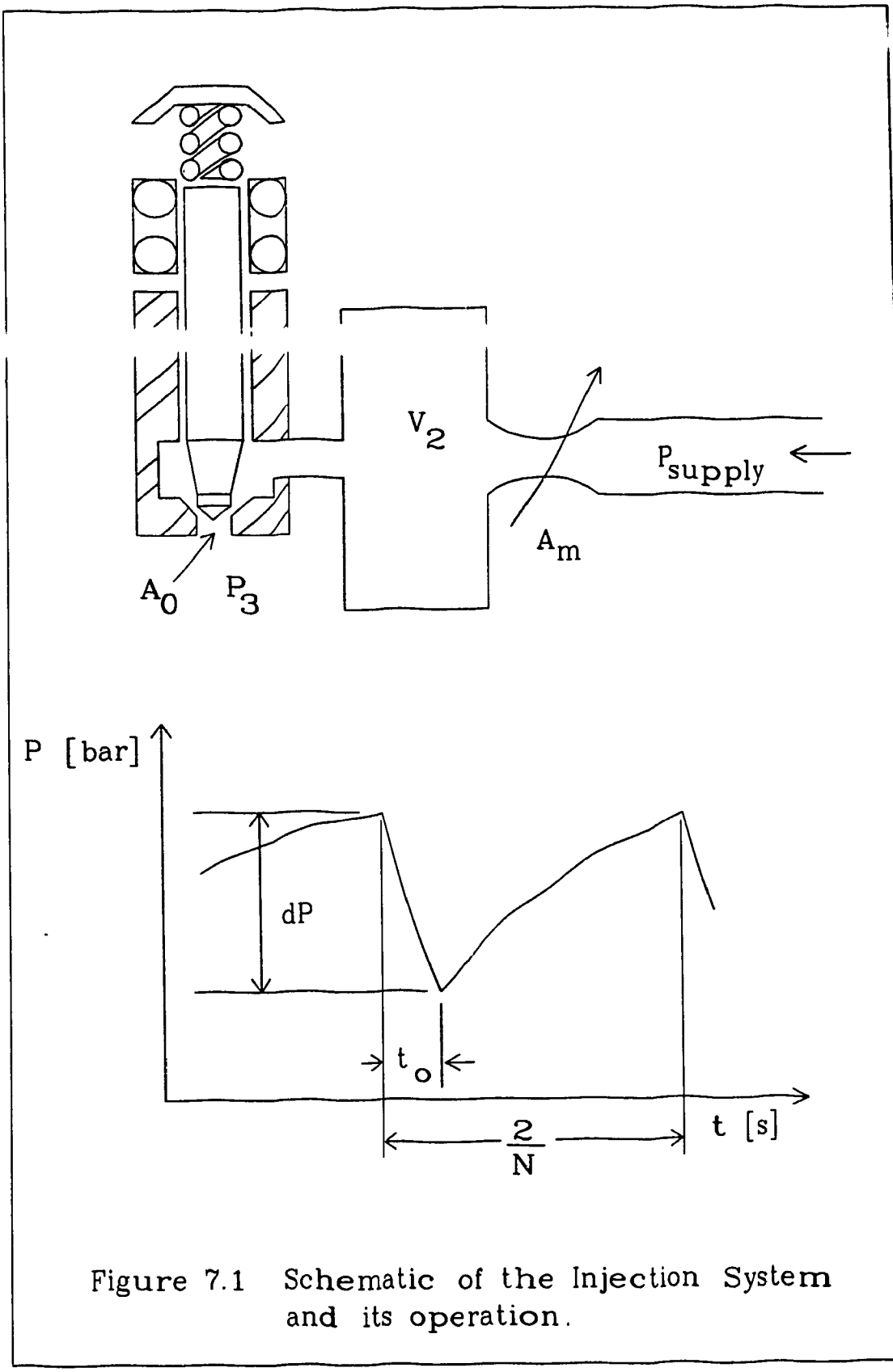

Figure 7.1 Schematic of the Injection System and its operation.

These parameters will be used in order to help to optimize the gaseous fuel injection system, via the simplified model simulations.

7.1 SIMPLIFIED MODEL OF THE GASEOUS FUEL INJECTION SYSTEM

Based on Figure 7.1, the simplified mathematical model can be developed and used to calculate the injected gas dose under certain engine operating conditions. For this purpose, there is no special need to fully simulate the unsteady flow characteristics, i.e no pressure wave influence would be considered. Instead, only the injection system lumped volume between the metering valve and the injector would be included in the simulation. This volume in the open system, between the metering valve restriction and the injector nozzle orifice, will be considered to be a control volume, as shown in Figure 7.2.

The following equations are used to describe the events surrounding the control volume:

$$\dot{m}_i = \dot{m}_e + \frac{dm_{cv}}{dt} * dt \qquad (7.1)$$

or

$$A_{12} U_{12} \rho_{12} = A_o U_o \rho_o + \frac{dP_2}{dt} * \frac{V}{RT} * dt \qquad (7.2)$$

Calculations are done for Δt intervals from t_o to t_f to find the velocity of the gas, U_o, and thus the dose will be calculated by integrating $\dot{m}_e$ from t_0 to t_{inj}.

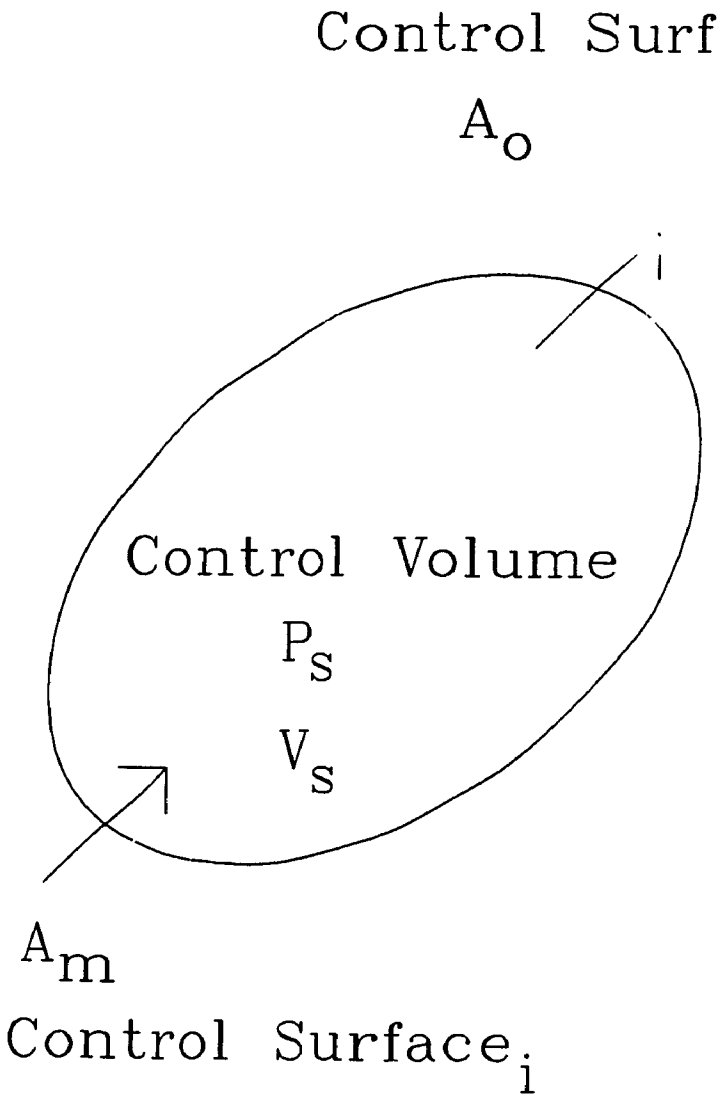

Figure 7.2 Control Volume approach mass calculation

The following is a list for the model simplification assumptions:

1) The changes of physical properties of the gas inside the control volume are instantaneous, i.e. the propagation of the pressure waves across the control volume occurs at an infinite velocity. This assumption is justified by the following: assuming an injection duration of 5 ms, the distance between the metering valve and the injector orifice is 0.250 m and the velocity of sound is 300 m/sec for Natural Gas and 1300 m/sec for Hydrogen Gas at 100 bar pressure. Then, for the case of Natural Gas, the time for the pressure wave to traverse the distance is 0.83 ms; thus, the pressure wave traverses 3 times during the injection period. It allows us to assume that the pressure in the injection system can be considered constant for the simplified calculations.

2) The injector processes are assumed isothermal. They occur in ambient room temperature (see test description in Chapter 5) without any heat release and adiabatic compression or expansion processes.

3) The alternative gaseous fuels, Hydrogen and Natural Gas, can be considered as ideal gases under isothermal conditions, i.e. with no significant changes in the gas constant of either gas.

7.1.1 Results and Validation of the Simplified Model

Calculations have been performed using the aforementioned simplified injection system model. The gas doses obtained were calculated for the same conditions as the test results, shown in Chapter 5. The results of these calculations are shown in Tables 7.1 and 7.2 for Natural Gas and Hydrogen Gas respectively.

Table 7.1 Comparison of Simulated Results and Experimental Results using Configuration 1 with Natural Gas

Eng. Point (rpm)	Injection time (ms)		Metering Position (rev)		Fuel Dose (mg)		Pressure Drop (bar)	
	exp	sim	exp	sim	exp	sim	exp	sim
2000	5.2	4.9	3.5	4.0	27.8	27.5	21.4	18.6
1600	6.2	5.8	10.	10.	36.0	35.9	13.8	16.1
600	7.2	6.9	10.	10.	44.1	43.6	16.5	18.5

Table 7.2 Comparison of Simulated Results and Experimental Results using Configuration 1 with Hydrogen Gas.

Eng. Point (rpm)	Injection time (ms)		Metering Position (rev)		Fuel Dose (mg)		Pressure Drop (bar)	
	exp	sim	exp	sim	exp	sim	exp	sim
2000	5.6	5.4	7.5	7.5	13.9	13.9	40.0	45.4
1600	6.1		13.	13.	18.2	17.5	34.5	31.5
600	9.0	1.	8.0	7.0	22.6	22.6	55.2	59.1

Notice from the two tables how close the comparisons are in both fuel dose and metering valve positioning, as compared to the simulations done in Chapter 6. There is a higher degree of error in the injection time and in the pressure drop, but not for all cases. This is probably due to the model neglecting the pressure wave effects on the injection process and to the inaccurate positioning of the metering valve. If the metering valve positioning were to be corrected, the error could perhaps be smaller on the injection duration. Also, the bouncing of the needle has to be taken into account, since it results in an additional amount of fuel: there is no accounting done for the bouncing effect in the model presented.

Summarizing, the range of error is well within 10 percent and the simulated results in general conform with the experimental results. Thus, the simplified model can be considered useful in developing a gas injection system and predicting its behavior.

7.2 EFFECT OF DESIGN PARAMETER VARIATIONS ON THE INJECTED GAS DOSE AND PRESSURE DROP IN THE INJECTOR

The calculated gas doses presented in Tables 7.1 and 7.2 have been included in the plots showing fuel dose versus the opening of the metering valve flow area for various configurations. Also, the pressure drop in the injector volume has been plotted versus the metering valve flow area, and the gas dose has been plotted versus the injection time. The graphs in Figures 7.3 through 7.16 are showing the results obtained for Natural Gas and Hydrogen injections, for three different engine speeds: maximum power, maximum torque and starting.

The obtained simulation results can be used to predict the effect of the design parameters of the fuel injection system on the dose of gas injected and on the pressure drop in the injector volume. By substituting different design parameters and calculating the gas dose and pressure drop, the relationship between the dose and the design parameter variation can be calculated and plotted on a graph. Thus, having such graphs for several design parameters, optimization of the design of the injection system could be performed. Such graphs are useful since they reduce the need to test different configurations; thus, reducing the necessary time and costs in developing a new gaseous fuel injection system.

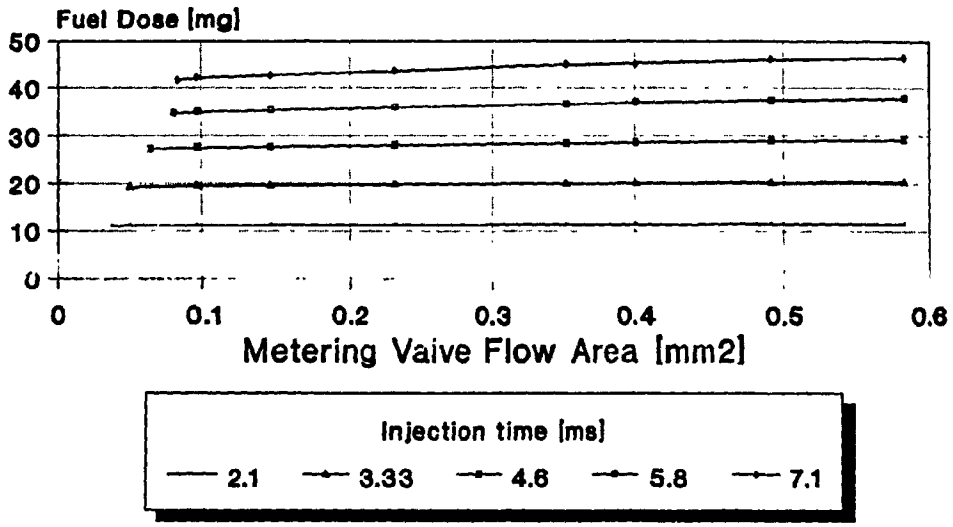

Figure 7.3 Fuel Dose vs Metering Valve Flow Area at 2000 rpm for Natural Gas.

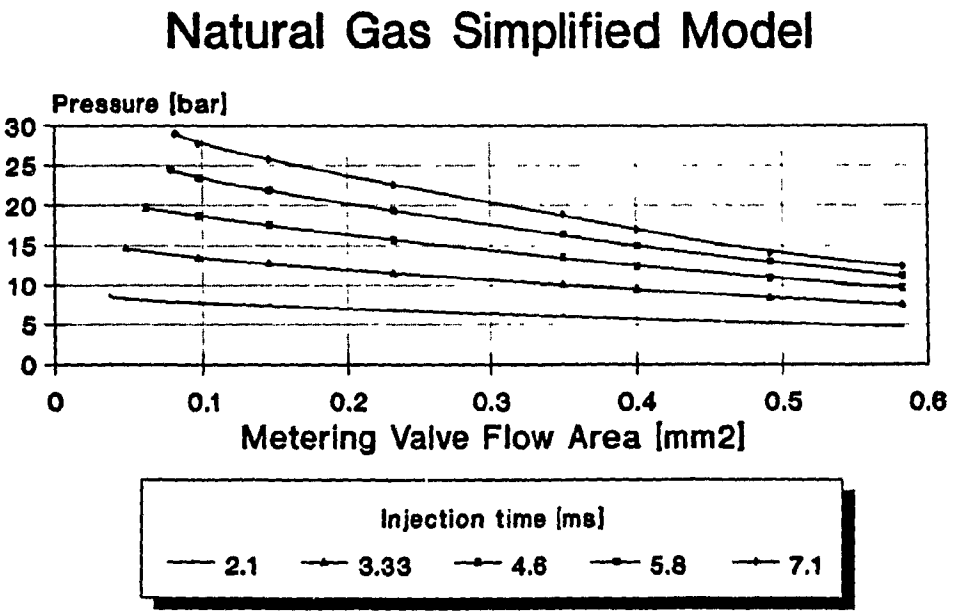

Figure 7.4 Pressure vs Metering Valve Flow Area at 2000 rpm for Natural Gas.

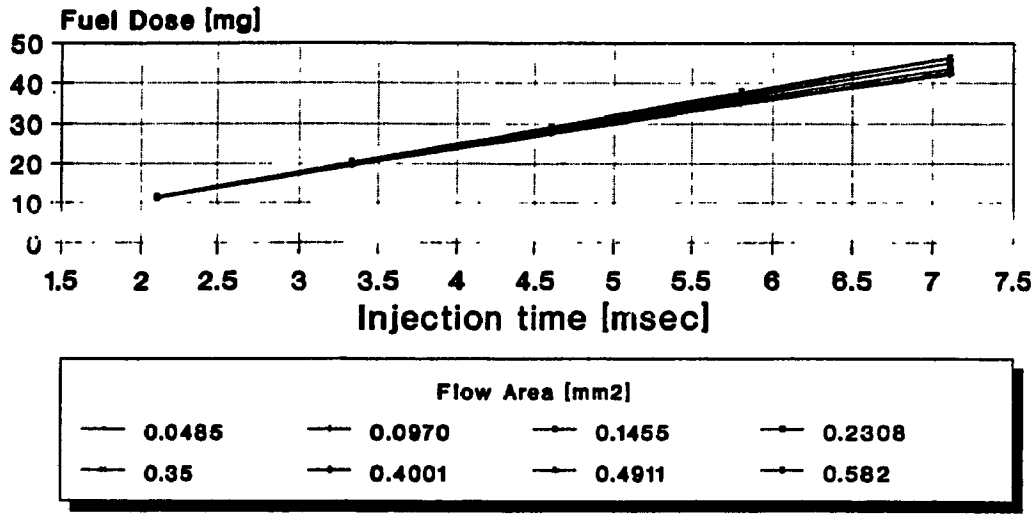

Figure 7.5 Fuel Dose vs Injection Time for Natural Gas at 2000 rpm.

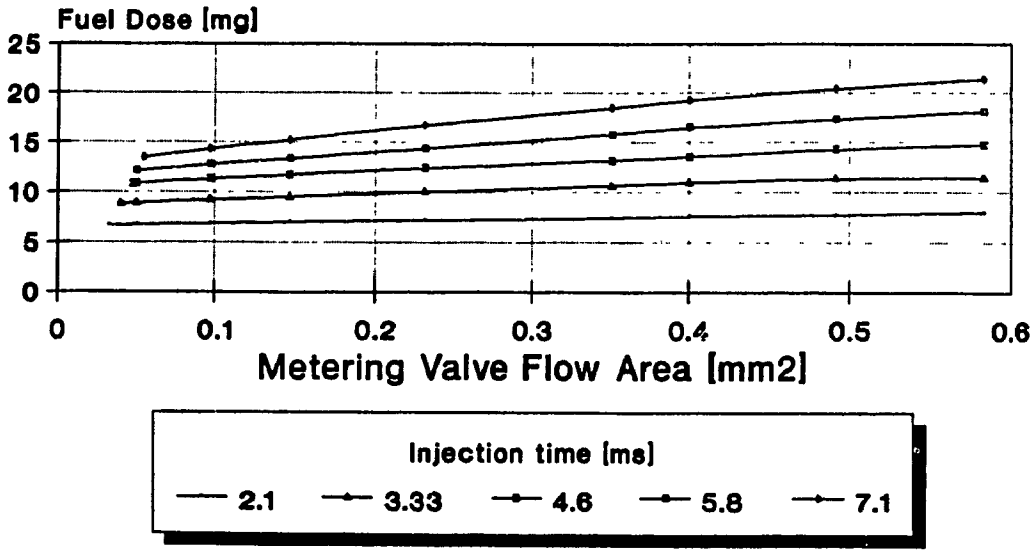

Figure 7.6 Fuel Dose vs Metering Valve Flow Area at 2000 rpm for Hydrogen Gas.

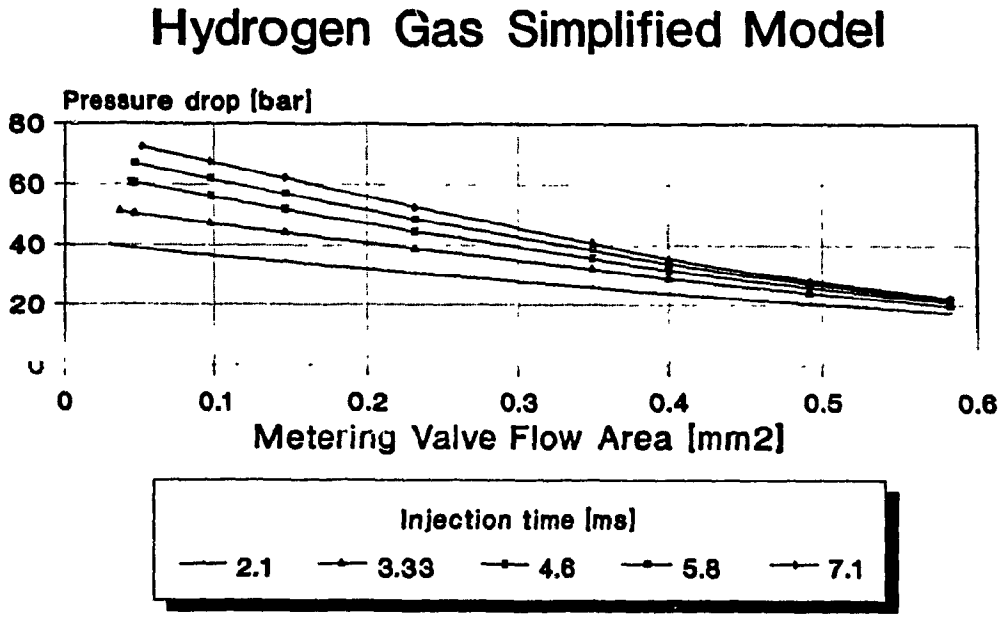

Figure 7.7 Pressure vs Metering Valve Flow Area at 2000 rpm for Hydrogen Gas.

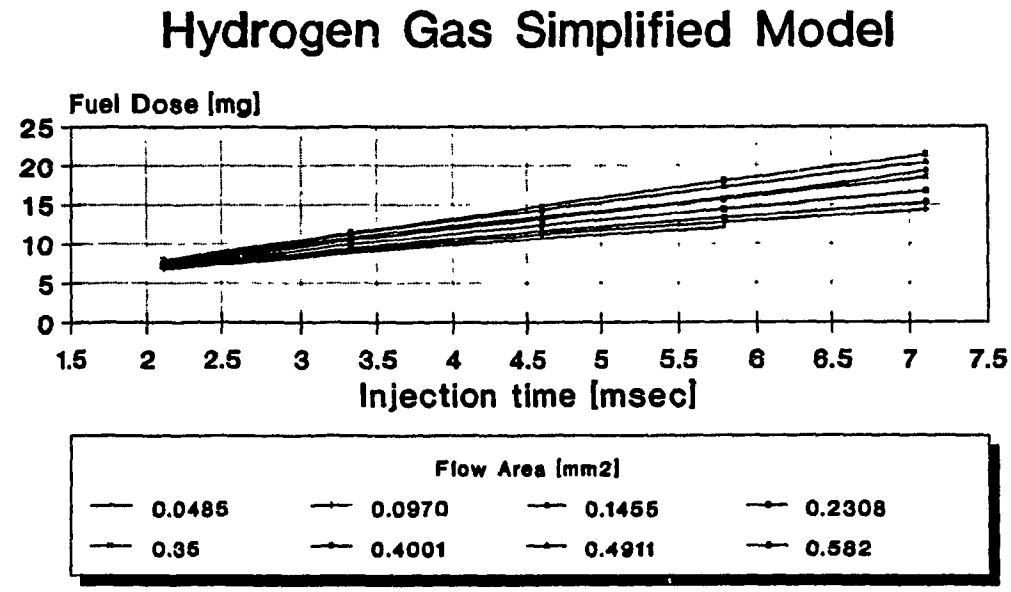

Figure 7.8 Fuel Dose vs Injection Time for Hydrogen Gas at 2000 rpm.

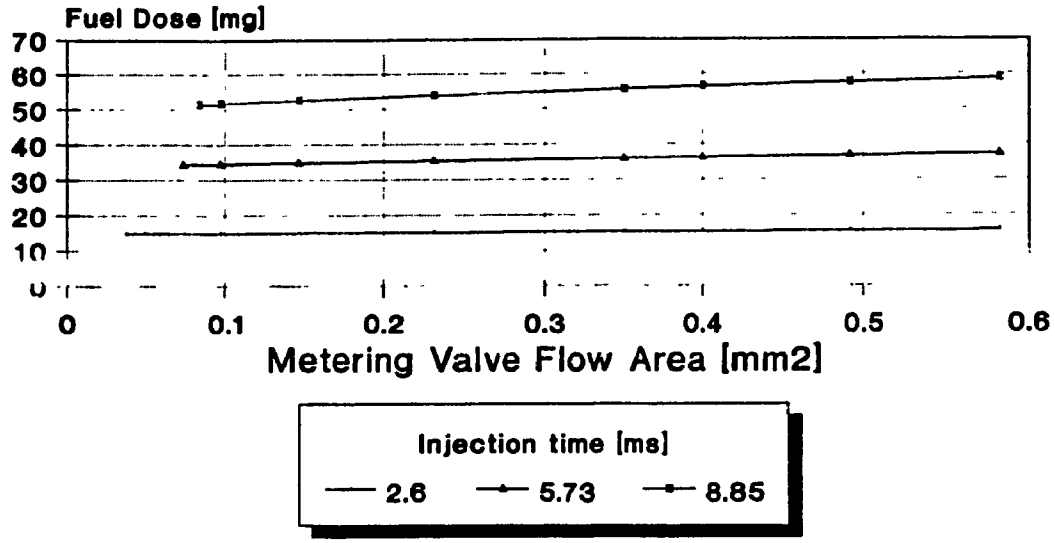

Figure 7.9 Fuel Dose vs Metering Valve Flow Area at 1600 rpm for Natural Gas.

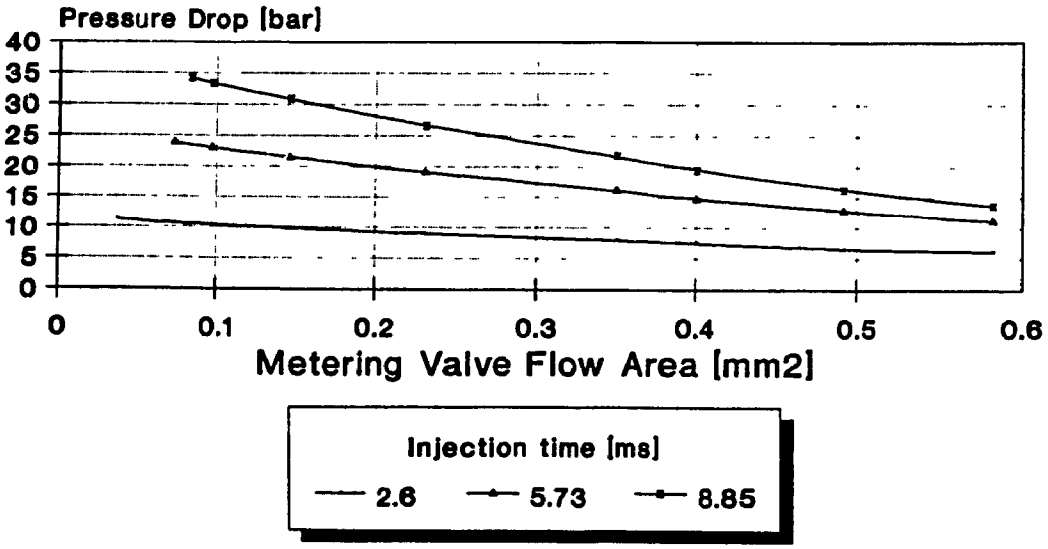

Figure 7.10 Pressure vs Metering Valve Flow Area at 1600 rpm for Natural Gas.

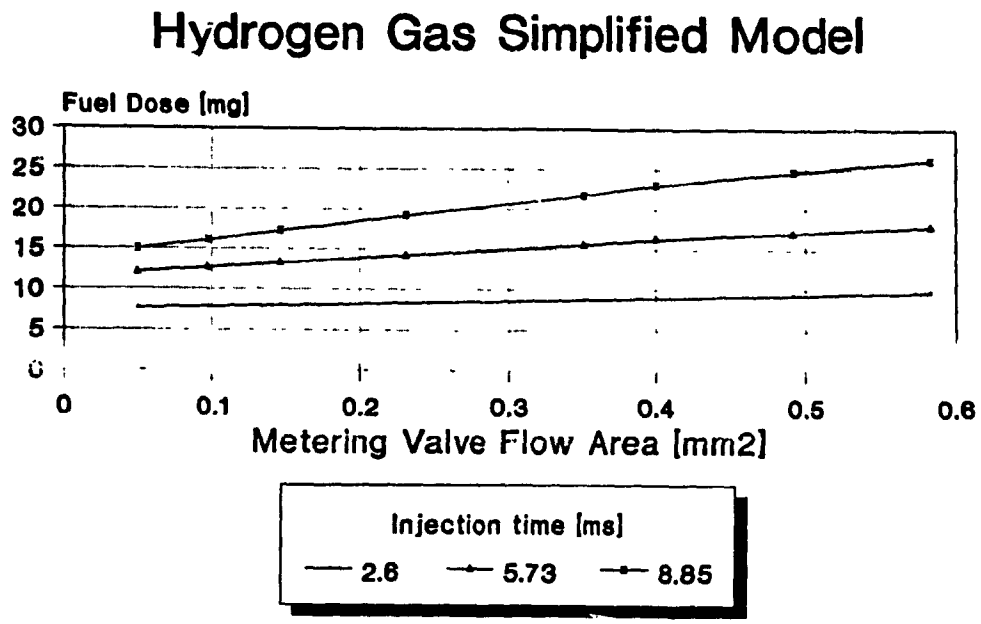

Figure 7.11 Fuel Dose vs Metering Valve Flow Area at 1600 rpm for Hydrogen Gas.

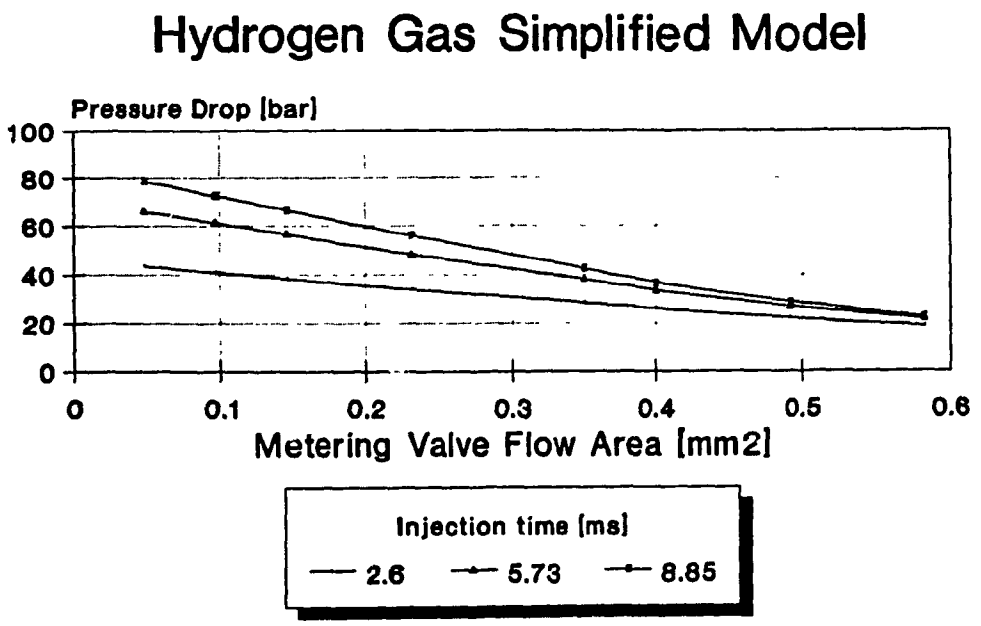

Figure 7.12 Pressure vs Metering Valve Flow Area at 1600 rpm for Hydrogen Gas.

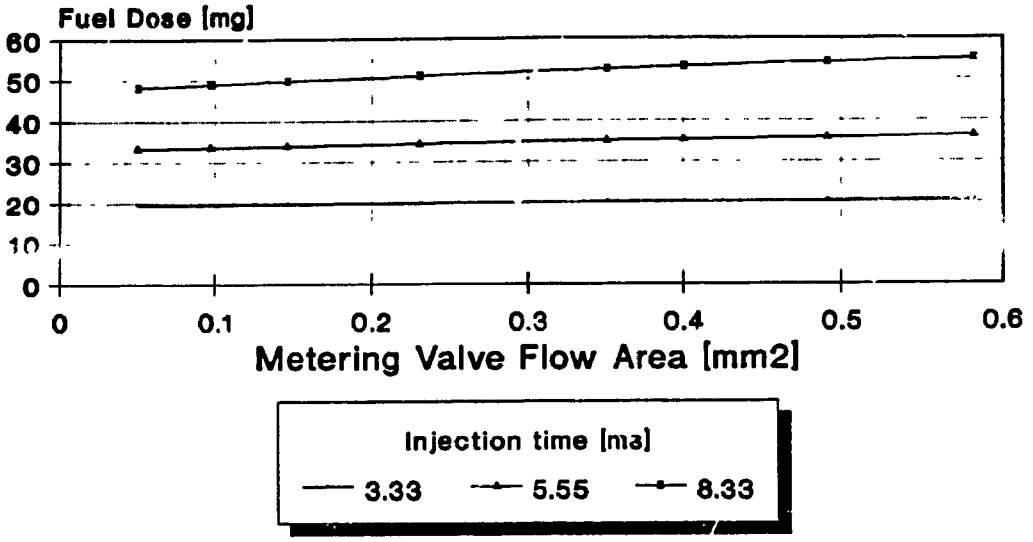

Figure 7.13 Fuel Dose vs Metering Valve Flow Area at 600 rpm for Natural Gas.

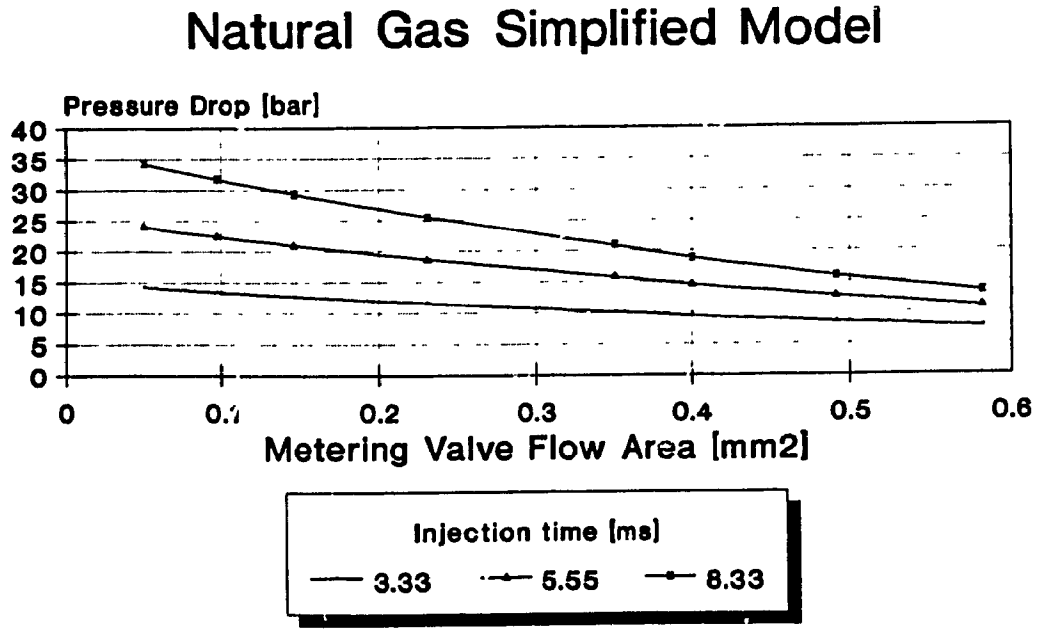

Figure 7.14 Pressure vs Metering Valve Flow Area at 600 rpm for Natural Gas.

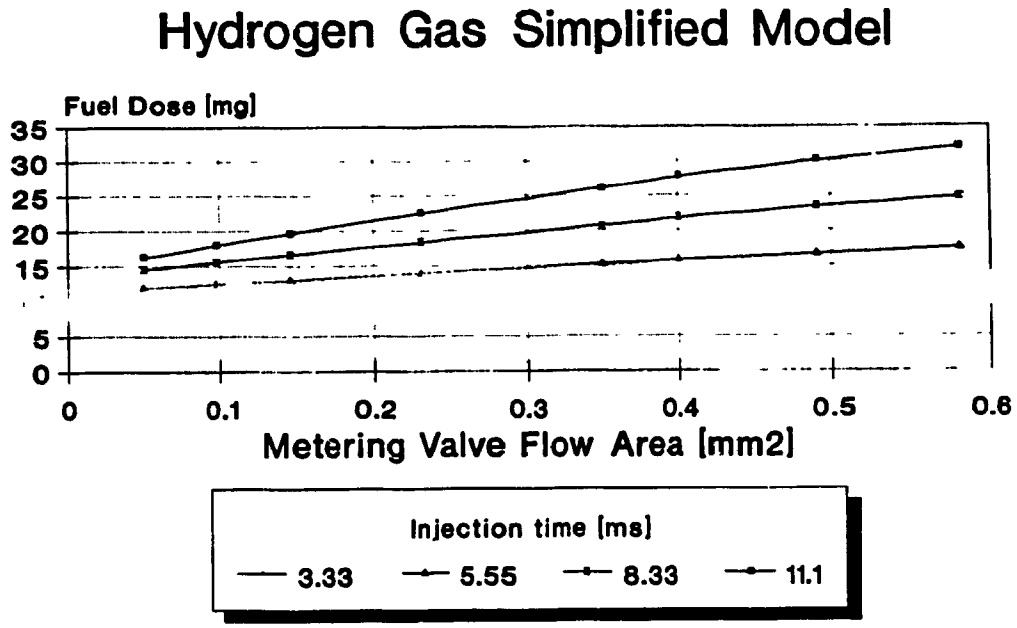

Figure 7.15 Fuel Dose vs Metering Valve Flow Area at 600 rpm for Hydrogen Gas.

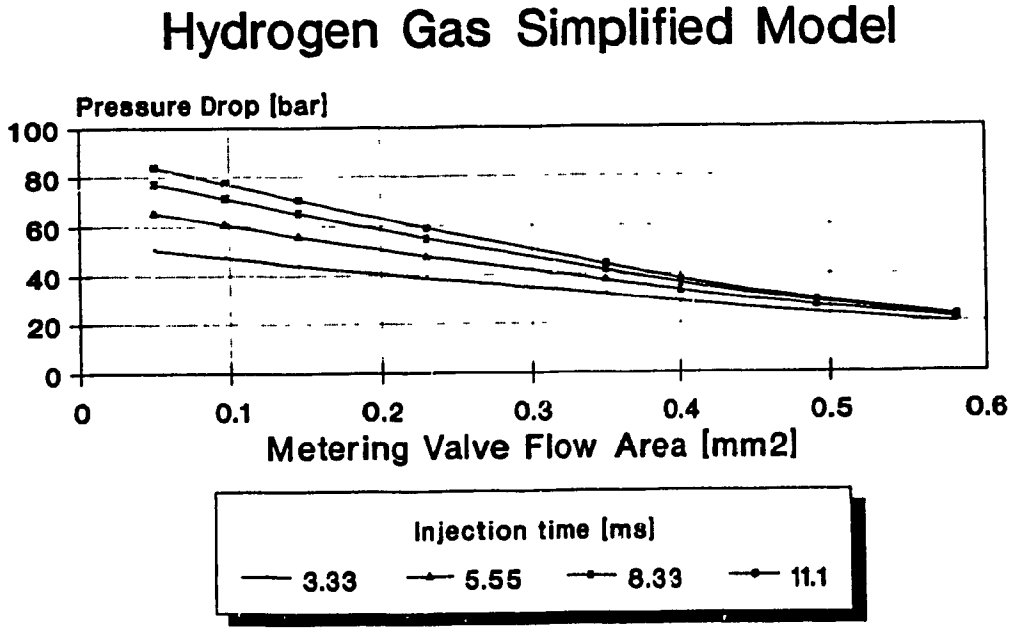

Figure 7.16 Pressure vs Metering Valve Flow Area at 600 rpm for Hydrogen Gas.

7.3 CRITICAL ASSESSMENT OF THE TEST RESULTS

After having computed the gas dose and comparing with the experimental results, some inaccuracies in the test results have been detected

1) There was a significant inaccuracy in the setting of the metering valve position during the experimental investigation, which was based on the notches machined on the metering valve thimble. The clearance in the thread on the screw of the micrometer handle and on the metering valve spindle resulted in some kind of hysteresis in the valve positioning. Not enough attention was paid to approach the desired metering valve position from one side only, by returning it to its datum point and then opening the metering valve.

2) The results for Configuration 1 were more scattered. This can be explained by the fact that in Configuration 1 the gas volume is small and the impact of the metering valve opening is more dominant for the gas dose and pressure drop.

3) The gas dose and pressure measurements, for which an oscilloscope was used, were not very accurate and contributed to the deviations being observed in Chapter 5.

All these factors had some effect on the actual accuracies of the test results and contributed to some

deviation in model validation. The largest source of error was on the metering valve positioning, as discussed in Chapter 6, this is what caused the simulation results to differ from the experimental results, obtained in Chapter 5. This is due to the improper attention paid to valve positioning. Had more concern been paid to this detail, the experimental results would have been more closely matched to the simulation results.

8. CONCLUSIONS AND RECOMMENDATIONS

The following chapter consists of conclusions and recommendations regarding the investigation into electronically controlled multi-point gaseous injection systems.

The first section will deal with an overview of the work presented and will draw several conclusions on the outcome of the investigation.

The last section will deal with some recommendations for future research and investigation into electronically controlled gaseous injection systems.

8.1 SUMMARY AND CONCLUSIONS

In summary, the main objectives of this work was to perform simulations of gaseous fuel injection for use in high speed diesel engines.

First, a mathematical model was developed in order to simulate an injection process with the use of Natural Gas and Hydrogen and to simulate the impact of the pressure waves on the injection system. The results of simulation were then matched with the experimental results to find out the pressure wave effect on the injected gas dose.

A test set-up, with an electronically controlled injector and a computer controlled data acquisition with a novel dose measuring chamber, was equipped with instrumentation to measure the needle displacement and the injector pressure. This allowed to find different injection characteristics for required gas doses of an engine's operating characteristics. The dose was found versus the opening of the metering valve and the pulse width of the current controlling the solenoid actuated injector.

The comparison of the injection characteristics with the simulated results allowed to validate the mathematical model that was developed to emulate an injection system. This validation was also helpful to predict the gas dose

obtained from the injection system. Also, a simplified model was developed whereby the pressure waves were neglected and the injector and the metering valve were placed close to each other. This approach reduced the necessary calculation time significantly with the results being close to the experimental results. Several simulations were performed for different metering openings and injection times, which allowed to predict the gas dose of either Natural Gas and Hydrogen, as well as the pressure drop obtained in the injection system. This method was sought to be used when developing a new gas injection system for predicting the gas injection process for different engine sizes.

Thus, the following conclusions can be formulated from the summary mentioned above:

1) The investigated systems responded well to the metering valve opening and to the pulse width of the current sent to the solenoid actuated injector. This provides a great deal of flexibility for the designer who can choose the best manner of operation for a particular injection system.

2) The impact of the pressure waves between components located at some distance was found not to be significant to the amount of the gas dose injected and to the pressure drop in the injection system. The same was found in the case of the multi-point injection system. It can be

concluded that the most important factor was the volume of fuel between the metering valve and the injector nozzle; much less significant was the actual volume distribution.

3) Based on the previous conclusion, the simplified method of dose calculation can be recommended for design purposes, giving to the designer the known values of metering valve opening, pulse width, current and [illegible] drop for a certain dose requirement.

4) The equipment used to operate the multi-point injection system was slightly inadequate since it lacked a high-speed A/D converter for data acquisition. The conversion speed was too slow and not enough data points were collected for the injection process which lasted a few milliseconds; thus, a cathode oscilloscope was used for the injection process records.

8.2 RECOMMENDATIONS

The following is a list of possible recommendations for future work regarding multi-point electronically controlled gaseous injection systems.

1) The solenoid controlled injectors that were used in this investigation were not designed as state of the art equipment. The solenoids were heavy and bulky, which affected the response time to the pulse width current. Thus, more modern and more compact solenoids should be used to operate the injectors.

2) The injectors that were used always had a tendency to seize after several cycles of operation. They needed to be lubricated often. Thus, the injectors to be used for future work should have a higher clearance to avoid seizures, and also the needle needs to be more pressure balanced in order to avoid sealing of the gas flow along the nozzle guide.

3) It can be predicted that the metering valve may not always be required in an injection system. In case when the gas supply to the injector is not obstructed or affected by any pressure waves, it would eliminate the need for a metering valve, without affecting the gas pressure level in the injectors. Then, the only tool to modify the injection characteristics would be the pulse width

modulation to vary the injected gas dose.

4) More investigation should proceed with the design of multi-point injection systems for gaseous fuels. The designs should involve more than just two injectors fed from the same reservoir and controlled from one metering valve. As aforementioned in the conclusions section, the most important feature was the volume between the metering valve and the injectors and not the volume distribution.

5) The control and data acquisition equipment also need to be at the state of the art, as well as the programming of the control codes. There is a definite need for a multiprocessing and multitasking system in order to enhance the capabilities and flexibility of the injection system. This means that the control equipment should be able to effectively execute several control routines simultaneously, by CPU time slices or parallel processors.

REFERENCES

1. Homan, H.S., De Boer, P.C.T., and McLean, W.J., "The Effect of Fuel Injection on NOx Emissions and Undesirable Combustion For Hydrogen-Fuelled Piston Engines", Int. J. Hydrogen Energy, Vol 8, No. 2,pp. 131-146, 1983.

2. Varde, K.S. and Frame, G.M., "A Study of Combustion and Engine Performance Using Electronic Hydrogen Fuel Injection", Int. J. Hydrogen Energy, Vol. 9, No. 4, pp. 327-332, 1984.

3. Peschka, W., "Liquid Hydrogen Fuelled Automotive Vehicles in Germany - Status and Development", Int. J. Hydrogen Energy, Vol. 11, No. 11, pp. 721-728, 1986.

4. Strobl, W. and Peschka, W., "Liquid Hydrogen as Fuel of the Future for Individual Transport", BMW AG Presse, July 1986.

5. Furuhama, S. and Kobayashi, Y., "A Liquid Hydrogen Car with a Two-Stroke Direct Injection Engine and LH2-Pump", Int. J. Hydrogen Energy, Vol. 7, No. 10, pp. 809-820, 1982.

6. Furuhama, S. and Kobayashi, Y., "Development of a Hot -Surface-Ignition Hydrogen Injection Two-Stroke Engine", Int. J. Hydrogen Energy, Vol. 9, No. 3, pp. 205-213, 1984.

7. Furuhama, S. and Fukuma, T., "High Output Power Hydrogen Engine with High pressure Fuel Injection, Hot Surface Ignition and Turbocharging", Int. J. Hydrogen Energy, Vol. 11, No. 6, pp. 399-407, 1986.

8. Hinds, H.R., Hydrogen Energy - News and Views, Int. J. Hydrogen Energy, Vol. 12, No. 6, pp. 427-431, 1987.

9. Martorano, L. and Dini, D., "Hydrogen Injection in Two -Stroke Reciprocating Gas Engines", Int. J. Hydrogen Energy, Vol. 8, No. 11/12, pp. 935-938, 1983.

10. Ikegima, M., Miwa, K. and Shioji, M., "A Study of Hydrogen Fuelled Compression Ignition Engines", Int. J. Hydrogen Energy, Vol. 7, No. 4, pp. 341-353, 1982.

11. MacCarley, C.A., "Development of a High Speed Injection Valve for Electronic Hydrogen Fuel Injection", Proceedings of the 3rd World Hydrogen Energy Conference, Vol. 2, pp. 1119-1133, 1980.

12. Taxon, M. and Gieseking, J., "The United Technologies Alpha Series Fuel Injector - High Performance at a Reduced Cost", SAE Paper 851656, 1985.

13. DeGrace, L.G. and Bata, G, "The Bendix DEKA Fuel Injector Series - Design and Performance", SAE Paper 850559, 1985.

14. [illegible] "Aisan Fuel Injector for Multipoint Injection System", SAE Paper 860486, 1986.

15. Krepec, T., Tebelis, T. and Kwok, C., "Fuel Control Systems for Hydrogen-Fuelled Automotive Combustion Engines - A Prognosis", Int. J. Hydrogen Energy, Vol. 9, No. 1/2, pp. 109-114, 1984.

16. Krepec, T., Giannacopoulos, T. and Miele, D., "New Electronically Controlled Hydrogen-Gas Injector Development and Testing", Int. J. Hydrogen Energy, Vol. 12, No. 12, pp. 855-861, 1987.

17. Krepec, T., Miele, D. and Sudano, A., "Preliminary Concept of Semicryogenic Tank for Storage and Direct Injection of Natural Gas in Internal Combustion Engines", SAE Paper 880148, 1988.

18. Tebelis T. and Krepec, T., "A Concept of Electronically Controlled Hydrogen-Gas Injector for High Speed Compression Ignition Engines", Proceedings of the Second International Symposium on Hydrogen Produced for Renewable Energy, Cocoa Beach, Florida, 1985, pp. 397-408.

19. Giannacopoulos, T., Krepec, T. and Lisio, C., "Preliminary Investigations on a Microprocessor Controlled Gaseous Hydrogen Injector", Proceedings of ASME International Computers in Engineering Conference, Chicago, Illinois, July 1986.

20. Giannacopoulos, T., "A Feasibility Study on an Electronically Controlled Hydrogen Gas Injector", Master's Degree Thesis, Concordia University, Montreal, Quebec, Canada, March 1986.

21. Krepec, T., Miele, D., and Lisio, C., "New Concept of Hydrogen-Fuel Storage and Supply for Automotive Applications", Presented at the 7th World Hydrogen Energy Conference in Moscow, U.S.S.R. on September 25-29, 1988.

22. Vargaftik, N.B., Tables on Thermophysical Properties of Liquids and Gases. In Normal and Dissociated States. Hemisphere Publishing Corporation, Washington, 1975.

23. Lichty, L.C., Combustion Engine Processes, McGraw-Hill, New York, New York 1967

24. McCloy, D. and Martin, H.R., The Control of Fluid Power, Longman Group Limited, London, England, 1973.

25. Andersen, B.W., The Analysis and Design of Pneumatic Systems, John Wiley and Sons Inc., N. Y., N. Y., 1967.

26. Zalmanzon, L.A., Components for Pneumatic Control Instruments, The Static and Dynamic Characteristics of Pneumatic Resistance, Capacitance, and Transmission Lines. Permagon Press, London, 1965.

27. Seilly, A.H., "HELENOID Actuators - A New Concept in Extremely Fast Acting Solenoids", SAE Paper 790119, 1979.

28. Seilly, A.H., "COLENOID Actuators - Further Development in Extremely Fast Acting Solenoids", SAE Paper 810462, 1981.

29. Glikin, P.E., Fuel Injection in Automotive Diesel Engines", SAE Paper 851458, 1985.

30. Komiyama, K., Okazaki, T., Togashi, K., Hashimoto, H., and Takaya, K., "Electronically Controlled High Pressure Injection System for Heavy Duty Diesel Engine - KOMPICS", SAE Paper 810997, 1981.

31. Hames, R.J., Straub, R.D., and Amann, R.W., "DDEC-Detroit Diesel Electronic Control", SAE Paper 850542, 1985.

32. Schechter, M.M. and Asik, J.R., "Direct Fuel Injection with Electromagnetic Spill Control - Investigation with the EME-4 Pump", SAE Paper 840308, 1984.

33. Wylie, E.B., Bolt, J.A., and El-Erian, M.F., "Diesel Fuel Injection System Simulation and Experimental Correlation", SAE Paper 710569, 1971.

34. El-Erian, M.F., Wylie, E.B., and Bolt, J.A., "Analysis and Control of Transient Flow in the Diesel Injection System, Part I - The Analytical Control Method", SAE Paper 730661, 1973.

35. El-Erian, M.F., Wylie, E.B., and Bolt, J.A., "Analysis and Control of Transient Flow in the Diesel Injection System, Part II - Design Results of Controlled After-Injection", SAE Paper 730662, 1973.

36. Scullen, R.S. and Hames, R.J., "Computer Simulation of the GM Unit Injector", SAE Paper 780161, 1978.

37. Goyal, M., "Modular Approach to Fuel Injection System Simulation", SAE Paper 780162, 1978.

38. Smith , D.H. and Spinweber, D.A., "A General Model for Solenoid Fuel Injector Dynamics", SAE Paper 800508, 1980.

39. Marcic, M. and Kovacic, Z., "Computer Simulation of the Diesel Fuel Injection System", SAE Paper 851583, 1985.

40. Wylie, E.B. and Streeter, V.L., Fluid Transients, Corrected Edition, FEB Press, Ann Arbor, Michigan, 1983.

41. Krepec, T., To, C.H., and Krepec, M., "Evaluation of Diesel Injectors Dynamic Properties", Proceedings of the Sixth Congress on Theory of Machines and Mechanisms, 1983.

42. Lindsay, J.F. and Katz, S., Dynamics of Physical Circuits and Systems, Matrix Publishers, Inc., Beaverton, Oregon, 1978.

43. James, M.L., Smith, G.M., and Wolford, J.C., Applied Numerical Methods for Digital Computation, Third Edition, Harper and Row Publishers, New York, New York, 1985.

44. Blaum, Dr.-Ing. Eddo, Das Einspritzgesetz der schnellaufenden Dieselmachine, Zeitlicher und mengeumafliger Verlauf der Einspritzung, VDI-VERLAG GMBH, Berlin 1942.

45. Yuan, W.S., Foundation of Fluid Mechanics, Prentice-Hall Inc., Englewood, New Jersey 196

APPENDIX A

Peugeot Engine Operating Characteristic

The engine used for the purpose of this investigation is a 25 HP Peugeot Idenor Diesel engine, with a maximum speed of 2300 rpm. Four of its basic operating characteristics were used to analyze the conversion of this engine to operate on gaseous fuels such as Natural Gas and Hydrogen. The four basic points are: minimum idle, maximum torque, maximum power,and maximum idle. The following table summarizes the speed of the engine and the fuel requirements at each of the four points. The only dose missing from the table is the starting dose, which is equivalent to 160 % of the maximum power dose at 600 rpm.

Table A.1. Engine Operating Points.

point	engine speed	Fuel Requirement
min. idle	600 rpm	20% of max. power
max. torque	1600 rpm	200 g / HP-hr
max. power	2000 rpm	220 g / HP-hr
max. idle	2300 rpm	20% of max. power

In order to obtain a fuel dose versus speed graph, it

is essential to calculate the fuel dose at each point. Knowing that the engine outputs 25 HP and that the torque droop is 15%, the best point to calculate the dose as an example would be at maximum torque. Solving for maximum torque requires to first calculate the torque at maximum power, and the following equation is used,

$$T_{mp} = \frac{7120 * HP}{N} \qquad (A.1)$$

Substituting in values of 25 for HP and 2000 rpm for N,the torque at maximum power equals 89 N-m. Thus, the maximum torque can be calculated from the torque droop equation, as shown below,

$$\text{Torque droop} = \frac{T_{max} - T_{mp}}{T_{max}} * 100 \qquad (A.2)$$

Substituting for torque droop and T_{mp}, the maximum torque, T_{max}, is found to be 104.71 N-m. By rearranging equation (A.1) to solve for HP at maximum torque, and by substituting the engine speed and the torque, the power at maximum torque is found to be 23.53 HP. Now, solving for the required fuel dose the following equation is used:

$$\dot{m}_f = \dot{W} * ge \qquad (A.3)$$

Substituting in 23.53 HP for $\mathring{W}$ and the fuel requirement of 200 g/HP-hr at maximum torque, ge, the mass flow of fuel is calculated to be 4706 g/hr. To obtain the fuel dose per cylinder per injection, the following equation is used,

$$m_f = \frac{2\,\mathring{m}_f}{N\,n_c * 60} \qquad (A.4)$$

Substituting the mass flow, the speed, N, as 1600 rpm, and the number of cylinders, n_c, as 4, the mass dose per cylinder per injection is found to be 2.451 (10^{-5}) kg of diesel fuel. The other points can be solved in a similar manner and Table A.2 summarizes the results.

Table A.2. Engine Fuel Dose Results.

point	engine speed	Fuel Dose (10^{-5})kg
min. idle	600 rpm	0.4851
max. torque	1600 rpm	2.4510
max. power	2000 rpm	2.2920
max. idle	2300 rpm	0.4851

From this table, a rough but useful engine operating characteristic curve can be plotted, as seen in Figure A.1.

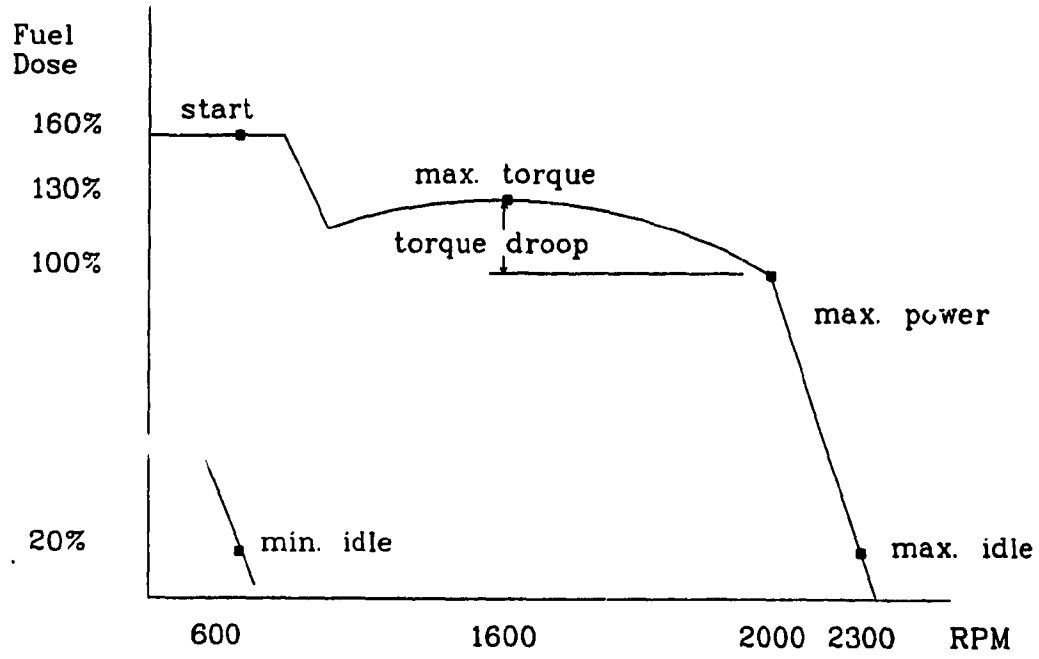

Figure A.1 Engine Operating Characteristics

APPENDIX B

Derivation of Original Pintle Nozzle and Modified Pintle Nozzle Flow Areas

The pintle nozzle and modified pintle nozzle shapes have been shown in Chapter 3, as well as the plots showing the flow area versus the needle lift or displacement. The pintle nozzle has five critical flow areas, while the modified pintle nozzle only has three. The first two critical flow areas are identical to both nozzles [44].

First the shared critical flow areas will be presented, followed by the last critical flow area for the modified pintle nozzle and lastly the three remaining critical flow areas for the original pintle nozzle.

The first critical flow area for the nozzles is A_{se} and can be seen in Figure B.1 corresponding to segment CD. The flow areas can be described by the following equation:

$$A = 2 \Pi R L \qquad (B.1)$$

where,

A = critical flow area
R = average radius of the critical flow area
L = length of the cylinder of the flow area

Thus, for the flow area A_{se}, R and L must be solved for in terms of needle displacement h. From the flow area triangle in Figure B.2, the following derivation fo. che

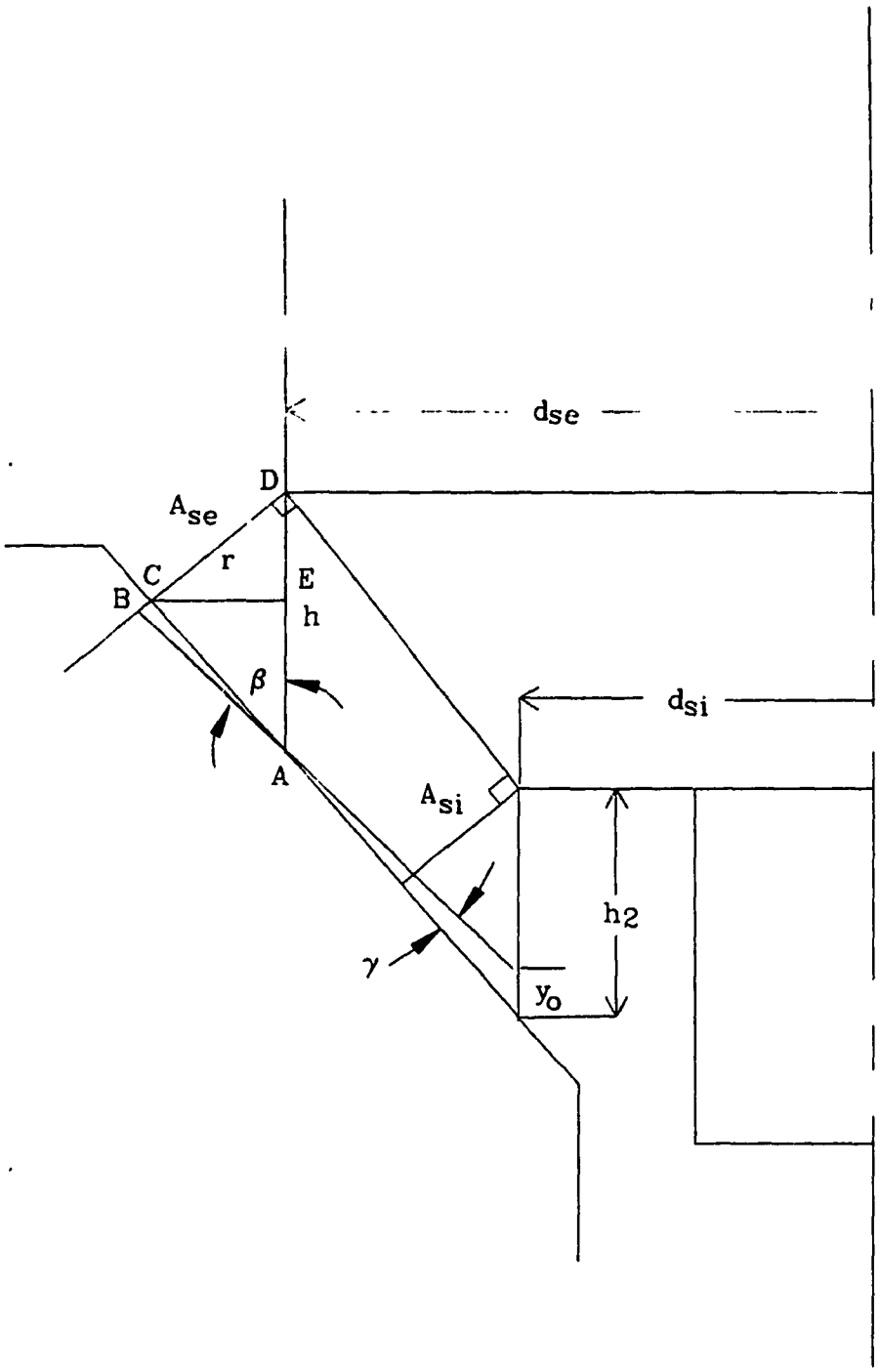

Figure B.1 Original Pintle Geometry for Flow Area.

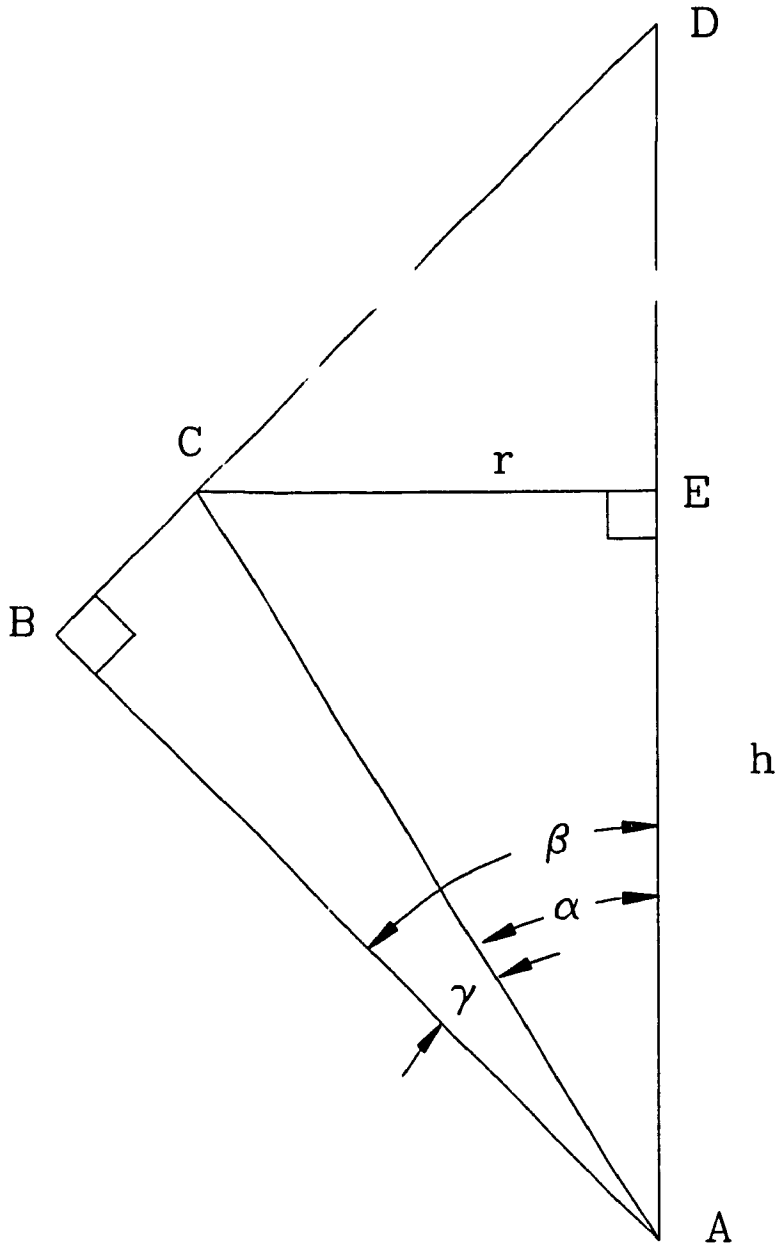

Figure B.2 Close Up of Geometry

flow area can be said for the length L,

$$L = \overline{CD} = \overline{BD} - \overline{BC}$$

where,

$$\overline{BD} = h \sin \beta = \overline{AB} \tan \beta$$

and,

$$\overline{BC} = \overline{AC} \sin \gamma = \overline{AB} \tan \gamma$$

whereby,

$$\overline{AB} = h \cos \beta$$

thus, substituting all the above in the equation for the length L, the following is obtained.

$$L = \overline{CD} = h \cos \beta \ (\tan \beta - \tan \gamma)$$

For the radius R,

$$R = \frac{d_{se}}{2} + \frac{\overline{CE}}{2}$$

where,

$$\overline{CE} = \overline{CD} \cos \beta$$

recalling that $\overline{CD} = L$ and substituting and solving for R, the following is obtained,

$$R = \frac{d_{se}}{2} + \frac{h \cos^2 \beta}{2} \ (\tan \beta - \tan \gamma)$$

Thus, substituting L and R into equation (B.1), the flow area A_{se} is solved for as show below.

$$A_{se} = \Pi d_{se} h(\sin \beta - \tan \gamma \cos \beta) + \Pi h^2 \cos^3 \beta (\tan \beta - \tan \gamma)$$

and, when $\gamma << 1$,

$$A_{se} = \Pi\, d_{se} h\, (\sin \beta - \cos \beta) + \Pi\, h^2 \cos \beta \sin \beta$$

Similarly from the geometry in Figure [illegible] the second critical flow area, A_{s1} can be solved for as in the case for the first critical flow area. Thus, the equation obtained is as follows:

$$A_{s1} = \Pi\, d_{s1} h_2 (\sin \beta - \cos \beta) + \Pi\, h_2^2 \cos \beta \sin \beta$$

where,

$$h_2 = h + y_o$$

and,

$$y_o = \frac{d_{se} - d_{s1}}{2 \sin \beta} * \frac{\sin \gamma}{\sin \alpha}$$

All that remains to derive now is the last critical flow area for the modified pintle and the remaining three critical flow areas for the original pintle nozzle. See Figure B.3.

The last critical flow area for the modified nozzle is the nozzle orifice area, which the equation is given below.

$$A_o = A_{23} = \frac{\Pi}{4} d_o^2$$

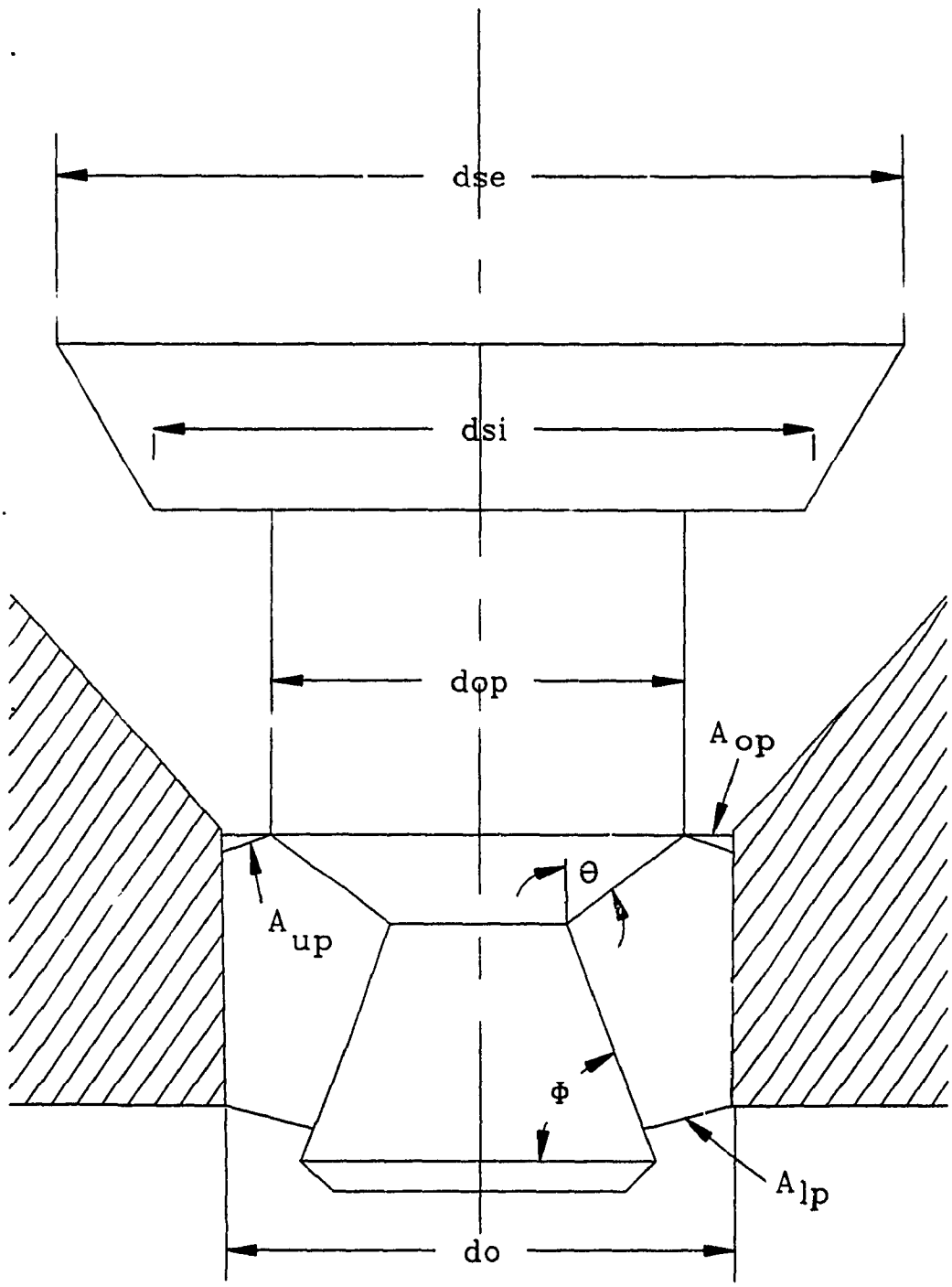

Figure B.3 Pintle Geometry for Flow Area

The three remaining critical flow areas for the original pintle nozzle are dependent on the actual value of the needle lift. That is that if the needle lift is not greater than a certain value, then that flow area is non existent. The three critical flow areas fall into existence with the following needle lift values: a) when needle lift is greater than or equal to ≅0.3 mm and b) when the needle lift is greater than or equal to ≅0.5 mm. And the flow areas are solved similarly as shown for the first critical flow area.

Before the needle lift approaches 0.3 mm, the critical flow area shifts from the first two aforementioned flow areas into the third critical flow area. It occurs between the pintle shaft and the nozzle housing giving an annular flow area. The equation describing this flow area is given below.

$$A_{op} = \frac{\Pi}{4} (d_o^2 - d_{op}^2)$$

This flow area ceases to exist once the pintle shaft is no longer interfacing with the nozzle housing, i.e. once the 0.3 mm needle lift is achieved in the injector.

Then the fourth critical flow area is achieved, between the upper pintle and the injector nozzle diameter. This equation is only valid until the 0.5 mm needle lift mark is achieved and then shifts to the last critical flow

area. The equation describing this flow area is given below as:

$$A_{up} = \frac{\Pi}{4} (d_o^2 - d_{op}^2) \; / \; \cos \theta$$

where,

$$\theta = \text{atan} \frac{h_{pi}}{d_o - d_{op}}$$

and,

$$h_{pi} = h - 0.3$$

Finally, the last critical flow area is present between the injector nozzle diameter and the lower pintle. The equation describing its flow area is shown below.

$$A_{lp} = \Pi \, d_o (h_o - h) \cos \Phi - \Pi \, (h_o - h)^2 \cos^2 \Phi \sin \Phi$$

APPENDIX C

CALIBRATION CURVES

This appendix will deal with the calibration curves of the various measuring instruments, electronic circuits and injection equipment that were used in the progress of this investigation.

The devices that were calibrated are: pressure transducers, linear variable differential transformer (LVDT), springs for the gaseous injector and a frequency to voltage (F/V) converter integrated circuit (IC). The calibration curves will be in the respective order, as mentioned above.

The pressure transducers used are Kistler quartz transducers Model No. 630B2 and Serial No. 5002 and C10864. Figure C.1 shows the output voltage from the change in pressure, for both transducers. The calibration values for the transducers are as follows: for No. 5002, the value is 10 mV/bar, and for No. C10864, the value is 10 mV/bar.

The linear variable differential transformer, by AVL, was calibrated by measuring maximum displacement of the injector needle movement possible after assembly of the injector. The calibration curve is shown in Figure C.2 for the LVDT. There were two springs to choose from, a red

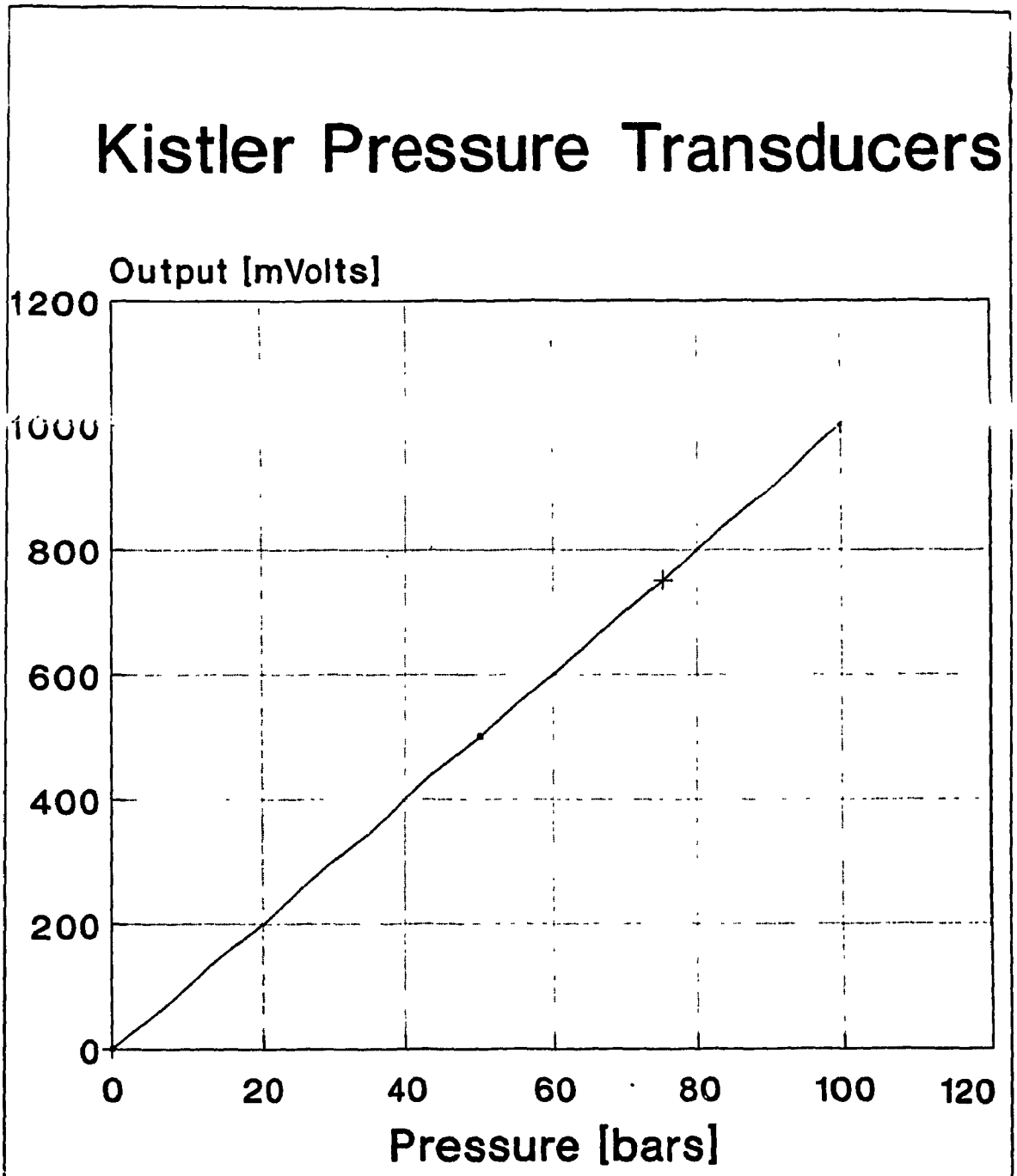

Figure C.1. Calibration Curve for Kistler Pressure Transducers used in Experimental Set-up.

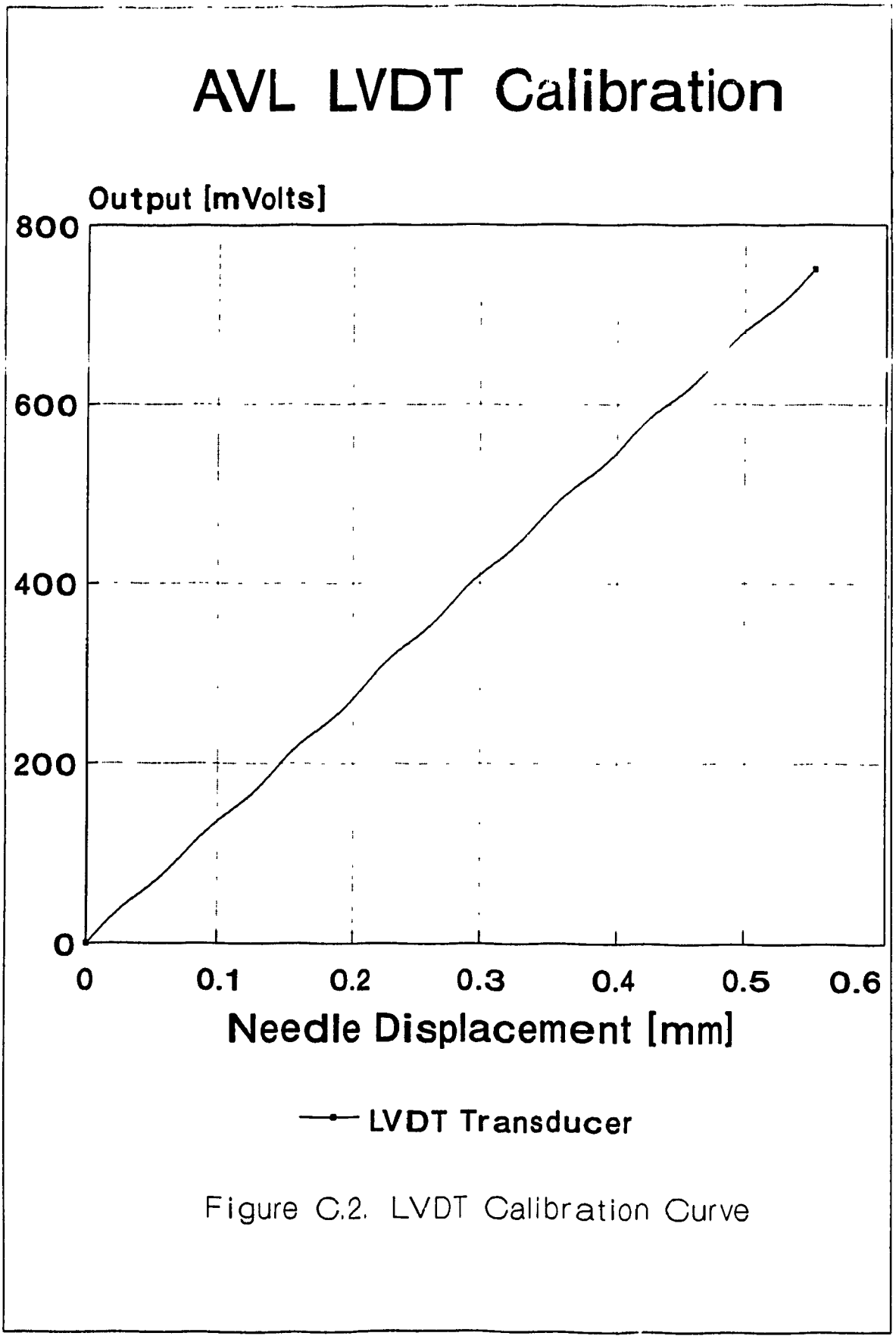

Figure C.2. LVDT Calibration Curve

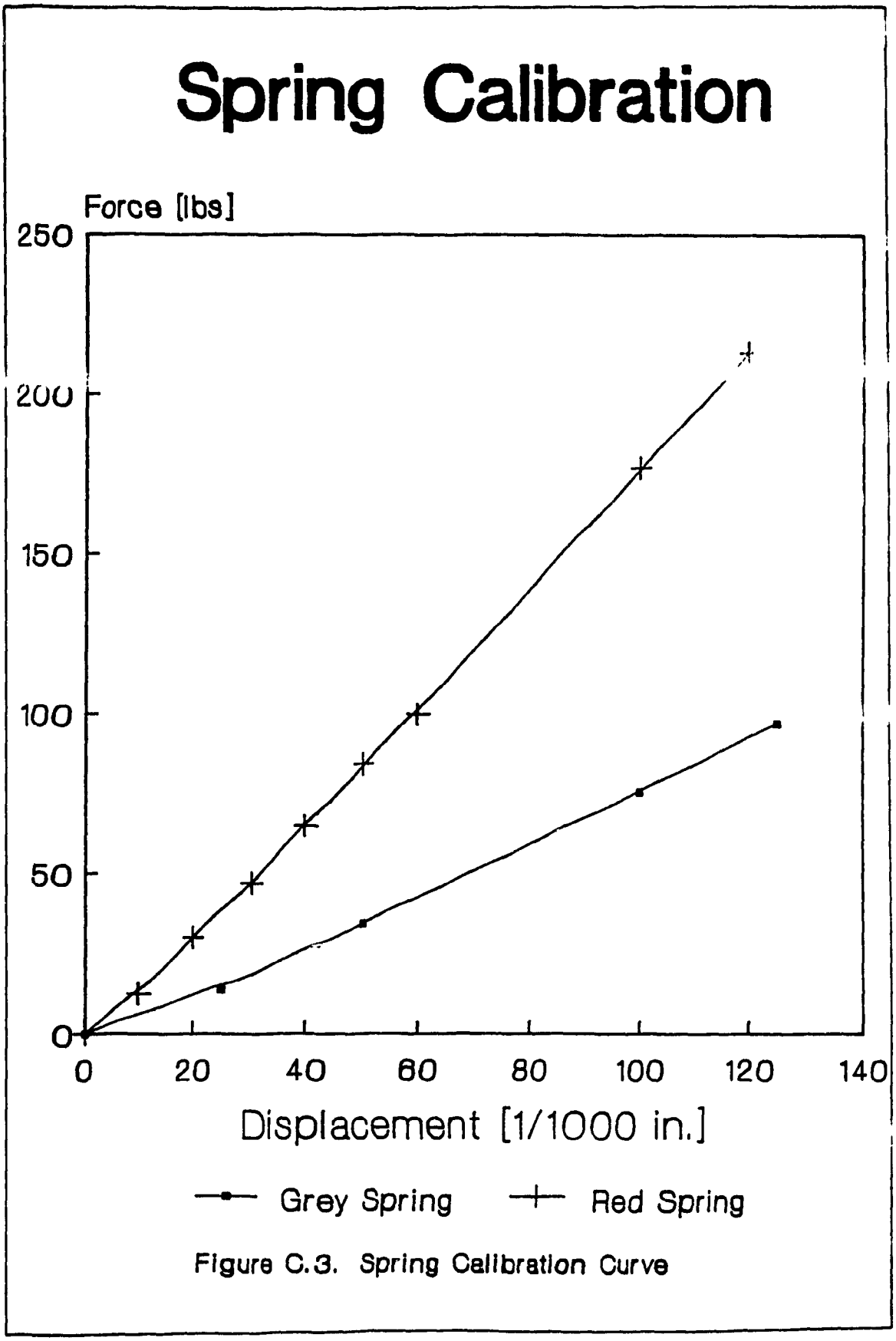

Figure C.3. Spring Calibration Curve

spring and a grey spring. The force versus displacement curves for the springs are shown in Figure C.3. The spring selection was based on the maximum force a spring could exert to maintain the closed position due to the number of threads available to set the preload on the spring. The red spring was chosen over the grey one due to its higher K value and its ability to maintain the injector in the closed position.

The calibration of the Teledyne 9400 F/V can be seen in Figure C.4. This curve shows several non-linear sections, a plateau, and a linear section between 500 and 2500 Hertz (Hz). The range which is desired for the diesel engine used in this investigation is between 500 and 2500 rpm, and by using a 60 tooth gear and magnetic pick-up it matches the linear range of the frequency to voltage converter. Figure C.5 points out the linear portion of the curve which is output from the F/V chip.

Lastly, the last two pages of this appendix provide the calibrations of the experimental set-up for the injectors and the metering valve.

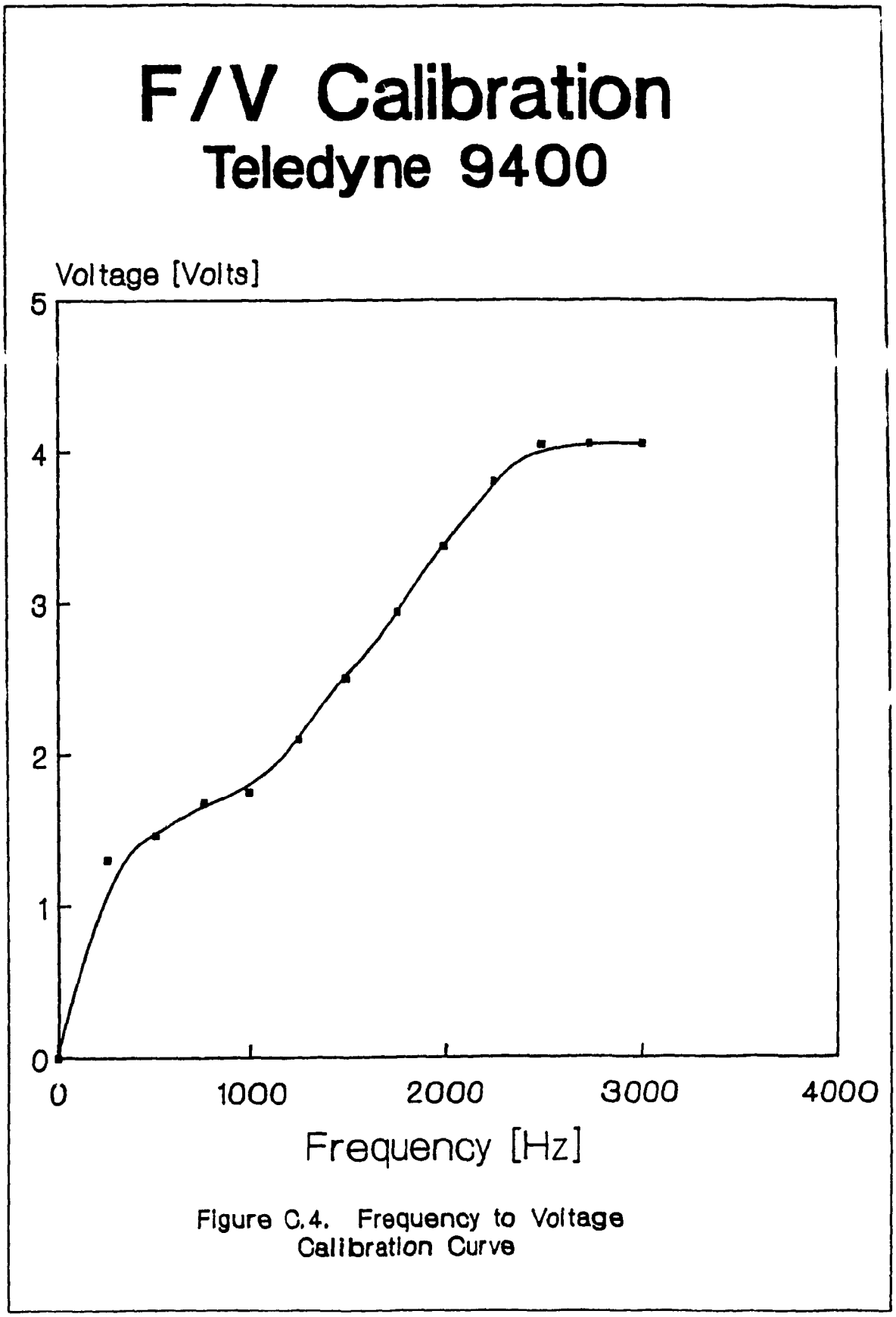

Figure C.4. Frequency to Voltage Calibration Curve

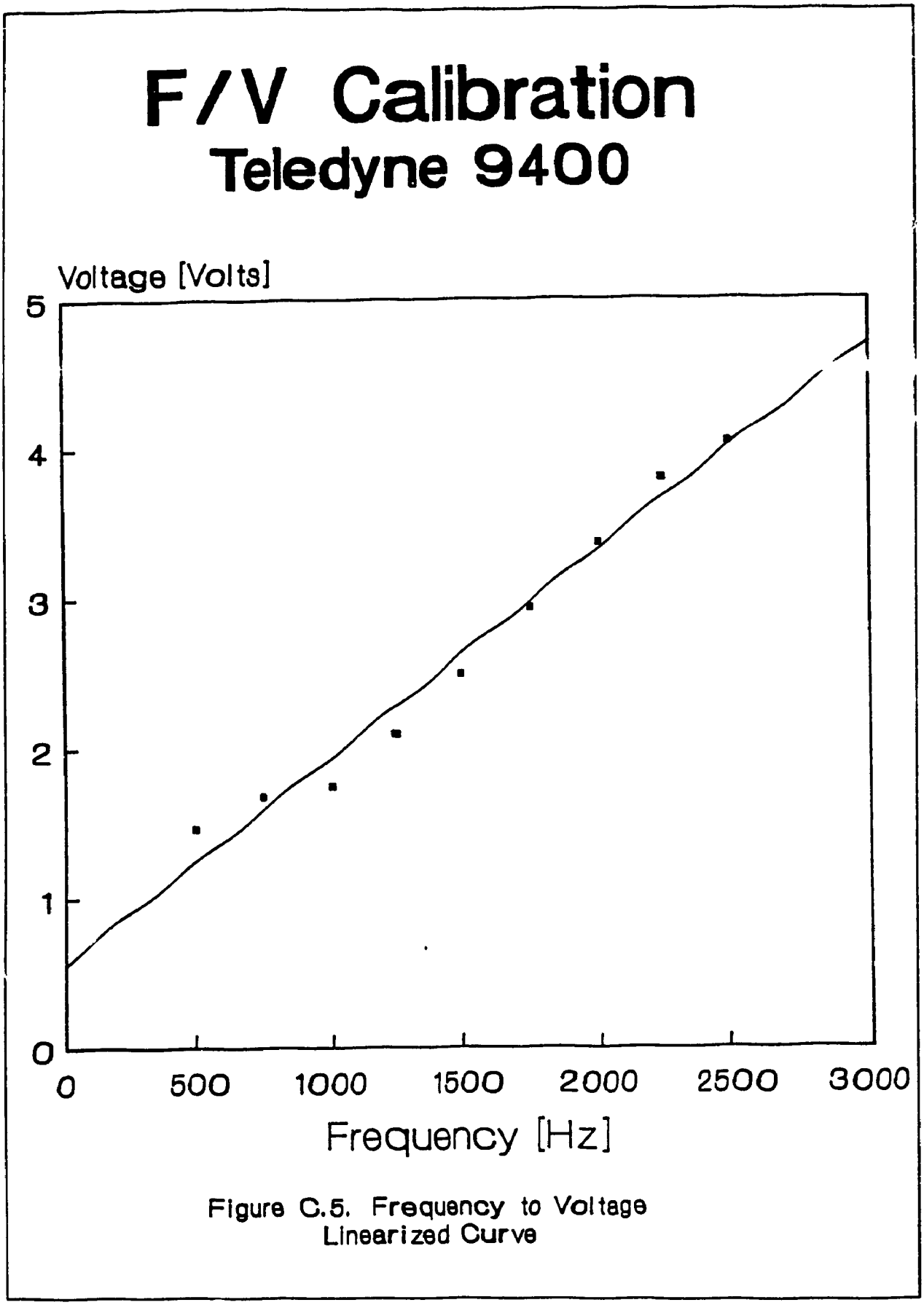

Figure C.5. Frequency to Voltage Linearized Curve

Table C.1 Injector Configurations and Instrumentation Calibrations for Experimental Test Set-Up.

INJECTOR CONFIGURATION No. 1

Injector Housing	: CAV BKB - 40S5146V
Injector Nozzle	: CAV BDN4SD508W
Spring Constant	: 143 kN/mm
Needle Lift Limit	: 0.58 mm

INJECTOR CONFIGURATION No. 2

Injector Housing	: CAV BKB - 40S5146V
Injector Nozzle	: CAV BDN4SD508W, with modified pintle
Spring Constant	: 321 kN/mm
Needle Lift Limit	: 0.55 mm

INSTRUMENTATION

Pressure Transducers	: Kistler
Injection Pressure Calibration	: Model 603B2 S/N C10864 Range 10 : 144.93 mV/bar
Dose Pressure Calibration	: Model 603B2 S/N 5002 Range 20 : 633.65 mV/bar Range 50 : 253.46 mV/bar
Lift Transducer	: AVL
Displacement Calibration	: Model 3075-A02 S/N 471 Injector 1 : 1557.1 mV/mm Injector 2 : 689.7 mV/mm

Table C.2 Metering Valve Configurations

METERING VALVE CONFIGURATIONS

Metering Valve Type	: Hoke S/N 1315M4B 3° taper 1.19 mm diameter

Pipe Parameters

Pipe Lengths	: 125 mm, 250 mm
Pipe Diameters	: 3.0 mm, 4.5 mm

Configurations:

Config. #1 : no pipe, metering valve only

Config. #2 : 125 mm pipe between injector and metering valve, of diameter 4.5 mm
#2b : same as above, pipe diameter 3.0 mm

Config. #3 : 250 mm pipe between injector and metering valve, of diameter 4.5 mm
#3b : same as above, pipe diameter 3.0 mm

Config. #4 : metering valve attached to a tee separating two injectors connected by two 125 mm pipes of 4.5 mm diameter.
#4b : same as above, pipe diameter 3.0 mm

APPENDIX D

Metering Valve Flow Area Characteristics

The metering valve used in the experimental apparatus is a HOKE metering valve, model 1335M4B. The valve is a conical poppet type with a taper angle of 3 degrees on the needle and a hole diameter of 1/16 inches. The valve dimensions and angles can be seen in Figure D.1. From the figure, the angle, α, is half the taper angle and Y is the height of the metering valve from its seated position. D_{met} is the diameter of the hole, and L represents the width of the flow area.

The flow area can be derived as follows: first, the width, L, is calculated in terms of the height, Y, and half of the taper angle, α, [26].

$$L = Y * \sin \alpha \qquad (D.1)$$

Then, the circumference is taken at the midpoint of the width, L. This circumference can be found by subtracting the difference between the metering valve radius and the distance s, as seen in the previous figure. Thus,

$$R_c = R_{met} - s \qquad (D.2)$$

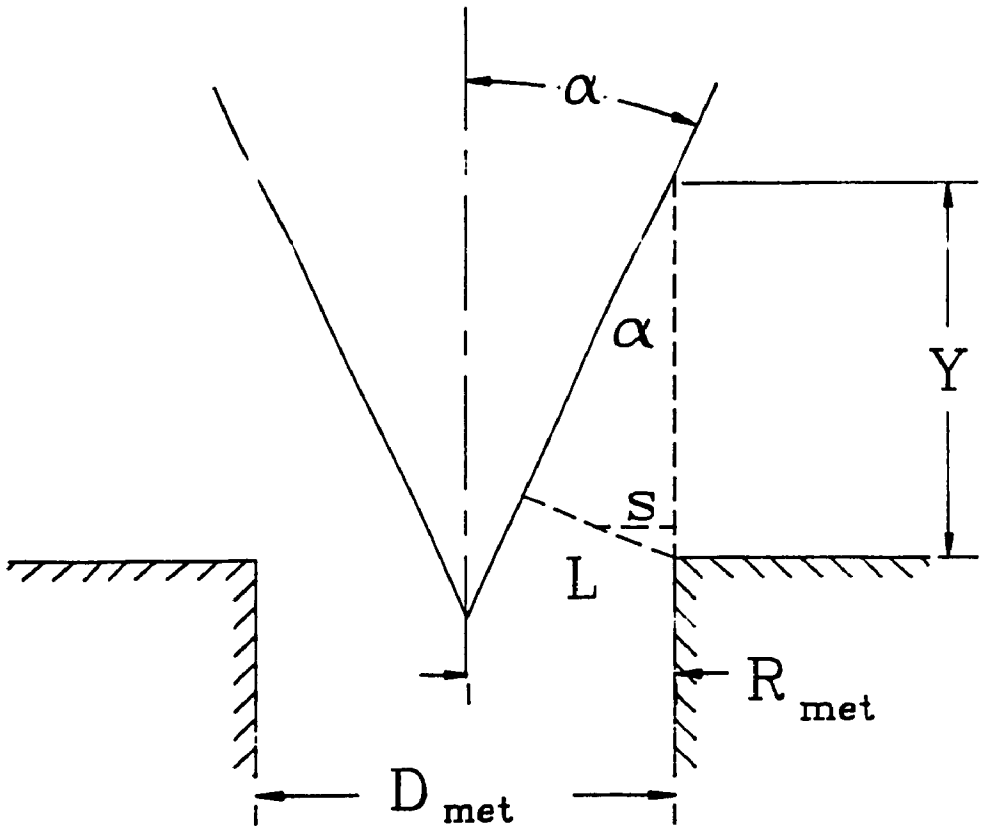

Figure D.1. Metering Valve Poppet Geometry [24].

where,

$$s = 0.5 * L * \cos \alpha \qquad (D.3)$$

from the geometry in Figure D.1.; thus, the equation for the flow area due to the lift, Y, is the product of the width, L, multiplied by the circumference at the mid-point of the width.

$$A_{met} = L * 2 \quad [R_{met} - 0.5 \, L \cos \alpha] \qquad (D.4)$$

Substituting the equation (D.1) in equation (D.4) and rearranging the terms, the final equation for the conical poppet type metering valve becomes the following [26]:

$$A_{met} = Y \sin \alpha * [D_{met} - Y \sin \alpha \cos \alpha] \qquad (D.5)$$

Finally, substituting values for the angle and the diameter, the equation for the area is only in terms of the lift, Y.

$$A_{met} = 0.003479 \, Y - 0.01525 \, Y^2 \qquad (D.6)$$

The manufacturer's data have also been presented in Chapter 3 and in Appendix C.

APPENDIX E

Derivation of Viscous Damping Force

The viscous damping force is based on flow between two parallel plates, or better known as Couette Flow [45]. The equation for Couette Flow is given as follows:

$$F_{damp} = -\Pi\, d_{needle} \int_0^L \tau_{yx}\, dh \qquad (E.1)$$

where,

$$\tau_{yx} = \mu \frac{du}{dy} \qquad (E.2)$$

and,

$$\frac{u}{U} = \frac{Y}{\delta} + \alpha \frac{Y}{\delta}\left(1 + \frac{Y}{\delta}\right) \qquad (E.3)$$

where

$$\alpha = \frac{\delta^2}{2\mu U}\left(\frac{-dP}{dh}\right) \qquad (E.4)$$

In this particular case, for the injector needle motion, y is the radial distance and x is the central axis of the injector needle. L is the needle length along which the Couette Flow occurs and δ is the clearance between the injector needle and the injector housing. Thus by substituting equations (E.4) in (E.3), and solving for u,

which is the velocity of the fluid flow, it can be substituted in equation (3.2), which is then substituted in equation (3.1) in order to obtain the following expression:

$$F_{damp} = -\Pi\, d_{needle} \int_0^L \mu \frac{d}{dy} \left(\left(\frac{yU}{\delta} + \frac{\delta}{2\mu} \left(\frac{-dP}{dh} \right) \left(y - \frac{y^2}{\delta} \right) \right) \right) \qquad (E.5)$$

By simplifying the above expression in equation (3.5) and by letting $y = \delta$, it is reduced to the following:

$$F_{damp} = -\Pi\, d_{needle}\, \mu \left(\int_0^L \frac{U}{\delta}\, dh + \int_0^L \frac{\delta\, dP}{2\mu} \right) \qquad (E.6)$$

Integrating for this expression from L to 0, that is from the top of the injector needle, close to ambient pressure P_4, and the injection chamber, at pressure P_2. The following final equation is obtained:

$$F_{damp} = C_1 U + C_2 \qquad (E.7)$$

where,

$$C_1 = -\Pi\, L\, d_{needle} \frac{1}{\delta}$$

$$C_2 = -0.5\, \Pi\, \delta\, d_{needle} (P_4 - P_2)$$

$$U = \frac{dh}{dt} = \text{needle velocity}$$

Thus, the solution for the viscous damping force is provided in equation (3.7) and is used as such in the mathematical model for the injector motion.